CARBON ISOTOPE STRATIGRAPHY OF EARLY EOCENE HYPERTHERMALS IN THE BIGHORN BASIN, WYOMING, USA: ANALOGUES FOR MODERN ANTHROPOGENIC CARBON EMISSIONS

by

Bianca Jean Maibauer

A thesis submitted to the faculty of
The University of Utah
in partial fulfillment of the requirements for the degree of

Master of Science

in

Geology

Department of Geology and Geophysics

The University of Utah

December 2013

The University of Utah Graduate School

STATEMENT OF THESIS APPROVAL

The thesis of **Bianca Jean Maibauer**

has been approved by the following supervisory committee members:

Gabriel Bowen	, Chair	**October 9, 2013** Date Approved
Lauren Birgenheier	, Member	**October 9, 2013** Date Approved
Thure Cerling	, Member	**October 9, 2013** Date Approved

and by **John Bartley** , Chair/Dean of

the Department/College/School of **Geology and Geophysics**

and by David B. Kieda, Dean of The Graduate School.

ABSTRACT

Paleoclimate records indicate that the early Cenozoic Era was punctuated by several abrupt, transient hyperthermal events, most notably the Paleocene-Eocene Thermal Maximum (PETM, ca. 55.5 Ma) and the Eocene Thermal Maximum 2 (ETM2, ca. 53.6 Ma). These abrupt warming events occur coeval to a significant perturbation to the global carbon cycle. Although the timing and magnitude of these ancient hyperthermal events were similar to projected future changes associated with anthropogenic carbon emissions, the application of these events as analogues to anthropogenic global change is complicated by widely divergent interpretations of the rate, patterns, and sources of carbon release. Recently drilled scientific cores that span these hyperthermals were collected at three terrestrial sites from the Bighorn Basin, Wyoming, USA.

Pedogenic carbonate isotope data from the Gilmore Hill (GMH) site exhibit relatively stable background $\delta^{13}C$ and $\delta^{18}O$ values over a host of multicolored floodplain lithologies but lack the expected >2‰ shift of the ETM2 carbon isotope excursion (CIE). Bulk sedimentary organic matter at Basin Substation (BSN) reveals a dramatic decrease in total organic carbon (TOC) preservation through the estimated PETM interval while $\delta^{13}C$ values are variable and lack the expected >2‰ PETM CIE. High-resolution carbon isotope data from Polecat Bench (PCB) pedogenic carbonate show that the PETM is characterized by a sustained >5‰ negative CIE, and the onset of this event is

characterized by two massive releases of between 600 and 10,000 gigatons of carbon (Gt C), each occurring in one thousand years or less.

We hypothesize that the ETM2 interval is located within poorly cemented, highly weathered sands that characterize the upper 25 m of core at GMH and may represent a climatic response to the warming event. The variability and lack of discernible CIE in our BSN $\delta^{13}C$ record suggests that additional external mechanisms, such as water stress or organic matter source, likely impacted the preserved TOC. The PCB record, however, shows volatile behavior in Earth's carbon cycle leading up to initiation of the PETM and indicates that the PETM is a strong analogue to current and future carbon cycle perturbation in both magnitude and rate of change.

“Twenty years from now you will be more disappointed by the things that you didn’t do than by the ones you did do. So throw off the bowlines. Sail away from the safe harbor. Catch the trade winds in your sails. Explore. Dream. Discover.”

-Mark Twain

TABLE OF CONTENTS

ABSTRACT…… iii

LIST OF FIGURES…… vii

LIST OF TABLES…….. ix

ACKNOWLEDGEMENTS…… x

INTRODUCTION.……. 1

GEOLOGIC SETTING…….. 6

BIGHORN BASIN CORING PROJECT DESCRIPTION……... 10

CARBON ISOTOPE STRATIGRAPHY AND CARBON CYCLE CHANGE ACROSS THE PALEOCENE-EOCENE BOUNDARY: EVIDENCE FROM PEDOGENIC CARBONATE AT POLECAT BENCH, BIGHORN BASIN, WY, USA……..…….. 13

Abstract…… 13
Background…….. 14
Methods..…..…… 18
Results and Discussion..…….. 20
Conclusions…….. 33

CARBON ISOTOPE RECORDS OF PALEOGENE HYPERTHERMAL EVENTS FROM BULK SOIL ORGANIC CARBON AND PEDOGENIC CARBONATE IN THE BIGHORN BASIN, WYOMING……... 53

Abstract…….…….. 53
Background…….…… 54
Methods…….…. 58
Results and Discussion..……. 63
Conclusions…….…… 78

SUMMARY AND FUTURE WORK..……...… 112

REFERENCES…… 115

LIST OF FIGURES

Figure		Page
1.	Map of study area…….	9
2.	Evaluation of the influence of atmospheric CO_2 on the $\delta^{13}C$ values of pedogenic in Polecat Bench cores. ……..	35
3.	Diagenetic sparry calcite in Polecat Bench pedogenic carbonate nodules…….	36
4.	Carbon and oxygen isotope data from pedogenic carbonate at Polecat Bench ……..	37
5.	Photomicrographs comparing matrix (top row) and nodule (bottom row) texture …….	38
6.	Lithologic and isotopic records from Polecat Bench drill core and outcrop ……	39
7.	Core stratigraphy, core $\delta^{13}C$ values and outcrop $\delta^{13}C$ values for the PETM interval at Polecat Bench.…….	41
8.	Schematic of the Paleogene exogenic carbon pools ……	42
9.	Variation in primary micritic calcite versus secondary sparry calcite in pedogenic carbonate collected from Gilmore Hill (GMH) cores and Polecat Bench (PCB) cores and outcrop ……..……	82
10.	Pedogenic carbonate carbon isotope stratigraphy and lithostratigraphy at Gilmore Hill.……..……	83
11.	Comparison of outcrop and core lithostratigraphy and carbon isotope records from terrestrial Eocene strata in the Bighorn Basin, WY.....	85
12.	Comparison of cored lithostratigraphy and carbon isotope stratigraphy from two Bighorn Basin sites. ……...…….	87

13. Lithostratigraphy, total organic carbon (TOC) concentrations, and bulk organic matter carbon isotope stratigraphy at Basin Substation. 89

14. Test for the presence of inorganic carbonate in Basin Substation bulk organic matter samples 90

15. Basin Substation bulk organic carbon isotope record highlighting values derived from sandstone lithologies 91

16. TOC trend corrections calculated and applied to $\delta^{13}C_{org}$ data at Basin Substation. 93

17. Lithostratigraphy, total organic carbon (TOC) concentrations, and corrected bulk organic matter carbon isotope stratigraphy at Basin Substation 95

18. Location and stratigraphy of four Bighorn Basin bulk organic matter studies 96

19. Comparison of total organic carbon records from four sites located in the Bighorn Basin, WY 98

20. Comparison of bulk organic carbon isotope records from four sites located in the Bighorn Basin, WY 100

LIST OF TABLES

Table		Page
1.	Carbon and oxygen isotope stratigraphy from Polecat Bench core collected carbonate nodules.……	43
2.	Carbon cycle mass balance modeling parameters for the Paleocene Epoch ……..……	50
3.	Carbon cycle mass balance calculations for the pre-onset excursion ..…...	51
4.	Carbon cycle mass balance calculations for the PETM CIE...…… …..	52
5.	Sand blank test for residual organic carbon during sample analysis……..	102
6.	Carbon and oxygen isotope stratigraphy from Gilmore Hill core collected carbonate nodules ……..……	103
7.	Carbon cycle mass balance calculations for the ETM2…….	106
8.	Carbon isotope stratigraphy and total organic carbon (TOC, wt% C) from Basin Substation bulk sedimentary organic matter …….	107
9.	Raw and corrected $\delta^{13}C$ values for Basin Substation bulk organic matter..	110

ACKNOWLEDGEMENTS

I would first like to thank my truly wonderful advisor, Gabe Bowen. Not only did he believe in me from the very beginning, but he has provided so many fantastic opportunities that have enabled a more than successful graduate school experience, in addition to helping build the foundation for a successful future. I would also like to thank my committee members, Thure Cerling and Lauren Birgenheier, for understanding my unusual path and progress and agreeing to work with me nonetheless. I also want to recognize members of the SIRFER, SpaTIAL, and PSI Labs, specifically Clement Bataille, Amy Steimke, Vishnu Srinivasaraghavan, and Justin VanDeVelde, as well as Brenda Bowen for technical and ideological contributions. Several members of the Bighorn Basin Coring Project Science Team have also provided invaluable discussion and ideas throughout the course of my work, including Elizabeth Denis, Allie Baczynski, Rachael Acks, Mary Kraus, Phil Jardine, Thomas Westerhold, and Ursula Röhl, as well as the three PIs on our project Scott Wing, Phil Gingerich, and Will Clyde. I would also like to acknowledge the National Science Foundation for providing the funding for this research (NSF Grant #0958821).

I would also like to express gratitude towards my high school Outdoor Education teacher, Charles Deveney, for recognizing the importance of the outdoors and our impact on the planet and instilling those values on not only me, but many years of students before and after me. My friends at Purdue University and the University of Utah have

greatly added to my overall graduate school experience, both personally and academically, providing support, camaraderie, and lasting friendship. I would specifically like to thank Alex Gonzalez, Alex Turner, Tyler Szwarc, Marko Gorenc, Brenton Chentnik and Julia Mulhern. Finally, I would like to thank my family, without whom I wouldn't be here to write these acknowledgements, let alone this thesis. They have supported and encouraged my every move and are the reason why I have made it this far in my education. More than anyone, I want to thank my late grandfather Harold Emmanuel Julius Knappe, for recognizing the beauty of nature and for appreciating the outdoors and rocks enough to instill that appreciation is his children, including my mother Connie. My grandfather and mother passed that appreciation on to me and they are the reason why I'm a geology nerd ☺.

INTRODUCTION

In the last decade, the subject of greenhouse warming and climate change has become a prominent topic of conversation amongst scientists, policy makers, and the general public. Observations of the global surface temperature indicate average total warming of ~1 °C since the start of the industrial revolution (ca. 1850) (IPCC, 2007). Measurements made at the Mauna Loa Earth Observatory in Hawaii reveal that atmospheric pCO_2 is on the rise as well, with an increase of about 80 ppmv in the last 54 years (NOAA/ESRL, 2013). The coupled relationship between temperature and CO_2 has been well documented in Earth's recent history through studies of ice cores spanning glacial and interglacial cycles (Petit et al., 1999). These records also reveal that atmospheric pCO_2 today represents the highest measured level in the last 425,000 years (IPCC, 2007; Petit et al., 1999). Anthropogenic fossil fuel combustion and deforestation, which release greater than 35 Gt of CO_2-eq per year, account for ~75% of anthropogenic CO_2 release and directly contribute to the measured increases in global temperatures and atmospheric pCO_2 (IPCC, 2007). The amount and rate of carbon being released today into the atmosphere will likely result in fundamental changes to ecosystems, climate, and the carbon cycle. In order to better understand and predict these expected changes, we can look to the most recent periods in Earth's history with similar conditions.

During the early Cenozoic, there were several large and abrupt pulses of CO_2 into exogenic reservoirs (oceans, atmosphere, biosphere, soils) that occur coeval to a marked

temperature rise (Zachos et al., 2008). These temporary greenhouse intervals represent rapid perturbations to the global carbon cycle, and some studies suggest that carbon may have been released at roughly the same rate and magnitude as anthropogenic carbon release measured in recent decades (Bowen et al., 2006). Perhaps the largest and most well studied of these Cenozoic hyperthermals is the Paleocene-Eocene thermal maximum (PETM, ca. 55.5 Ma) (Westerhold et al., 2012). The PETM is characterized by >5 °C of warming and a >3‰ negative carbon isotope excursion (CIE), both occurring synchronously in less than 10,000 years (McInerney and Wing, 2011; Zachos et al., 2008). This CIE represents an abrupt release of >2,000 gigatons (Gt) of ^{13}C-depleted carbon into exogenic reservoirs (Zachos et al., 2008). In addition to changes in the global carbon cycle, several other notable changes occurred to Earth's physical and biological systems. For example, floral and faunal communities exhibited significant fluctuations in habitat range and body/leaf size, the modern ancestors of several prominent mammalian lineages first appeared in the stratigraphic record, and Earth's oceans became very acidic resulting in, among other things, a 35–50% extinction in benthic foraminifera (Bowen et al., 2006; Gingerich, 2006). Several smaller but similar $\delta^{13}C$ anomalies, occurring within ~3 myr of the PETM, have been well documented in marine sections (Lourens et al., 2005). Recent terrestrial studies reveal the presence of these subsequent greenhouse intervals, known as the Eocene Thermal Maximum 2 (ETM2) and H2, suggesting that these smaller-scale warming events were global in scale and resulted in continental environmental perturbations as well (Abels et al., 2012). Although the causes and effects of these successive, smaller-scale warming events are less well-understood than the

PETM, constraint of Paleogene carbon cycle dynamics will help advance ongoing and future work regarding the relationship between paleo- and modern greenhouse intervals.

Although numerous studies have documented these hyperthermals, especially in marine sections, significant uncertainty remains about these events, highlighting the need for further research and understanding. For example, the magnitude, source, and timing of carbon release at the onset of the PETM CIE remain poorly constrained. While marine carbonate and foraminifera generally show a negative CIE of 2.5–4.0‰, many terrestrial archives record a negative $\delta^{13}C$ shift >5.0‰ (McInerney and Wing, 2011). In addition to offset in the CIE magnitude, the pattern of $\delta^{13}C$ change during the onset of the CIE also behaves differently in many records, with some archives revealing an abrupt, coherent shift to low values (Magioncalda et al., 2004; Sluijs et al., 2006) while others indicate a step-like onset (Bains et al., 1999; Bowen et al., 2001; Zachos et al., 2005; Zachos et al., 2006). This variation in recorded CIE shifts could be due to a variety of mechanisms including, but not limited to, mixing rates and carbonate dissolution in the oceans and/or productivity and respiration rates in the terrestrial realm (McInerney and Wing, 2011). This offset in both the magnitude and pattern of $\delta^{13}C$ change has important implications for the amount and timing of carbon release at the onset of the PETM. For example, in order to produce a −3‰ CIE, ~2,700 Gt carbon (C) of a −60‰ source (i.e., methane hydrates [Dickens et al., 1997]) or ~9,000 Gt C of a −22‰ source (i.e., oxidized terrestrial biomass [Higgins and Schrag, 2006]) would be required. Poor constraint of carbon cycle change during the onset of the PETM makes it difficult to predict which mechanism is responsible and how rapidly carbon was released during the PETM.

The ETM2 and H2 hyperthermal events, which occur within a few hundred thousand years of one another during the early Cenozoic warming trend, are smaller in magnitude and duration than the PETM (Lourens et al., 2005; Abels et al., 2012). They exhibit similar (but lesser) geochemical and biotic responses to warming and enhanced pCO_2, including a distinct excursion in $\delta^{13}C$. Studies of the timing of these smaller hyperthermal events suggest that they correspond to maxima in orbital parameters, specifically eccentricity, and that they are likely orbitally-paced (Lourens et al., 2005). If orbital forcing triggered carbon release and subsequent warming during ETM2 and H2, it is possible that the cause all of the Paleogene hyperthermals may be linked, indicating a larger and longer time scale control on these short-term events.

In order to assess the potential for Paleogene hyperthermals to serve as an analogue to current and future anthropogenic change, the rates and magnitude of carbon release must be constrained. Significant discrepancies exist between marine and terrestrial archives, as well as within records from similar depositional environments. Carbon isotope records from continental strata spanning the Paleocene-Eocene (P-E) boundary have been studied extensively in outcrop exposures; however, differences remain in the pattern and pace of carbon release interpreted from these records as well. These discrepancies, likely due to weathering, imprecise stratigraphic control, or variance in deposition or erosion, make it difficult to assess the pattern of carbon cycle and environmental change related to CO_2 release. Through the Bighorn Basin Coring Project (BBCP), continental strata spanning these Paleogene greenhouse intervals were drilled for the first time ever. These pristine, unweathered cores provide the opportunity for high-resolution coupled geochemical and sedimentological studies, including stable

isotope analyses, compound specific isotope analyses, pollen and biomarker analyses, and assessment of the hydrological and sedimentological responses during greenhouse intervals. This research will focus on stable isotope analyses of both pedogenic carbonate ($\delta^{13}C$ and $\delta^{18}O$) and bulk soil organic matter ($\delta^{13}C$) and will provide the foundation with which to compare ongoing research by colleagues. The purpose of the research is to (1) develop continuous, high-resolution $\delta^{13}C$ curves spanning the PETM or ETM2 from inorganic pedogenic carbonate and/or bulk organic matter, (2) compare and contrast these cored stratigraphic archives to existing regional and global records, and (3) constrain carbon cycle dynamics during the PETM and ETM2.

GEOLOGIC SETTING

The Bighorn Basin (BHB) in northwestern Wyoming is a Rocky Mountain foreland basin developed during the Laramide orogeny (Fig. 1) (Kraus and Gwinn, 1997). During Laramide compression, the Precambrian-cored Owl Creek, Bighorn, and Beartooth Mountains were uplifted and emplaced, developing the southern, eastern, and northwestern boundaries of the intermontane foreland basin, respectively (WSGS, 2013). A combination of basin subsidence and sediment accumulation governed the fluvially dominated synorogenic deposition in the basin during the early Cenozoic (Clyde, 1997; Kraus and Gwinn, 1997). Volcanism beginning in the middle Eocene developed the Absoraka volcanic complex, the western boundary of the BHB (Kraus and Gwinn, 1997), which postdates the strata discussed in this text. Deposition continued in the BHB during the Oligocene and Miocene, followed by epeirogenic uplift which eroded up to 1500 m of strata, leaving Paleocene and Eocene sediments exposed on the surface (Clyde, 1997).

Strata on the basin margins are characteristic of alluvial fan deposits flowing from the surrounding mountain ranges towards the central basin and feature mainly sandstones and conglomerates of Precambrian igneous and metamorphic detritus and post-Precambrian sedimentary detritus (Neasham and Vondra, 1972). Along the central portion of the basin, a northwest flowing meandering river system characterized by rapid in-channel aggradation and lateral point-bar migration with periodic episodes of overbank deposition and sourced from the surrounding mountain belts served as the primary

mechanism of sedimentation during late Paleocene and early Eocene times in this region of the Bighorn Basin (Neasham and Vondra, 1972; Bown and Kraus, 1987). These central-basin fluvial deposits of the Fort Union (late Paleocene) and Willwood (early Eocene) Formations consist of mudrocks with moderate to strong pedogenic overprinting and heterolithic deposits with weakly developed paleosols and sandstones (Kraus and Gwinn, 1997). Well-developed paleosols indicate slow and episodic accumulation on the floodplain, likely from overbank flooding of the main channel and in-situ modification of existing bedrock (Neasham and Vondra, 1972). Weakly developed heterolithic deposits indicate rapid sedimentation on the floodplain, likely due to temporary, episodic abandonment of the main trunk channel (Kraus and Riggins, 2007). The thick, laterally continuous channel and sheet sandstones represent deposits of the main channel of the meandering river system (Kraus and Riggins, 2007). Studies of floodplain deposition and modern river avulsions in the Saskatchewan River in Canada support these interpretations (Kraus and Wells, 1999).

The Bighorn Basin preserves the thickest and most expanded stratigraphic sections spanning the Paleocene-Eocene boundary in the world (Gingerich and Clyde, 2001), making it well-suited for research of early Cenozoic climatic and ecologic change. Although floodplain environments are characterized by episodic river flooding and deposition as well as erosional periods, strata in the Bighorn Basin are relatively stratigraphically and temporally continuous (Gingerich and Clyde, 2001) and feature high sedimentation rates relative to the extensively studied marine sections, which have lower sedimentation rates and may be subject to significant time averaging from dissolution or bioturbation (Sluijs et al., 2012). Substantial outcrop work has been conducted over the

last two decades focusing on the litho-, magneto-, chemo-, and biostratigraphic distribution of features across the Fort Union and Willwood Formations and these existing studies provide the ideal foundation for this study.

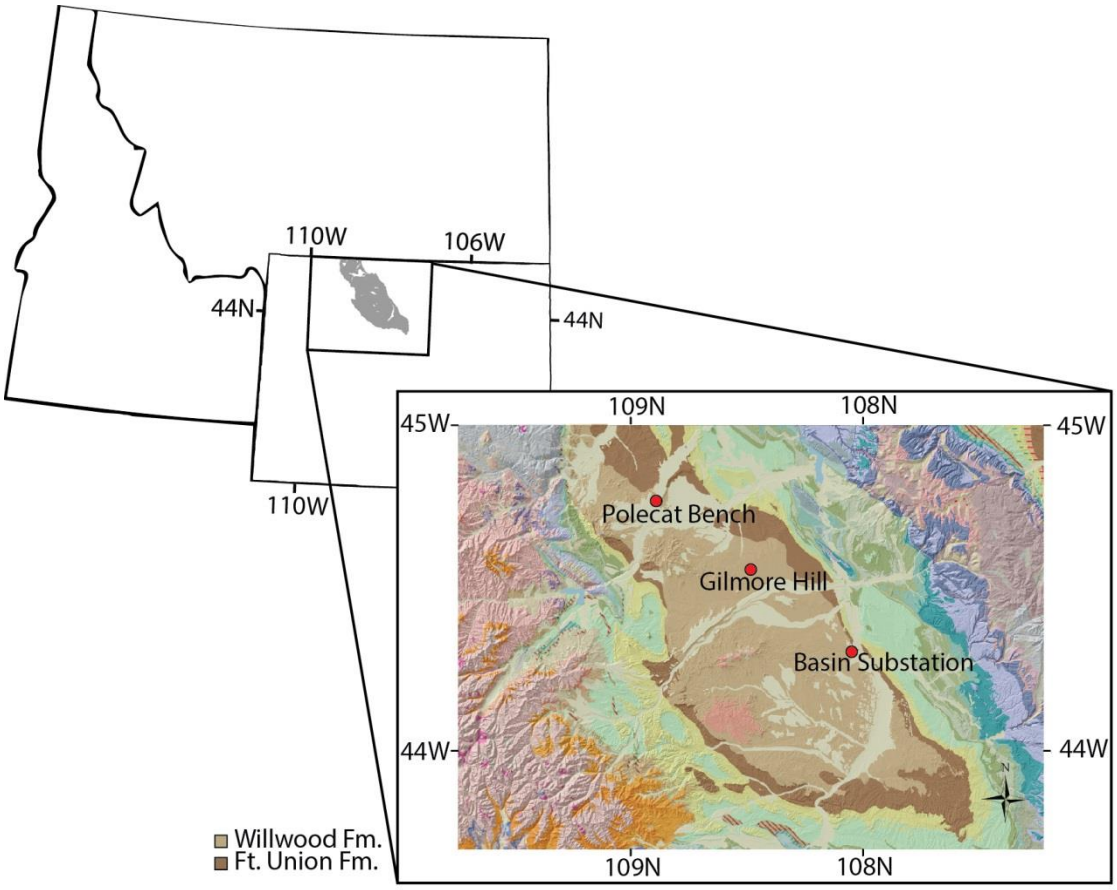

Fig. 1. Map of study area. Location of the Bighorn Basin in northern Wyoming (gray field and inset) and the drilling sites for the Bighorn Basin Coring Project (Polecat Bench, Gilmore Hill, and Basin Substation; red circles) are shown. The targeted formations were the Paleocene Ft. Union Formation (dark brown) and the Eocene Willwood Formation (tan).

BIGHORN BASIN CORING PROJECT DESCRIPTION

Between July 13, 2011 and August 5, 2011, the BBCP collected 921 m of sediment core from three drilling locations in the Bighorn Basin (BHB), northern Wyoming (Clyde et al., 2012; Clyde et al., 2013) (Fig. 1). Two holes were drilled at each site to ensure maximum recovery. These drilled terrestrial strata spanning the P-E boundary offer the opportunity for high-resolution studies of unweathered, thick, stratigraphically continuous climate archives. The overall goal of the BBCP is to better understand the causes of these early Paleogene hyperthermals and how the continental biogeochemical and ecological environments were impacted both during and after the warming events.

The first drilling site, Basin Substation (BSN-1A and BSN-1B; 44.416N, 108.105W) is approximately 6.6 km (4 miles) northwest of Basin, WY and 277 m of core was collected (~138.5 m per hole) with >98.6% core recovery (Clyde et al., 2013). This site is located in the southeastern region of the BHB in an alluvial backswamp paleodepositional environment, with detrital fluvial input sourced from the southeast direction (Neasham and Vondra, 1972). Strata here are characterized by organic-rich (relative to other sites), drab sandstones and mudstones with carbonaceous shales (Wing and Harrington, 2001). The second drilling location, Polecat Bench (PCB-2A and PCB-2B; 44.768N, 108.887W) is approximately 10.4 km (6.5 miles) west-northwest of Powell, WY and collected 375.1 m of core (130 m for PCB-2A and 245.1 m for PCB-2B) with

>99% core recovery. This drilling location is in the northwestern region of the basin and is characterized by strata deposited in a well-drained distal (from the main trunk channel) floodplain, with the main meandering fluvial system sourced from the southeast and flowing in the northwest direction (Neasham and Vondra, 1972; Clyde, 1997). These first two sites were targeted for their known coverage of the PETM. The final site, Gilmore Hill (GMH-3A and GMH-3B; 44.515N, 108.645W) is 47 km (29 miles) west of Greybull, WY. It was targeted for its expected coverage of ETM2 and 269.1 m of core (202.4 m for GMH-3A and 66.7 m for GMH-3B) was collected with ~98.6% core recovery. This site is located in the central McCullough Peaks region and is also characterized by well-drained distal floodplain deposition with the meandering river system flowing to the northwest. Cores were labeled, described, digitally documented, drained of excess fluids, and then shipped to the Integrated Ocean Drilling Program (IODP) Bremen Core Repository (BCR) at MARUM-University of Bremen (Bremen, Germany).

At the BCR, the BBCP Science Team met to split, describe, scan, sample, and archive these cores (Clyde et al., 2013). The archive halves were line scanned for high-resolution color imagery, visually described, and then packaged for storage. Working halves of the cores were color scanned, sampled, and then stored as well. To account for offsets in depth obtained either during drilling or due to core expansion, a composite depth scale (meters composite depth, MCD) was developed by collaborators after methods described in Clyde et al. (2013) (data tables can be found online at http://www.pangaea.de/). Briefly, the color reflectance data collected between 400–700 μm (visible spectrum) provided the color space a* (red over green ratio), which was used

with the high-resolution core images to correlate the two cores and develop offsets between key lithologic intervals. These offsets were used to align the A and B cores to the composite MCD scale, as well as to correlate laterally continuous stratigraphic units to adjacent outcrop studies, if available (data tables can be found online at http://www.pangaea.de/).

CARBON ISOTOPE STRATIGRAPHY AND CARBON CYCLE CHANGE ACROSS THE PALEOCENE-EOCENE BOUNDARY: EVIDENCE FROM PEDOGENIC CARBONATE AT POLECAT BENCH, BIGHORN BASIN, WY, USA

Abstract

Abrupt climate warming and carbon cycle perturbation during the Paleocene-Eocene thermal maximum (PETM, ca. 55.5 Ma) (Westerhold et al., 2012) was similar in magnitude to projected future changes associated with anthropogenic carbon emissions (IPCC, 2007). Interpretation of the event as an analogue for anthropogenic global change, however, is complicated by uncertainty about the rate, pattern, and sources of PETM carbon release (McInerney and Wing, 2011). We present carbon isotope data from terrestrial deposits spanning the PETM in the Bighorn Basin (WY, USA) that show that the beginning of the PETM is characterized by two, not one, massive releases of carbon within 4 thousand years. During each release, carbon entered the surface ocean and/or atmosphere at rates similar to modern fossil fuel emission rates. The new record shows volatile behavior in Earth's carbon cycle and indicates that the PETM is a strong analogue to current and future carbon cycle perturbation in both magnitude and rate of change.

Background

Superimposed on an existing early Cenozoic warming trend, the PETM represents an abrupt and transient hyperthermal event and the hottest time in global history in the last 65 Ma (Zachos et al., 2001). A massive release of ^{12}C-enriched carbon into the ocean, atmosphere and biosphere in <20 kyr is expressed as a greater than 3‰ negative carbon isotope excursion with an accompanying 5–9 °C of warming (Zachos et al., 2005; Bowen and Zachos, 2010; McInerney and Wing, 2011). Although the temporal relationship between carbon release and warming is poorly understood, a minimum of 1,500 gigatons (Gt) of isotopically light carbon (assuming a −60‰ source) must have been released and incorporated into exogenic reservoirs in order to achieve a 3‰ CIE (Zeebe et al., 2009; Bowen and Zachos, 2010). Due to differences in mixing rates between carbon reservoirs and discrepancies between records, the exact timing, magnitude, and source of carbon release is poorly constrained. Studies of the pattern and pace of carbon release and subsequent ecological and environmental responses during the PETM can provide important insight into the expected feedbacks and reactions to modern day warming.

The exact source of the carbon released during the PETM is still debated, though some possible mechanisms include thermal dissociation of deep marine methane hydrates, widespread burning or oxidation of terrestrial organic matter, and/or igneous intrusion into organic rich-strata (Dickens et al., 1995; Dickens et al., 1997; Svensen et al., 2004; Higgins and Schrag, 2006; Moore and Kurtz, 2008; McInerney and Wing, 2011; DeConto et al., 2012). Methane clathrates or hydrates are methane molecules bound by ice that are stable in deep-sea sediments at low temperatures and high pressures. Increasing deep ocean temperatures from changing ocean circulation or

pressure loss from slope failure can both cause this isotopically light ($\delta^{13}C$ = −60‰) source of carbon to destabilize (Dickens et al., 1995). Enhanced wildfire burning of Paleocene peat and/or coal, with a $\delta^{13}C$ signature of −22‰, could in part explain the observed negative shift in carbon isotope values. Although several mechanisms may have caused extensive burning, sediment cores lack evidence for an increase in combustion byproducts (Moore and Kurtz, 2008). Desiccation of a large epicontinental seaway ($\delta^{13}C$ = −22 to −25‰ [Higgins and Schrag, 2006]) or thawing of permafrost ($\delta^{13}C$ = −30‰ [DeConto et al., 2012]) could also be potential causes of early carbon release; however, the rapid timing and large magnitude of carbon injection that would be required by these mechanisms to achieve a −3‰ CIE in <20 kyr makes them less likely candidates. Finally, intrusion of magma into organic-rich sediments, such as the North Atlantic seafloor, could result in the rapid release of thermogenic methane with a $\delta^{13}C$ of −30‰ (Svensen et al., 2004). Although it is unknown whether one or multiple sources contributed to the observed >3‰ negative CIE, these reservoirs represent several proposed sources of PETM carbon release.

In addition to the very clear shift in $\delta^{13}C$ observed at the P-E boundary, both marine and terrestrial floral and faunal communities experienced significant changes as well. The abrupt decline in marine carbonate preservation and increase in clay-dominated sedimentation marks one of the early indicators of major environmental change during the PETM, reflecting enhanced ocean acidification and carbonate dissolution resulting from increased input of CO_2 into the oceans (Zachos et al., 2005). This brief absence of carbonate in marine records represents the largest benthic foraminifera extinction to occur in the last 90 myr (Kennett and Stott, 1991) and reveals just one of the often

complicating factors associated with studying marine PETM records. In the terrestrial realm, the first appearance of modern artiodactyls, perissodactyls, and primates in North America at the P-E boundary signifies one of the largest mammalian turnover events in the Cenozoic (Gingerich, 2006). Additionally, fossils collected in Eocene deposits in the BHB reveal dwarfing of Wa-0 fauna, generally limited to the PETM time period (Clyde and Gingerich, 1998). Ecologic change during the PETM was not limited to just faunal communities, as Wing et al. (2005) revealed. Not only did North American flora experience significant and rapid shifts in habitat range, but warming and decreases in water availability at the onset of the PETM resulted in changes in leaf size and shape (Wing et al., 2005). If the PETM represents our best (in terms of timing and magnitude) and most recent analogue to modern day anthropogenically enhanced greenhouse warming, then these observed paleoecologic changes may be highly representative of the responses we can expect in the future.

Significant discrepancies exist between the $\delta^{13}C$ record in marine and terrestrial archives, as well as within records from similar depositional environments. Due to lower sedimentation rates and a high possibility for carbonate dissolution or mixing of sediment via bioturbation in marine strata (Sluijs et al., 2012), we can look to terrestrial records to measure and model PETM carbon cycle changes. The influx of ^{13}C-depleted carbon into the atmosphere would shift the overall isotopic composition of atmospheric CO_2 on a global scale, resulting in uptake of this CO_2 via the terrestrial biosphere and preservation of this widespread shift in continental sections. One particularly useful proxy that can be used to document and constrain these global carbon cycle changes is paleosol carbonate (Cerling et al., 1989). Pedogenic carbonate forms in moderate to well-drained soils with

seasonal climates and mean annual precipitation of <760 mm (Royer, 1999). As carbonate precipitates, it records the stable oxygen and carbon isotopic composition of the soil CO_2 in which it forms. Atmospheric and respired CO_2 serve as the two primary contributions to soil gas; however, below ~30 cm depth in the soil, the contribution of atmospheric CO_2 is negligible, meaning that plant respiration is the dominant control on the $\delta^{13}C$ of soil CO_2. Plants fix carbon from atmospheric CO_2 during the isotope-fractionating process of photosynthesis. Although C_3 and C_4 plants have different photosynthetic pathways which would result in an offset in the isotope compositions of their respired CO_2, there is no evidence of C_4 plants during the Paleocene or Eocene (Jacobs et al., 1999). With an offset of ~19‰ between atmospheric $\delta^{13}CO_2$ and C_3 plants, the $\delta^{13}C$ of soil CO_2 governed by plant respiration should track changes in $\delta^{13}C_{atm}$. Data from modern soils and other PETM records show that soil carbonate can record changes in the isotopic composition of atmospheric CO_2 (Cerling, 1984; Bowen et al., 2001; Koch et al., 2003).

Carbon isotope records from continental strata spanning the P-E boundary have been studied extensively in outcrop exposures; however, discrepancies remain in the pattern and pace of $\delta^{13}C$ change in these records. These inconsistencies, likely due to weathering and imprecise stratigraphic control, make it difficult to assess the pattern of carbon cycle and environmental change related to PETM CO_2 release. Here I present a new high-resolution isotope analysis of paleosol carbonate from *drilled* strata at Polecat Bench (Bighorn Basin, WY, USA). These pristine, stratigraphically continuous continental sections spanning the P-E boundary provide the ideal framework for a complete evaluation of terrestrial PETM environmental and carbon cycle change.

Methods

Two hundred ninety pedogenic carbonate nodules were collected from Polecat Bench cores (Bighorn Basin, WY, USA) (Fig. 1) at approximately two hundred fifty-five stratigraphic intervals. Polecat Bench (PCB) is a flat-topped Pleistocene stream terrace that is actively eroding along its margins, exposing well-studied surface sections of late Paleocene-early Eocene fluvial strata (Fort Union and Willwood Formations) (Gingerich, 2001). Pedogenic carbonate nodules were identified in cores as discrete, small (~2 mm to >5 cm in diameter), well-cemented, rounded to subrounded accumulations of micritic carbonate, some of which contain observable secondary, diagenetic spar. Carbonates occurring within strata lacking features associated with pedogenesis (disturbance of original depositional layering, mottling, root traces, burrows), such as laminated sandstones, were not sampled due to their potential exogenous origins.

Pedogenic carbonate sampled for paleo-environmental isotopic reconstruction is commonly sampled from more than 20 to 30 cm below the paleosol surface, where the isotopic composition of soil carbonate is relatively constant (Cerling et al., 1989). Due to the aggradational, welded character of the paleosols present in the PCB cores, we were not able to unambiguously discern the depth of carbonate formation for most samples and did not screen our samples based on depth of formation. Previous work on outcrop samples from Polecat Bench, however, has demonstrated that no relationship exists between the thickness of preserved paleosol horizons and pedogenic carbon isotope values (Bowen et al., 2001), suggesting that most nodules in these strata formed at sufficient depths to record stable soil CO_2 isotope ratios. Our $\delta^{13}C$ record shows strong, coherent stratigraphic patterns throughout the record, including intervals with contrasting

and variable paleosol type and horizon thickness, and shows no apparent relationship between the soil profile thickness and measured isotope ratios (Fig. 2). Based on these considerations we assert that our isotopic records are likely representative of soil CO_2 isotope ratios at depth in the ancient soils and are unlikely to be affected by variable mixing between atmospheric and respired CO_2 in shallow paleosoil horizons.

The exterior surface of each nodule sample was physically cleaned using deionized water and samples larger than ~1 cm diameter were slabbed to expose a clean flat surface. For smaller samples, the exterior surface of the nodule was etched away using a dental drill. Primary micrite and secondary diagenetic spar were collected with a dental drill under a binocular microscope. Aliquots of approximately 100 μg were weighed into 10 mL Exitainer vials (for analyses conducted at the University of Utah, 4 mL at Purdue University). The vials were flushed with helium to remove atmospheric carbon dioxide from the headspace, placed on a heating block held at 75 °C, and orthophosphoric acid was manually injected into each vial. The samples were reacted for a minimum of one hour and analyzed using a ThermoFinnigan Gas Bench II coupled to a Delta Plus Isotope Ratio Mass Spectrometer (IRMS) at the University of Utah's SIRFER lab or a ThermoFinnigan Delta V Isotope Ratio Mass Spectrometer at Purdue University's Stable Isotope lab. Analyses of reference carbonates (Carrara Marble, NBS-19 and LSVEC) were used to correct the measured values for peak area and through-run drift and to calibrate the values to the Vienna PeeDee Belemnite (VPDB) scale. Analytical precision was approximately 0.1‰, for both $\delta^{13}C$ and $\delta^{18}O$, at both labs based on replicate analyses of reference carbonates throughout the course of the analyses.

Repeatability of the pedogenic carbonate analyses averaged 0.20‰ for $\delta^{13}C$ and 0.24‰ for $\delta^{18}O$ (1 standard deviation) based on replicate analyses of 94 samples.

Pedogenic carbonate nodules that are exposed to meteoric waters may undergo diagenetic alteration and form secondary sparry calcite (Fig. 3A). The isotopic composition of microsampled sparry calcite from the PCB core samples is similar to that previously documented from outcropping Polecat Bench sediments (Bowen et al., 2001) and in most cases features $\delta^{18}O$ values that are lower than those of co-occurring micritic carbonate and $\delta^{13}C$ values that are variably offset from those of micrites (Fig. 3B). We applied a quantitative, systematic screening approach in order to eliminate values from our dataset that were not likely representative of changes in paleosoil CO_2 $\delta^{13}C$ values through time, either due to diagenetic alteration or formation of nodule micrite under anomalous soil conditions. Individual nodules were excluded from our composite record if their carbon or oxygen isotope value fell outside of the range defined by the mean ± 4 standard deviations of the surrounding 6 samples (3 stratigraphically above and 3 below). Using this approach, 17 of the 299 nodules (6%) were removed from the dataset (Table 1; Fig. 4). These samples were stratigraphically distributed throughout the cores, and their exclusion does not have a substantial influence on the character of $\delta^{13}C$ change represented through the PETM record.

Results and Discussion

Polecat Bench Core Chemo- and Lithostratigraphy

Isotopic records from pedogenic carbonate in the two PCB cores show excellent agreement with one another (Table 1; Fig. 4). The most prominent feature of the

composite $\delta^{13}C$ record is an abrupt CIE of >5‰ occurring between 118 and ~55 meters composite depth (MCD). This large negative excursion to −14‰ is sustained for approximately 43 m, and values gradually increase back to background levels between 75 and 55 MCD. Following the recovery interval, from ~55 MCD to the top of the section, the remainder of the PCB core record exhibits relatively stable values (average −8.7‰). The PCB core record also provides long-term context for $\delta^{13}C$ trends through the interval immediately preceding the PETM, revealing that $\delta^{13}C$ values were relatively stable throughout most of the latest Paleocene (average −8.0‰) but became more variable and shifted ~1.5‰ lower during the 15 m immediately preceding the CIE onset.

There are apparent trends in the composite $\delta^{18}O$ record, especially when the 5-point running average is displayed; however, the magnitude of these trends is similar to the range of variability in the data. The average $\delta^{18}O$ value across the full composite section is −8.2‰, with a total range of 3.9‰. Measurements were subdivided into PETM and non-PETM values based on their $\delta^{13}C$ values (PETM is between 55.6 and 122.6 MCD, average $\delta^{13}C$ = −12.8‰; non-PETM is above 55.6 and below 122.6 MCD, average $\delta^{13}C$ = −8.6‰). Average non-PETM $\delta^{18}O$ values are −8.3‰ (n = 129), and average PETM values are −8.0‰ (n = 144), and results from a two-sample Student's t-test reveal that these averages are significantly different at a 95% confidence level ($p < 0.0001$).

The clear shifts in $\delta^{18}O$ values in the PETM CIE interval, which stratigraphically match the trends in the $\delta^{13}C$ record, indicate the likelihood for coupled carbon cycle and hydrological cycle changes. The trend towards higher $\delta^{18}O$ values, indicating soil waters that are more enriched in ^{18}O, could be indicative of local warming, an increase in evaporation, or a change in global climatic patterns (Bowen et al., 2001; Koch et al.,

2003). Based on modern relationships between the $\delta^{18}O$ of precipitation and temperature (Rozanski et al., 1993) and the $\delta^{18}O$ of calcite and temperature (Bottinga and Craig, 1968), our $\delta^{18}O$ record indicates that if there were no changes to the hydrological cycle, then temperatures warmed by approximately 2 °C during the PETM. Numerous marine and terrestrial records form various proxies support the idea of increased temperatures globally; however, recent studies are inconsistent in terms of changes to the hydrological cycle (McInerney and Wing, 2011), with some studies suggesting more humid conditions at the start of the PETM (Bowen et al., 2004) while others suggest a more arid environment (Kraus et al., 2013). Although it is challenging to constrain changes in global atmospheric circulation patterns during the PETM, regional studies, especially in the North American midlatitudes, largely point towards a shift to more arid conditions, with the possibility of an increase in more seasonally intense storms (Kraus et al., 2013; McInerney and Wing, 2011). Thus, the observed shift in $\delta^{18}O$ from pre-PETM to PETM values is likely a combination of both increased temperature and aridity.

High-resolution data within and prior to the onset also reveal previously unrecognized structure in the $\delta^{13}C$ record (Fig. 4). The data suggest that the beginning of the PETM at PCB is marked by at least two discrete, negative carbon isotope events. The first of these, occurring stratigraphically lower and temporally first, has been labeled the pre-onset excursion (POE). It is characterized by a ~3‰ shift occurring abruptly between 123.6 and 122.6 MCD and decaying gradually to background $\delta^{13}C$ values over the following 1.5 m. The second shift occurs stratigraphically above the POE between two adjacent samples collected at 119.26 and 118.19 MCD and involves a 5.7‰ decrease to full PETM minimum CIE values, marking the onset of the CIE. These stratigraphically

distinct shifts are closely matched by the $\delta^{18}O$ record, indicating a coupled shift in the hydrological and carbon cycles. Whereas the abrupt decline in $\delta^{13}C$ values at the onset of the CIE has been well documented in previous studies, this pre-PETM excursion and recovery captured in the PCB record represents previously unrecognized variability in the time leading up to the event.

The systematic screening approach (described above) used to exclude outliers in the dataset removed several values that lied in the interval of variability immediately preceding the CIE, including two samples with $\delta^{13}C$ values less than −12‰ (126.1 and 127.8 MCD) (Fig. 4). Unlike the POE samples, these are individual nodules whose low $\delta^{13}C$ values are not replicated by data from stratigraphically adjacent samples, and as a result they are rejected based on the screening criteria outlined above. However, if these data are in fact representative of paleosoil $\delta^{13}C$ values, it is possible that they may reflect additional, very short-term perturbations of the carbon cycle preceding the POE.

In order to ensure that $\delta^{13}C$ variability we observed in the pre-PETM section of our record, particularly during the $\delta^{13}C$ recovery between the POE and CIE, is not a result of detrital deposition of eroded, older nodules, we examined paired thin sections from five representative nodules and their host matrices occurring through this interval. Two of these pairs, chosen from intervals of highly variable $\delta^{13}C$, are highlighted in Fig. 5. In all five representative samples, the host lithologies are primarily very fine sandstones to coarse siltstones supported by microcrystalline clay cement. These host matricies contain predominantly angular to rounded grains between ~25–100 μm in size of the subarkose variety (Neasham and Vondra, 1972) and minimal organic matter fragments. The carbonate nodules, ranging from ~2 mm to >5 cm in diameter, contain occluded lithics of

similar grain size to the host lithology, supported by micritic calcite cement. In some cases, veins of secondary sparry calcite ranging from a few tens of microns to several hundreds of microns in diameter are evident (Fig. 3A). Some carbonate nodules also contain occluded organic matter. In all cases we observed similar compositions, shapes, and size distributions for sand and silt-sized grains within the host matrix and those occluded within the carbonate nodules (Fig. 5). This result is consistent with the growth of these nodules in situ within the host matrix, as also suggested by macroscopic observations made during sampling (e.g., distribution of nodules throughout pedoturbated units and lack of association with primary depositional features or units preserving primary fabric, nodules much larger than associated siliciclastic grains).

Core to Outcrop Correlations

The individual and composite PCB records are highly concordant with previously published data from nearby PCB outcrops (Fig. 6) (Bowen et al., 2001). The PCB records show the close association of the CIE onset with a major episode of mammalian faunal turnover (Bowen et al., 2001) and the abrupt recovery of $\delta^{13}C$ values (75–55 MCD), which has been associated with an organic carbon burial feedback at the termination of the event (Bowen and Zachos, 2010). These two features have been well documented at numerous locations both within the Bighorn Basin, as well as from across the globe. BHB outcrop-based evidence did not provide substantial long-term context for $\delta^{13}C$ trends prior to the PETM. The new record, however, reveals that $\delta^{13}C$ values were relatively stable throughout most of the latest Paleocene and became more variable and shifted ~1‰ lower during the 15 m (~37.5 kyr based on long-term accumulation rates of 0.4

m/kyr [Clyde et al., 2007]) immediately preceding the CIE onset (Fig. 6). This pattern of changes in the PCB record suggest that local or global carbon cycling may have been destabilized leading up to the PETM, and the association between this change and pre-PETM climate warming (Secord et al., 2010; Sluijs et al., 2007) deserves additional attention.

The $\delta^{18}O$ record from outcrop collected pedogenic carbonate reveals an overall increase in values during the PETM interval from ~ −9.1‰ to ~ −8.5‰, with initial shifts associated with the onset of the CIE as high as 1–1.5‰ (Fig. 6) (Bowen et al., 2001). The core $\delta^{18}O$ record shows a similar magnitude increase in pre-PETM to PETM values of ~0.5‰, from approximately −8.3‰ to −7.8‰. While the outcrop records lack substantial long-term context for Paleogene climate leading up to the PETM, core $\delta^{18}O$ records indicate general stability, with most intervals of variability stratigraphically aligned with shifts in the $\delta^{13}C$ record.

A closer look at the relationship between outcrop and core carbon isotope records within the PETM interval reveals generally strong agreement in the magnitude of $\delta^{13}C$ change with slight offsets in the pattern and stratigraphic position (Fig. 7). The onset of the PETM in the core record is characterized by two distinct negative shifts, separated by a full recovery of values, whereas in the outcrop $\delta^{13}C$ record the onset of the PETM is marked by one negative shift, with an intermediate "pause" in values (119.4–120.8 MCD). This observed difference in the pattern of the CIE onset is likely a result of the sampling resolution between core and outcrop. The outcrop record samples 8 levels over approximately 10 m of strata spanning the onset interval, while the same 10 m of strata in core contains 42 sampled intervals. Additionally, the minimum CIE values in the outcrop

record are achieved approximately 3.5–4.5 m above the start of the CIE in the core. This discrepancy may be due to several factors, including differences in sedimentation between the two sites, poor correlation between the outcrop and core strata in this interval, or the possibility of inaccurate measurements made in during outcrop analysis. Aside from these two differences in the pattern of $\delta^{13}C$ change between outcrop and core, the PETM interval in both sections is largely similar, revealing a relatively abrupt ~5‰ negative excursion that is sustained for roughly 40 m.

Global Spatial and Temporal Trends

Previous studies, including outcrop work at PCB and marine records, have shown a step-like onset of the PETM CIE, providing some suggestion that carbon release during the event may have occurred in multiple pulses (Bains et al., 1999; Bowen et al., 2001; Zachos et al., 2005; Sluijs et al., 2007). Our data support this interpretation and suggest a pattern of at least two abrupt pulses separated by a brief cessation of release and $\delta^{13}C$ recovery. A petrographic screening of nodules through this section of variability leading up to the onset supports the in situ formation of nodules in this interval (Fig. 5) and suggests that the observed pattern of change likely reflects temporal changes in the $\delta^{13}C$ values of paleosoil CO_2. Because these changes were of relatively large magnitude and are recorded consistently across several distinct lithological and pedological units, we suggest that they derive primarily from temporal changes in the $\delta^{13}C$ values of global, atmospheric CO_2.

In order to further constrain likely scenarios of carbon release that support the newly identified structure in the carbon isotope record, a basic carbon cycle mass balance model was used (Eq. 1) based on the work of Bowen (2013):

$$\Delta\delta^{13}C = \frac{\delta^{13}C_a M_a + \delta^{13}C_i M_i}{M_a + M_i} - \delta^{13}C_i \quad (1)$$

In this equation, the mass (M_a) and isotopic composition ($\delta^{13}C_a$) of carbon released into the exchangeable carbon reservoir as well as the mass (M_i) and isotopic composition ($\delta^{13}C_i$) of the total carbon reservoir prior to the event dictate the amplitude of the CIE ($\Delta\delta^{13}C$). Although studies have sought to constrain these reservoir characteristics during Paleogene times, the exact size of the exogenic carbon pool (M_i) prior to the PETM remains poorly understood. The total exogenic carbon pool is comprised of the atmosphere, biosphere and soils, surface ocean, and deep ocean. Using the parameters for carbon reservoir masses and isotopic signatures described in Bowen (2013) (Fig. 8) and the size of the POE and CIE in our record, as well as a mass weighted average of CIE magnitudes from many records as a representation of the global isotopic response to the PETM, sensitivity tests can be conducted to determine what carbon sources and amounts may cause the observed CIE.

One proposed mechanism which may have initiated PETM warming and carbon release is oceanic methane hydrates ($\delta^{13}C = -60‰$) released via sea floor slumping (Dickens et al., 1995; Katz et al., 1999). Catastrophic slope failure has the ability to release large amounts of carbon at very high rates. Other potential mechanisms of carbon release to initiate the PETM include thermogenic methane release from volcanically

driven igneous intrusion into organic-rich sediments (Svensen et al., 2004; Rampino, 2013), oxidation of organic matter through seaway desiccation (Higgins and Schrag, 2006), or thawing permafrost (DeConto et al., 2012). Carbon stored in Cretaceous and Paleogene mudstones in the North Atlantic Volcanic Province (up to 15,000 Gt of C as methane with a $\delta^{13}C$ of −35 to −50‰) and igneous melt emplacement rates (tens to thousands of years) suggest that thermogenic methane release represents a likely candidate for initiation of the PETM in both timing and magnitude (Rampino, 2013; Svensen et al., 2004). Seaway oxidation ($\delta^{13}C$ = −30‰) and thawing permafrost ($\delta^{13}C$ = −22‰) would take a minimum of 10 kyr to release a large enough mass of carbon (~5,000 Gt of C) to produce a −2.5 to −3‰ excursion (Higgins and Schrag, 2006). Using these previously hypothesized carbon sources, we can determine the range of possible carbon amounts that would be required to cause the measured CIEs and with constraints on timing, the rate of carbon release can then be calculated.

Initiation of the POE and CIE occurred geologically instantaneously in our record, as suggested by the abrupt shifts to lower $\delta^{13}C$ values over relatively short intervals (~1 m each) of stratigraphically adjacent lithologies. Maibauer et al. (in review) developed an age model specifically for drilled strata at Polecat Bench in order to constrain the timing of carbon release at the onset of the PETM. Several renditions of the age model were developed, based on a range of assumptions about sedimentation rates (dependent on the lithologic thickness, type and paleosol maturity) and constrained by two end member estimations for the duration of the CIE body (either 90 kyr [Röhl et al., 2007] or 135 kyr [Murphy et al., 2010]). The negative $\delta^{13}C$ shifts that characterize the POE and CIE onsets each occur between distinct lithological units with no intermediate $\delta^{13}C$ values and no

associated major sandstone units or erosional surfaces. Because of the discontinuous nature of pedogenesis, the amount of time represented by the isotopic shifts could not be constrained at a resolution beyond that of the lithological units, thus a range of age models and assumptions about the timing of nodule formation was used to evaluate possible interpretations of the record. The age model of Maibauer et al. (in review) suggests that the onset of the POE and CIE each lasted no more than ~1 kyr, with the recovery back to higher values, which separates the POE from the CIE lasting no longer than ~2 kyrs. Maibauer et al. (in review) also point out that this ~1 kyr duration for carbon release at the start of the POE and CIE is a conservative estimate, with simulations of initially large pulses in the first 100–200 years, followed by declining rates of release for the remaining ~1 kyr representing their best fit scenario.

Due to the short-lived nature of the POE, we predict that a large injection of ^{13}C-depleted carbon likely did not propagate fully into the deep ocean. Over these time scales, a carbon isotope perturbation affecting the atmosphere would propagate into the surface ocean and biosphere but not necessarily the deep ocean, and we therefore developed an alternate model scenario to represent this (Fig. 8). Removing the deep ocean component of the total exogenic carbon pool results in a much smaller total pool of 10,000 Gt of C (Table 2). In order to recreate the POE of −3‰ that we measure in our cored terrestrial record, between ~600 and 2,500 Gt of C would be required for a −60‰ to −22‰ source, respectively (Table 3).

Initiation of the CIE was also geologically instantaneous in our record and the internal age model developed by Maibauer et al. (in review) suggests that this event was also initiated in ~1 kyr or less. Sustained low values following the onset of the CIE

suggests a continued carbon cycle perturbation for tens of thousands of years after the initial carbon injection. Over these time scales, the deep ocean would be affected by a large isotopically distinct carbon pulse and thus is included in the total size of the exogenic carbon pool in our mass balance calculations (Fig. 8; Table 2). The $\delta^{13}C$ record from cored PCB pedogenic carbonate reveals a PETM CIE of −5.7‰, double that of the marine carbonate record, which on average records between a −2.5‰ and −3‰ CIE (McInerney and Wing, 2011). This large discrepancy in the magnitude of the CIE in marine versus terrestrial carbonate may be due to the larger impact that a pulse of isotopically light carbon would have on $\delta^{13}C_{atm}$ versus the $\delta^{13}C$ of oceans, however these reservoirs equilibrate on the order of ~1 kyr and thus should record similar magnitude CIEs over larger timescales (Bains et al., 2003). Another possibility for this observed disparity could be from increased soil respiration on land, leading to a decrease in the $\delta^{13}C$ of soil CO_2 (Cerling, 1999; Bains et al., 2003). Regardless of the cause of this discrepancy, a larger amount of isotopically light carbon would be necessary to facilitate the larger magnitude CIE measured in our terrestrial record versus the marine records. Specifically, between ~2,400 and 8,500 Gt (for a −60‰ and a −22‰ source, respectively) would be required to reproduce a −2.5 to −3 ‰ CIE in the marine realm compared to between ~5,900 and ~18,700 Gt (for a −60‰ and a −22‰ source, respectively) that would be required to reproduce a CIE of −5.7‰ (Table 4). The existing marine and our new terrestrial records of $\delta^{13}C$ change most likely represent the end member cases for the amount of carbon required to initiate the PETM. The most likely scenario is probably somewhere in the middle and these estimations fall within the rage of results from a compilation of recent studies (McInerney and Wing, 2011).

In order to constrain some of the uncertainties in the rates of carbon release at the onset of the PETM, we applied the internal age estimates developed by Maibauer et al. (in review) to the calculated carbon amounts required to recreate the $\delta^{13}C$ behavior in our record described above. We estimate that initial carbon release of ~0.6–2.5 Gt C/yr occurred for a duration of ~1 kyr or less during the POE, followed by a brief (~1–2 kyr) cessation of carbon release where this newly added carbon is mixed into the exogenic carbon pool and continued by another rapid injection of isotopically light carbon of between 2.5 to 18.7 Gt C/yr for a total duration of 1 kyr. The continuation of low $\delta^{13}C$ values, rather than the recovery of values seen following the POE, indicates that this transition into the PETM involved a more prolonged perturbation of the carbon cycle. These sustained low values can be simulated either via continued, low rates of isotopically light carbon release over the duration of the PETM CIE body (Zeebe, 2013) or via carbon cycle feedbacks involving enhanced respiration of organic carbon in soils and sediments (Bowen, 2013).

The newly determined rates of carbon release were then used to reassess the most likely sources of carbon that would be required to initiate the PETM. With a carbon isotope signature of −60‰, ~ 2,500 Gt of C could have been released in ~1 kyr or less if catastrophic slope failure resulted in the rapid destabilization of deep sea methane clathrates (Dickens et al., 1995). Additionally, carbon stored in Cretaceous and Paleogene mudstones in the North Atlantic Volcanic Province (up to 15,000 Gt of C as methane with a $\delta^{13}C$ of −35 to −50‰) and igneous melt emplacement rates (tens to thousands of years) suggest that thermogenic methane release represents a likely candidate for initiation of the PETM in both timing and magnitude (Svensen et al., 2004; Rampino,

2013). Seaway oxidation and thawing permafrost would take a minimum of 10 kyr to release a large enough mass of carbon (~5,000 Gt of C with a $\delta^{13}C$ of −22‰) to produce a −2.5 to −3‰ excursion (Higgins and Schrag, 2006), and they would not likely be able to release carbon in two distinct pulses. Thus, these two latter suggestions likely represent subsequent responses to carbon release and warming, rather than the cause of it (Bowen, 2013). Catastrophic sea floor slumping and/or rapid emplacement of igneous bodies, however, do have the ability to release massive amounts of carbon very rapidly (1 kyr) and in multiple pulses, which would match the recorded carbon isotope stratigraphy in PCB cores and the timing modeled by Maibauer et al. (in prep).

Refining our original estimates to include only those mechanisms capable of releasing carbon at rapid (1 kyr or less) rates (thermogenic methane or methane clathrates), we can further constrain the rates of carbon release required to cause a $\delta^{13}C$ of between −2.5 and −5.7‰ to cause the CIE. Within the constraints of our record, these onsets are geologically instantaneous and the 1 kyr estimates represent a *maximum* duration for initiation. Thus, rates of between 2.5 and 10.7 Gt of C for initiation of the CIE represent conservative estimates, and the likely scenarios may have released carbon at rates up to an order of magnitude greater. The presence of the POE and subsequent recovery of values between the POE and CIE imply volatility leading into the PETM.

Measured anthropogenic CO_2 emissions indicate that humans are responsible for releasing ~ 3 Gt of C/yr over the last 150 years (IPCC, 2013). Model projections over the next 100 years reveal anthropogenic emissions of between ~3 to 15 Gt of C/yr, with a total of between 750 to 2,000 Gt of C released into the exogenic carbon cycle (IPCC, 2013). Estimates calculated in this study reveal that the PETM carbon release rates were

similar to current and projected anthropogenic carbon emissions (Andres et al., 2012; IPCC, 2013), strengthening the case for the PETM as an analogue to modern human-induced greenhouse warming.

Conclusions

The shape of the carbon isotope stratigraphy across the PETM, combined with age and carbon cycle modeling at the onset of the event, reveal that two rapid (submillennial), distinct pulses of isotopically light carbon into the atmosphere characterize the early stages of PETM carbon release. This structured variability can provide important information favoring certain notable triggering mechanisms over others. Some hypothesized mechanisms suggest a singular triggering event (e.g., bolide impact [Cramer and Kent, 2005]) or protracted release at relatively low rates (e.g., seaway desiccation [Higgins and Schrag, 2006] or permafrost oxidation [DeConto et al., 2012]), which do not support the PCB data but could easily have contributed carbon over longer timescales as a feedback to PETM warming (Bowen, 2013). Models involving massive methane release in response to discrete regional events (e.g., volcanic intrusion and thermogenic methane release [Svensen et al., 2004; Rampino, 2013], seafloor slumping and methane clathrate release [Dickens et al., 1995; Katz et al., 1999]) are more easily reconciled with the new data. In particular, it should be noted that the approximate length of time separating the POE and CIE in the PCB record is similar to that estimated for the propagation of a thermal pulse to hydrate-bearing depths in seafloor sediments (Zeebe, 2013), suggesting that carbon release during the main CIE onset may have been a feedback to transient warming generated by an initial catastrophic release during the

POE. If this is the case, the PETM may provide geological evidence for a strong clathrate feedback on global warming at ~10^3-year timescales, implying that the long-term response of clathrates to anthropogenic warming deserves additional consideration (Archer, 2007).

The rapid, volatile pattern of carbon release at the onset of the POE and CIE suggest that the PETM may be a strong analogue for anthropogenic global change in terms of not only the nature but also the magnitude and rates of change. All modeled cases suggest that PETM carbon release and atmospheric pCO_2 change reached rates over intervals of ~1,000 years that were similar to those associated with modern anthropogenic carbon emissions (Andres et al., 2012). This is consistent with data from single-specimen analysis of foraminiferal tests (Thomas et al., 2002) but contrasts with results from marine margin records (Cui et al., 2011), which may be affected by significant time-averaging (Sluijs et al., 2012). This new perspective may now place some of the relatively severe and prolonged changes in global temperatures, ocean pH, and terrestrial plant and animal communities during the PETM (McInerney and Wing, 2011) within reasonable expectations for future centuries, further supporting the use of the PETM as an analogue to modern global change.

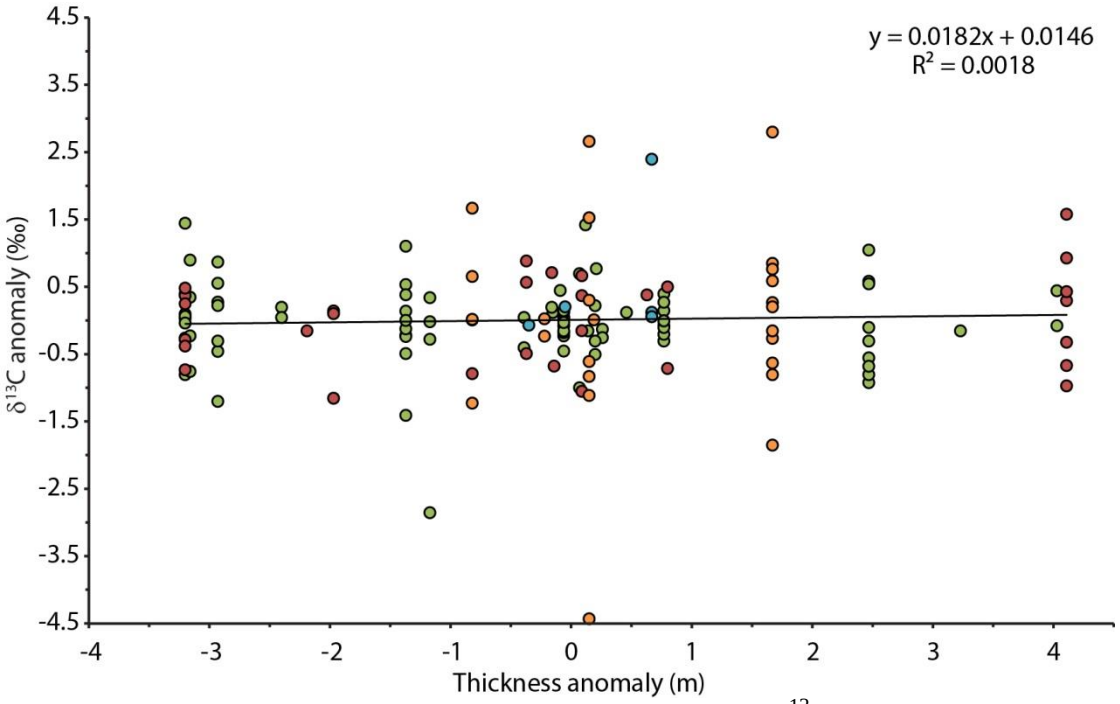

Fig. 2. Evaluation of the influence of atmospheric CO_2 on the $\delta^{13}C$ values of pedogenic in Polecat Bench cores. $\delta^{13}C$ and thickness anomalies represent the difference between values for an individual lithological or pedological unit and the mean values of the surrounding (one stratigraphically above and one below) two units. If samples from thin units are preferentially affected by ^{13}C-rich atmospheric CO_2, their $\delta^{13}C$ anomaly values should be systematically higher than suggests for thick units. The lack of relationship between $\delta^{13}C$ and thickness anomalies suggests that samples from thinner units were not preferentially affected by higher contributions of carbon from atmospheric CO_2 to pedogenic carbonate. Sample values are classified by stratigraphic position, blue = pre-POE (124.56 – 123.60 MCD), orange = POE and POE recovery (122.60 – 119.26 MCD), green = CIE body (118.19 – 76.02 MCD), and red = CIE recovery (75.96 – 60.59 MCD). CIE = carbon isotope excursion, POE = pre-onset excursion.

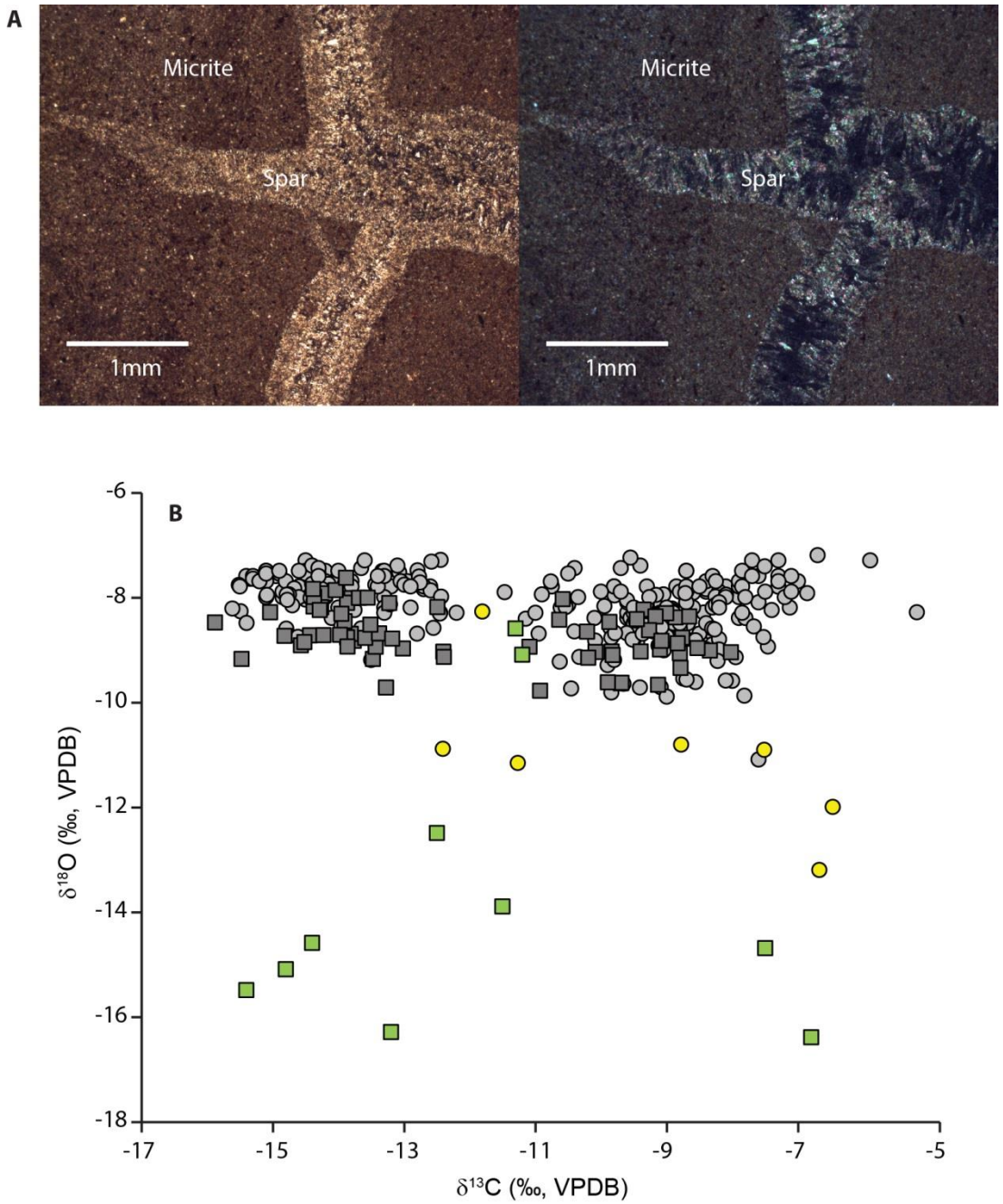

Fig. 3. Diagenetic sparry calcite in Polecat Bench pedogenic carbonate nodules. (A) Photomicrographs showing a matrix of micritic calcite with a vein of secondary sparry calcite at 2.5x magnification in both plane (left) and cross polarized light (right). (B) Carbon-oxygen isotope cross plot showing typical $\delta^{13}C$ and $\delta^{18}O$ values for primary micritic calcite (gray circles = core; gray squares = outcrop) and secondary diagenetic sparry calcite (yellow circles = core; green squares = outcrop) from PCB cores and outcrop (Bowen et al., 2001) collected carbonate nodules at Polecat Bench.

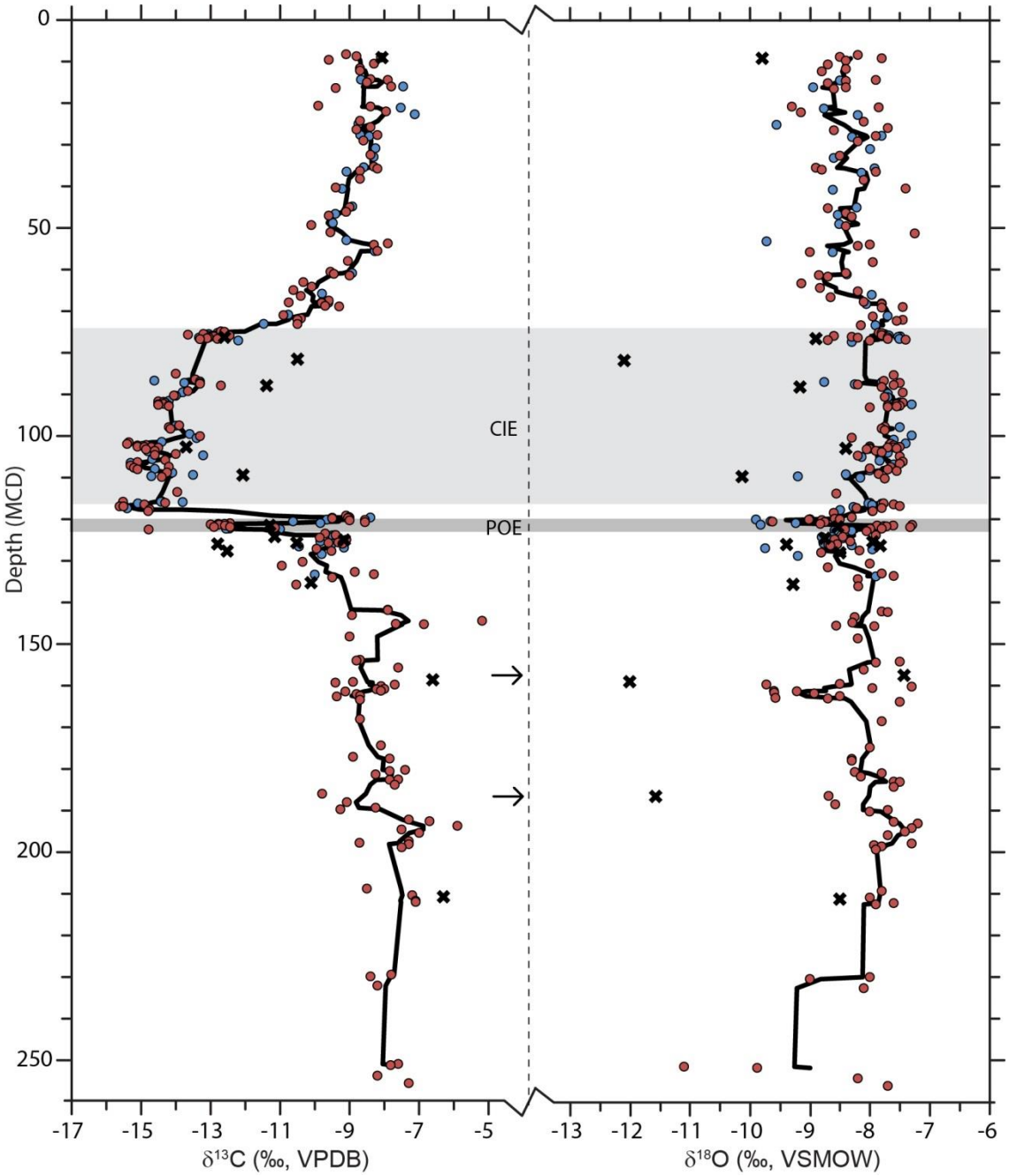

Fig. 4. Carbon and oxygen isotope data from pedogenic carbonate at Polecat Bench. Individual sampling intervals from core A (blue circles) and core B (red circles) are shown, with the 5-point running average based on the composite record from both cores shown as a black line. Points denoted by an 'x' were excluded from the composite stratigraphy based on screening criteria described in text. Arrows show the stratigraphic position of two excluded samples with very high $\delta^{13}C$ values falling outside of the plotted range.

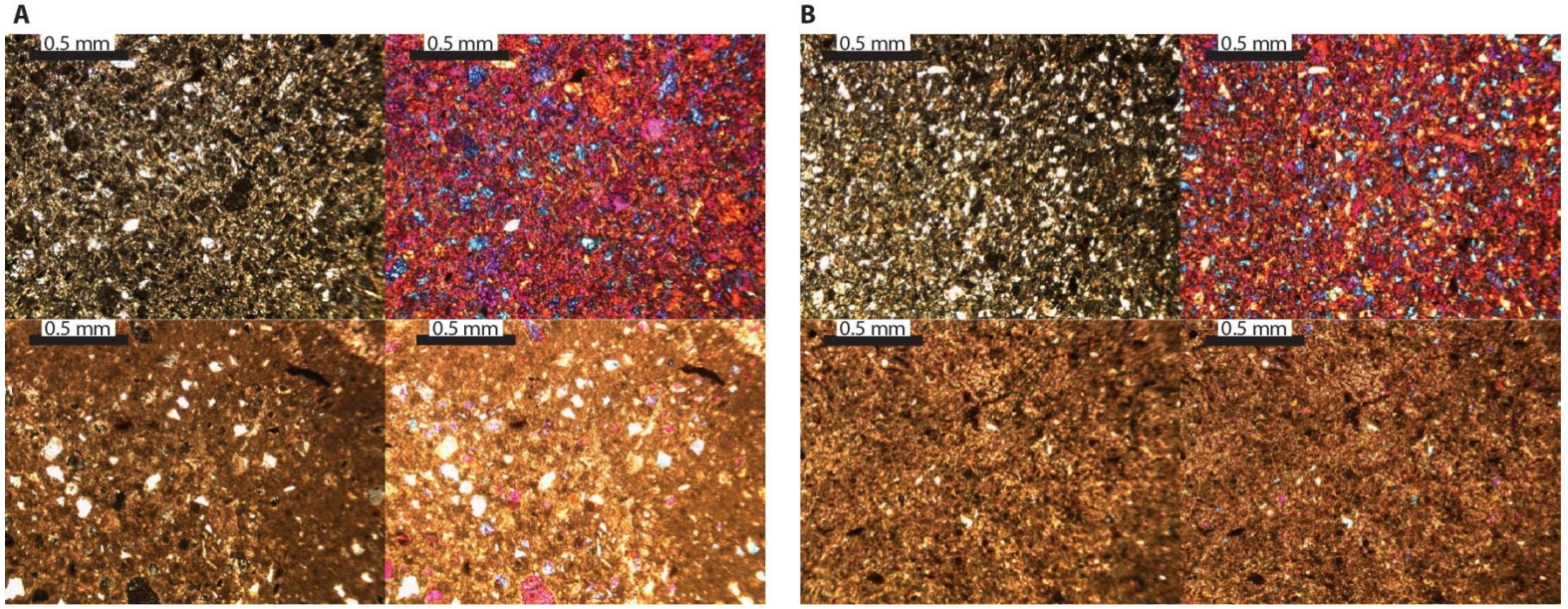

Fig. 5. Photomicrographs comparing matrix (top row) and nodule (bottom row) texture. Samples are representative of (A) the onset of the CIE (117.8 MCD) and (B) the $\delta^{13}C$ recovery interval between the POE and CIE (120.9 MCD). Note similar grain size, shape, and composition of clastic material in the matrix and nodules, consistent with displacive formation of the nodules in situ within the surrounding soil matrix. Both plane (left sides in each panel) and cross polarized (right sides) are shown at 6.3x magnification.

Fig. 6. Lithologic and isotopic records from Polecat Bench drill core and outcrop. From left to right: Litho-, bio- and chronostratigraphy of latest Paleocene-earliest Eocene outcrops exposed along the south end of Polecat Bench, Wyoming, including marker beds of Gingerich (2001); color line scan images of cores from Bighorn Basin Coring Project (BBCP) holes A and B at Polecat Bench; pedogenic carbonate $\delta^{13}C$ values from nodules collected in situ from outcrop exposures (Bowen et al., 2001) (stratigraphic level average values); new $\delta^{13}C$ records from pedogenic carbonate nodules collected from the PCB cores (hole A = blue, hole B = red), with 5-point moving average based on the composite record from both holes (black line); pedogenic carbonate $\delta^{18}O$ values from nodules collected in situ from outcrop exposures (Bowen et al., 2001), with 5-point moving average (black line) (stratigraphic level average values); and new $\delta^{18}O$ records from pedogenic carbonate nodules collected from the PCB cores (hole A = blue, hole B = red), with 5-point moving average based on the composite record from both holes (black line). The light gray field delineates the body of the PETM carbon isotope excursion (CIE), defined as the interval of sustained low $\delta^{13}C$ values in the PCB core record. The dark gray field highlights the period of variability just prior to the onset, labeled here as the pre-onset excursion (POE).

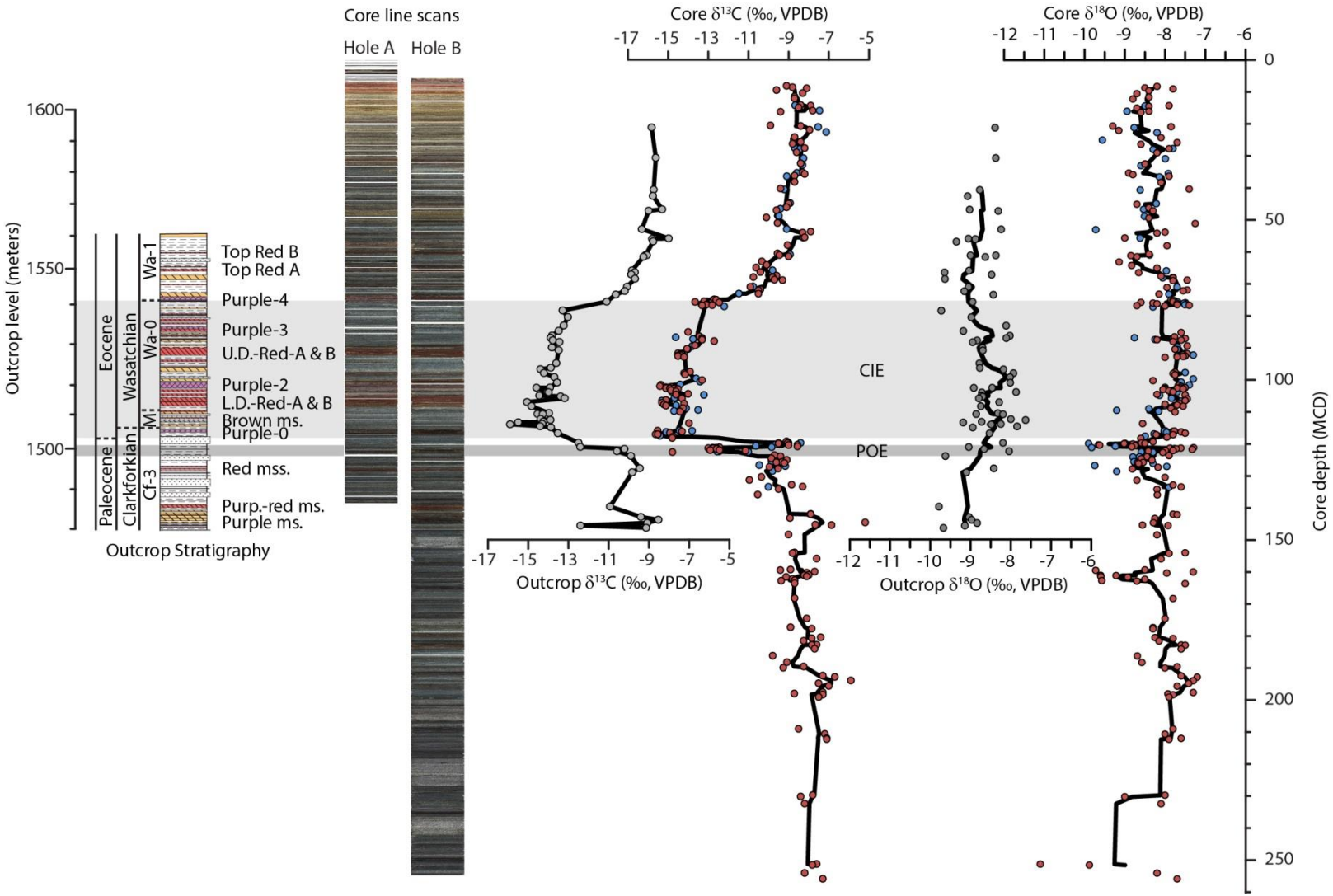
Core line scans
Hole A
Hole B
Core δ13C (‰, VPDB)
-17 -15 -13 -11 -9 -7 -5
Core δ18O (‰, VPDB)
-12 -11 -10 -9 -8 -7 -6
Outcrop level (meters)
1600
1550
1500
Eocene
Paleocene
Wasatchian
Clarkforkian
Wa-1
Wa-0
M
Cf-3
Top Red B
Top Red A
Purple-4
Purple-3
U.D.-Red-A & B
Purple-2
L.D.-Red-A & B
Brown ms.
Purple-0
Red mss.
Purp.-red ms.
Purple ms.
Outcrop Stratigraphy
CIE
POE
Outcrop δ13C (‰, VPDB)
Outcrop δ18O (‰, VPDB)
Core depth (MCD)
0
50
100
150
200
250

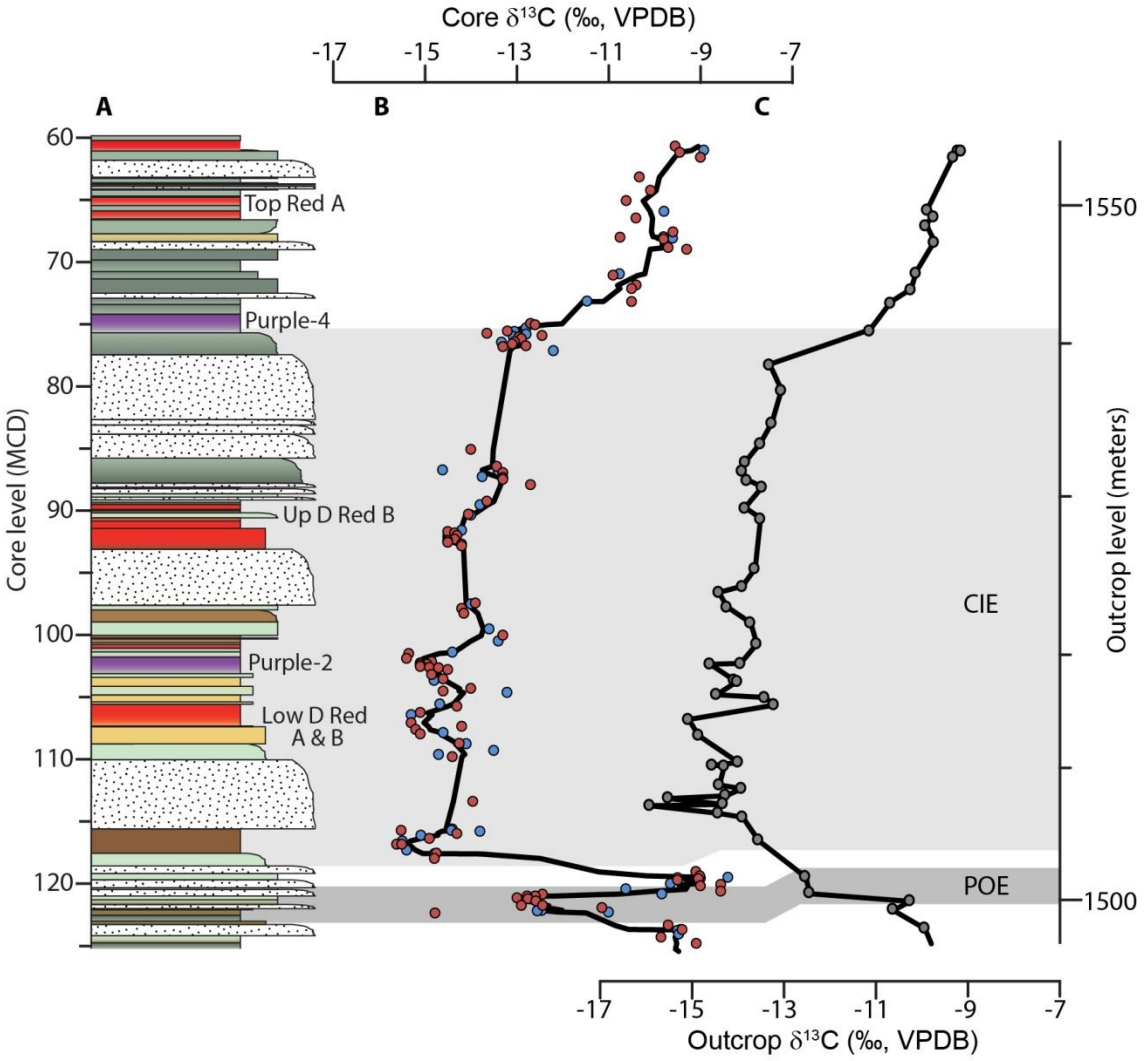

Fig. 7. Core stratigraphy, core $\delta^{13}C$ values and outcrop $\delta^{13}C$ values for the PETM interval at Polecat Bench. (A) Generalized stratigraphic column for the PCB cores, indicating the location of distinctive lithological units (Gingerich 2001) identified in core and outcrop. (B) Carbon isotope data from carbonate nodules in PCB cores from hole A (blue) and B (red). Symbols represent average values for individual nodules, and the black line gives a 5-point running average. (C) Carbon isotope data from carbonate nodules collected from PCB outcrops (Bowen et al., 2001). Symbols represent average values for individual paleosols. Gray background fields show hypothesized correlations of the pre-onset excursion (POE) and carbon isotope excursion (CIE) between core and outcrop. Stratigraphic offsets suggested in the POE interval honour the lithostratigraphic tie points and reflect 1) the similarity of intermediate outcrop $\delta^{13}C$ values previously recognized in the CIE onset interval to those documented in the PCB core POE, and 2) the recognition of uncertainty in the lithostratigraphic correlations for this interval of the record, which is dominated by thick and variable lithologies that are likely to exhibit strong lateral heterogeneity.

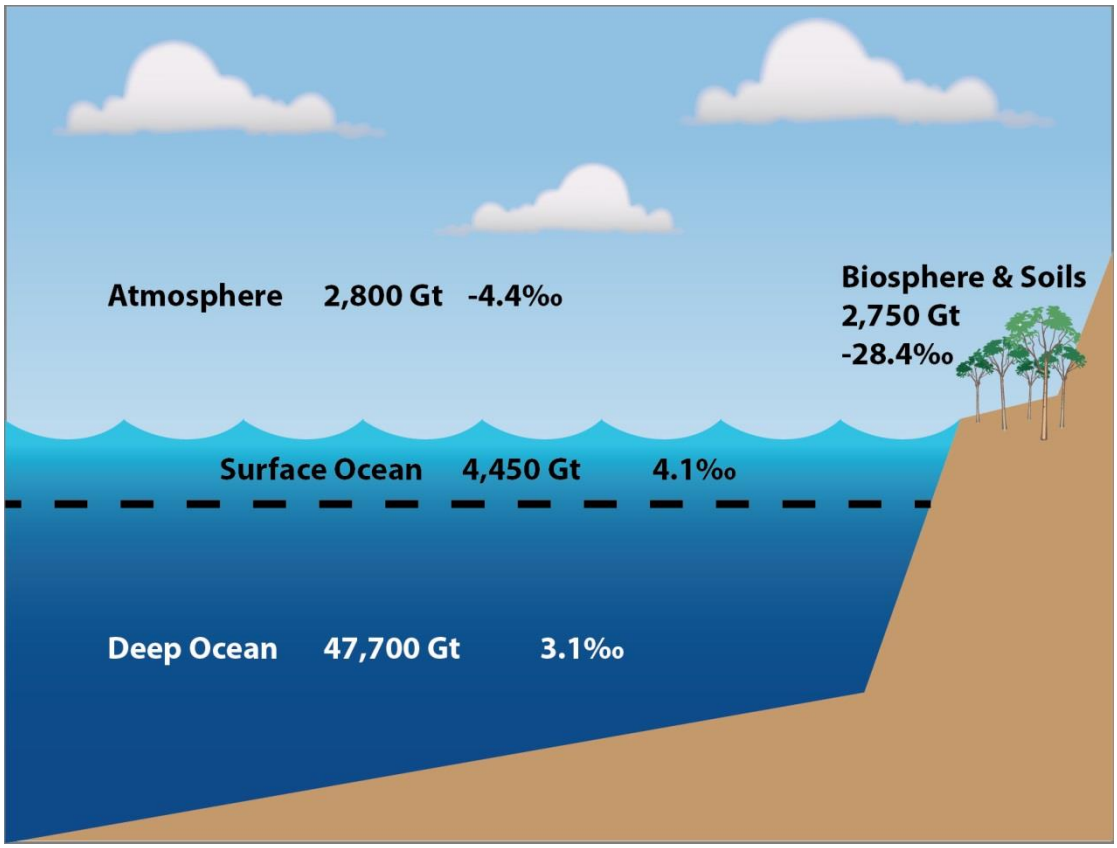

Fig. 8. Schematic of the Paleogene exogenic carbon pools. Reservoir sizes (in gigatons, Gt C) and their associated $\delta^{13}C$ values (‰) are derived from Bowen (2013).

Table 1. Carbon and oxygen isotope stratigraphy from Polecat Bench core collected carbonate nodules. All isotope values are reported in standard delta notation (δ) in per mil (‰) relative to the international standard Vienna PeeDee Belemnite (VPDB). Samples removed from the screening process are denoted in italics.

Site	Core	MCD	Sample ID	Avg. $\delta^{13}C$	Avg. $\delta^{18}O$	Count
PCB	B	8.23	3104094	−9.10	−8.20	1
PCB	B	8.70	3104096	−8.80	−8.50	1
PCB	B	9.03	3104098	−8.10	−7.80	1
PCB	*A*	*9.03*	*3102592*	*−8.07*	*−9.80*	1
PCB	B	9.57	3104100	−9.60	−8.40	1
PCB	B	10.52	3104102	−8.30	−8.70	1
PCB	B	11.60	3104108	−8.70	−8.40	1
PCB	B	12.18	3104110	−8.70	−8.80	1
PCB	B	14.24	3104116	−8.40	−7.90	1
PCB	A	14.35	3102628	−8.67	−8.50	1
PCB	B	14.43	3104118	−7.90	−8.40	1
PCB	B	14.99	3104120	−8.50	−8.70	1
PCB	A	16.00	3102644	−7.46	−8.94	1
PCB	B	16.01	3104122	−7.80	−8.40	1
PCB	B	16.37	3104126	−9.40	−8.60	1
PCB	B	20.64	3104142	−9.90	−9.30	1
PCB	A	20.82	3104148	−8.40	−7.85	2
PCB	B	21.09	3102670	−7.53	−8.77	1
PCB	A	22.01	3104146	−7.95	−9.15	2
PCB	B	22.67	3102692	−7.12	−8.20	1
PCB	A	24.25	3104160	−8.70	−8.10	1
PCB	B	25.00	3102708	−8.75	−9.56	1
PCB	B	25.76	3104168	−8.40	−7.70	1
PCB	A	26.32	3104172	−8.80	−8.60	1
PCB	B	27.63	3102726	−8.69	−7.80	1
PCB	A	27.67	3104178	−8.20	−7.90	1
PCB	B	27.95	3102728	−8.43	−8.30	1
PCB	A	29.00	3104188	−8.60	−8.20	1
PCB	B	30.84	3102754	−8.26	−7.99	1
PCB	A	32.44	3104198	−8.40	−8.50	1
PCB	B	32.96	3102764	−8.31	−8.60	1
PCB	A	35.30	3104206	−8.30	−8.90	1
PCB	B	35.45	3102792	−8.59	−7.92	1
PCB	B	35.78	3104208	−8.20	−8.80	1
PCB	A	36.31	3104210	−8.70	−7.90	1
PCB	B	38.23	3104244	−8.70	−8.10	1
PCB	A	40.31	3104252	−9.40	−7.40	1
PCB	A	40.59	3102832	−9.21	−8.62	1
PCB	B	44.86	3102868	−8.92	−8.22	1

Table 1 Continued

Site	Core	MCD	Sample ID	Avg. $\delta^{13}C$	Avg. $\delta^{18}O$	Count
PCB	A	46.16	3104276	−9.10	−8.40	1
PCB	A	47.06	3104278	−9.60	−8.30	1
PCB	B	48.84	3102892	−9.48	−8.51	1
PCB	B	49.35	3104286	−10.10	−8.40	2
PCB	A	51.09	3104288	−9.55	−7.25	2
PCB	B	52.99	3102932	−9.09	−9.72	1
PCB	B	53.75	3104302	−7.90	−8.00	2
PCB	B	54.08	3104304	−8.30	−8.20	2
PCB	A	55.56	3104310	−8.20	−9.00	2
PCB	B	55.62	3102972	−8.27	−8.62	1
PCB	B	57.98	3104324	−9.05	−7.95	2
PCB	A	60.60	3104338	−9.55	−8.40	2
PCB	B	60.92	3103048	−8.93	−8.38	1
PCB	B	61.08	3104342	−9.45	−8.85	2
PCB	B	61.47	3104344	−9.00	−8.70	2
PCB	B	63.09	3110308	−10.33	−9.14	1
PCB	A	64.16	3110310	−10.09	−8.83	1
PCB	B	65.01	3110311	−10.61	−8.20	1
PCB	B	65.85	3103110	−9.79	−7.97	1
PCB	B	66.40	3110312	−10.41	−8.65	1
PCB	B	67.51	3104400	−9.60	−8.10	2
PCB	A	67.91	3104402	−9.80	−7.80	2
PCB	B	67.97	3104408	−10.75	−7.80	2
PCB	B	68.03	3103146	−9.60	−8.06	1
PCB	B	68.09	3104410	−9.80	−7.80	2
PCB	A	68.78	3104412	−9.70	−7.45	2
PCB	B	68.91	3104414	−9.30	−7.80	2
PCB	B	70.91	3103196	−10.76	−7.70	1
PCB	B	71.03	3104428	−10.90	−7.95	2
PCB	A	71.83	3104430	−10.40	−7.45	2
PCB	B	72.09	3104432	−10.50	−7.55	2
PCB	B	73.14	3104438	−10.50	−8.15	2
PCB	A	74.93	3104440	−12.70	−7.85	2
PCB	B	75.03	3104448	−12.60	−7.80	2
PCB	A	75.27	3103242	−12.79	−7.75	1
PCB	B	75.54	3104452	−13.20	−7.80	2
PCB	A	75.59	3103246	−13.05	−7.68	1
PCB	B	75.72	3104462	−13.65	−8.60	2
PCB	A	75.80	3103248	−12.80	−7.49	1
PCB	B	75.91	3104458	−12.45	−8.30	2
PCB	B	75.96	3103266	−13.07	−7.53	1
PCB	B	76.02	3104464	−12.95	−7.70	2

Table 1 Continued

Site	Core	MCD	Sample ID	Avg. $\delta^{13}C$	Avg. $\delta^{18}O$	Count
PCB	*A*	*76.35*	*3104454*	*−12.60*	*−8.90*	1
PCB	B	76.42	3104456	−13.05	−7.70	2
PCB	B	76.42	3103270	−13.33	−7.50	1
PCB	B	76.60	3104468	−13.10	−7.40	1
PCB	A	76.72	3104472	−12.80	−8.70	1
PCB	B	76.82	3104470	−13.30	−8.00	1
PCB	B	77.14	3103272	−12.20	−8.30	1
PCB	*A*	*81.60*	*3103312*	*−10.50*	*−12.10*	1
PCB	A	85.12	3104484	−14.00	−7.60	1
PCB	B	86.48	3110315	−13.43	−7.76	1
PCB	A	86.76	3110367	−14.61	−8.76	2
PCB	B	86.84	3103358	−13.40	−7.80	1
PCB	B	87.00	3104494	−13.30	−7.50	1
PCB	B	87.32	3110368	−13.75	−8.25	1
PCB	B	87.38	3104496	−13.30	−8.20	1
PCB	A	87.51	3104498	−13.30	−7.60	1
PCB	*B*	*87.96*	*3103364*	*−11.39*	*−9.16*	2
PCB	A	87.98	3104504	−12.70	−7.80	2
PCB	A	89.30	3104508	−13.65	−7.45	2
PCB	B	89.61	3103382	−13.80	−7.70	1
PCB	B	90.36	3104518	−14.05	−7.75	4
PCB	B	90.41	3103406	−14.00	−7.70	1
PCB	A	91.64	3103432	−14.20	−7.50	1
PCB	B	91.74	3104528	−14.50	−7.45	2
PCB	B	91.88	3104532	−14.35	−7.55	2
PCB	B	92.15	3103436	−14.50	−7.30	1
PCB	B	92.38	3104538	−14.35	−7.70	2
PCB	B	92.48	3104534	−14.50	−7.50	2
PCB	A	92.64	3104542	−14.50	−7.55	2
PCB	B	92.78	3104544	−14.20	−7.70	2
PCB	B	92.90	3104546	−14.20	−8.00	1
PCB	A	97.53	3104552	−13.90	−7.75	2
PCB	B	97.62	3103466	−14.00	−7.50	1
PCB	A	97.96	3104554	−14.20	−7.80	2
PCB	A	98.36	3104558	−14.15	−7.75	2
PCB	B	99.63	3103514	−13.60	−7.30	1
PCB	B	100.14	3104566	−13.30	−8.30	2
PCB	B	100.62	3103544	−13.40	−7.60	1
PCB	B	101.51	3103554	−14.40	−7.40	1
PCB	B	101.60	3104578	−15.35	−7.65	2
PCB	B	102.01	3104582	−15.40	−7.60	2
PCB	B	102.26	3104586	−14.85	−8.00	2

Table 1 Continued

Site	Core	MCD	Sample ID	Avg. $\delta^{13}C$	Avg. $\delta^{18}O$	Count
PCB	B	102.37	3104588	−15.10	−7.50	2
PCB	B	102.52	3104592	−15.10	−7.70	2
PCB	B	102.65	3104594	−15.10	−8.00	2
PCB	B	102.73	3104596	−14.90	−7.55	2
PCB	*B*	*102.74*	*3103578*	*−13.70*	*−8.40*	1
PCB	A	102.79	3104598	−14.70	−8.00	2
PCB	B	102.93	3104612	−14.50	−8.05	2
PCB	B	103.32	3104614	−14.85	−7.90	2
PCB	A	103.67	3104616	−14.60	−7.80	1
PCB	A	103.78	3103586	−14.80	−7.70	1
PCB	B	104.45	3104620	−14.00	−8.20	1
PCB	B	104.64	3104622	−14.60	−7.50	2
PCB	A	104.77	3103614	−13.21	−8.14	3
PCB	B	105.69	3103616	−14.67	−7.84	2
PCB	B	105.89	3104624	−14.30	−7.45	2
PCB	B	106.41	3104634	−15.10	−7.50	1
PCB	A	106.56	3103640	−15.30	−7.60	1
PCB	B	107.22	3104638	−15.30	−7.65	2
PCB	B	107.52	3104640	−14.20	−8.00	1
PCB	A	108.00	3103666	−14.60	−8.00	1
PCB	A	108.13	3104644	−15.10	−7.55	2
PCB	B	108.87	3104646	−14.25	−7.85	2
PCB	B	108.93	3103686	−14.10	−8.40	1
PCB	A	109.46	3103696	−13.50	−9.20	1
PCB	*A*	*109.49*	*3104658*	*−12.07*	*−10.13*	3
PCB	B	109.78	3110369	−14.70	−8.16	2
PCB	A	109.95	3104660	−14.40	−7.75	2
PCB	B	113.57	3110316	−13.95	−8.56	1
PCB	A	115.81	3110370	−14.40	−7.99	1
PCB	B	115.93	3110371	−14.42	−8.02	1
PCB	A	115.94	3110317	−15.51	−7.77	1
PCB	B	115.98	3103746	−13.80	−7.80	1
PCB	B	116.17	3104682	−14.30	−7.60	1
PCB	A	116.32	3110372	−15.09	−7.96	1
PCB	B	116.57	3104684	−14.90	−7.50	2
PCB	A	116.78	3110373	−15.49	−8.27	1
PCB	B	117.04	3110318	−15.61	−8.22	1
PCB	B	117.05	3104706	−15.50	−7.80	1
PCB	B	117.50	3110374	−15.40	−8.49	1
PCB	A	117.77	3104708	−14.75	−7.95	2
PCB	B	117.81	3110376	−14.79	−7.96	1
PCB	A	118.19	3110319	−14.79	−8.60	1

Table 1 Continued

Site	Core	MCD	Sample ID	Avg. $\delta^{13}C$	Avg. $\delta^{18}O$	Count
PCB	B	119.26	3104724	−9.10	−8.30	2
PCB	B	119.60	3110320	−9.01	−8.58	1
PCB	B	119.75	3104726	−9.50	−8.50	1
PCB	B	119.80	3103806	−9.00	−9.90	1
PCB	A	119.83	3110321	−9.04	−9.02	1
PCB	B	119.93	3104742	−9.50	−8.80	1
PCB	A	120.24	3110379	−9.66	−9.65	1
PCB	B	120.30	3110322	−8.56	−9.62	1
PCB	B	120.41	3104750	−9.00	−8.75	2
PCB	B	120.66	3110380	−10.63	−9.23	1
PCB	B	120.85	3104752	−8.56	−8.83	2
PCB	B	121.06	3110381	−9.84	−9.82	1
PCB	A	121.10	3110323	−12.44	−7.29	1
PCB	B	121.24	3110325	−12.77	−7.61	1
PCB	B	121.38	3110326	−12.99	−7.77	1
PCB	B	121.46	3110327	−12.76	−7.72	1
PCB	*A*	*121.58*	*3110383*	*−11.30*	*−8.54*	1
PCB	A	121.64	3104776	−12.58	−7.33	4
PCB	A	121.98	3110330	−12.43	−7.99	1
PCB	B	122.00	3104778	−12.90	−7.80	1
PCB	B	122.19	3110331	−11.15	−8.41	2
PCB	A	122.38	3110384	−12.46	−8.32	1
PCB	B	122.43	3110385	−12.55	−8.59	1
PCB	A	122.53	3103844	−11.00	−8.30	1
PCB	B	122.60	3104780	−14.78	−8.05	5
PCB	A	123.60	3104806	−9.70	−7.90	1
PCB	B	123.94	3110386	−9.42	−8.64	1
PCB	B	123.95	3104808	−9.40	−8.45	2
PCB	B	124.03	3103860	−9.50	−8.80	1
PCB	*A*	*124.30*	*3110332*	*−11.16*	*−8.75*	2
PCB	B	124.30	3110387	−9.47	−8.45	1
PCB	A	124.56	3110333	−9.86	−8.59	1
PCB	B	125.05	3110334	−9.09	−8.32	1
PCB	*A*	*125.15*	*3104826*	*−9.15*	*−7.95*	2
PCB	B	125.51	3110388	−9.84	−8.77	1
PCB	B	125.71	3110335	−9.33	−8.54	3
PCB	*A*	*125.79*	*3110389*	*−10.52*	*−9.39*	1
PCB	A	125.83	3110336	−9.61	−8.69	1
PCB	B	126.02	3103884	−9.50	−8.30	1
PCB	B	126.03	3110337	−9.20	−8.66	1
PCB	*A*	*126.09*	*3110338*	*−12.80*	*−7.83*	4
PCB	A	126.69	3110391	−10.45	−9.75	1

Table 1 Continued

Site	Core	MCD	Sample ID	Avg. $\delta^{13}C$	Avg. $\delta^{18}O$	Count
PCB	B	126.99	3110392	−9.16	−7.96	1
PCB	B	127.24	3104856	−9.95	−8.17	3
PCB	B	127.76	3104864	−9.52	−8.81	3
PCB	A	128.53	3103936	−9.80	−9.20	1
PCB	B	130.38	3104880	−10.35	−8.00	2
PCB	B	131.31	3104904	−10.95	−8.70	2
PCB	B	132.78	3104922	−8.85	−7.80	2
PCB	B	133.45	3104022	−10.00	−7.90	1
PCB	B	134.12	3104944	−9.50	−8.20	1
PCB	*B*	*135.39*	*3110340*	*−10.11*	*−9.28*	1
PCB	B	135.85	3110341	−10.54	−8.19	1
PCB	B	141.89	3105046	−7.90	−7.80	1
PCB	B	142.02	3105048	−7.90	−7.70	1
PCB	B	143.21	3110343	−8.93	−8.25	1
PCB	B	144.58	3110344	−5.19	−8.29	2
PCB	B	145.28	3110345	−7.67	−8.56	2
PCB	B	145.42	3110346	−6.86	−7.92	2
PCB	B	148.35	3105114	−9.00	−8.20	1
PCB	B	153.95	3105154	−8.70	−7.50	1
PCB	B	154.14	3105156	−8.80	−7.90	1
PCB	B	155.85	3105182	−7.60	−8.10	1
PCB	*B*	*157.21*	*3110356*	*−1.39*	*−7.43*	2
PCB	*B*	*158.75*	*3110357*	*−6.61*	*−12.01*	2
PCB	B	159.28	3105208	−8.90	−8.50	1
PCB	B	159.44	3110358	−9.41	−9.72	1
PCB	B	159.93	3105224	−7.70	−7.30	1
PCB	B	160.29	3110359	−8.10	−7.96	1
PCB	B	160.97	3105222	−8.00	−9.60	1
PCB	B	161.04	3110360	−8.22	−9.22	1
PCB	B	161.40	3110361	−8.10	−9.59	2
PCB	B	161.57	3110362	−9.12	−8.93	2
PCB	B	162.22	3105238	−8.80	−8.50	1
PCB	B	162.63	3110363	−8.69	−9.57	1
PCB	B	162.78	3105240	−9.37	−8.70	3
PCB	B	163.58	3105254	−8.70	−7.50	1
PCB	B	168.25	3105292	−8.70	−7.80	1
PCB	B	174.54	3105354	−8.10	−8.00	1
PCB	B	177.31	3105376	−8.90	−8.30	1
PCB	B	177.74	3105384	−7.85	−8.30	2
PCB	B	180.43	3105406	−7.40	−8.25	2
PCB	B	180.74	3105408	−7.85	−7.80	2
PCB	B	181.53	3105422	−8.25	−8.15	2

Table 1 Continued

Site	Core	MCD	Sample ID	Avg. $\delta^{13}C$	Avg. $\delta^{18}O$	Count
PCB	B	182.74	3105436	−7.60	−7.60	2
PCB	B	182.84	3105444	−7.85	−7.50	2
PCB	B	186.19	3110365	−9.79	−8.69	1
PCB	*B*	*186.30*	*3110364*	*−3.99*	*−11.58*	1
PCB	B	189.55	3105496	−8.25	−7.70	2
PCB	B	189.94	3105498	−9.26	−8.00	2
PCB	B	192.41	3105526	−7.30	−7.60	1
PCB	B	192.81	3105528	−6.70	−7.20	1
PCB	B	193.93	3105540	−5.90	−7.30	1
PCB	B	194.77	3105550	−7.51	−7.41	2
PCB	B	195.63	3105552	−7.00	−7.70	1
PCB	B	197.61	3105570	−7.30	−7.30	1
PCB	B	198.01	3105582	−8.72	−7.93	1
PCB	B	198.31	3105584	−7.30	−7.80	2
PCB	B	199.07	3105590	−7.50	−7.90	1
PCB	B	209.02	3105656	−8.50	−7.80	1
PCB	A	210.61	3105658	−7.20	−8.00	1
PCB	*A*	*210.97*	*3105672*	*−6.30*	*−8.50*	1
PCB	A	211.94	3105674	−7.10	−7.60	1
PCB	A	212.23	3105688	−7.10	−7.90	1
PCB	A	229.70	3105782	−7.80	−8.00	1
PCB	B	230.16	3105792	−8.40	−9.00	1
PCB	B	232.36	3105812	−8.20	−8.10	1
PCB	B	251.22	3105926	−7.60	−11.10	1
PCB	B	251.50	3105928	−7.82	−9.88	3
PCB	B	254.02	3105954	−8.20	−8.20	1
PCB	B	255.83	3105978	−7.30	−7.70	1

Table 2. Carbon cycle mass balance modeling parameters for the Paleocene Epoch. Parameters are based on estimations from Bowen (2013) with a total exchangeable carbon reservoir including or not including the deep oceans, depending on the initial conditions used.

Carbon Reservoir	**Mass of C (Gt)**	**$\delta^{13}C$ (‰, VPDB)**
Atmosphere	2,800	−4.4
Biosphere + Soil	2,750	−28.4
Surface Ocean (Biomass + DIC)	4,450	4.1
Deep Ocean (DIC)	47,700	3.1
Total Exchangeable Carbon Reservoir	57,700	1.31
Exchangeable Carbon Reservoir without deep ocean	10,000	−7.21

Table 3. Carbon cycle mass balance calculations for the pre-onset excursion. The mass of carbon required (M_a) to cause a POE of −3‰ ($\Delta\delta^{13}C$) was calculated using multiple carbon sources ($\delta^{13}C_a$) and an initial size (M_i) and isotopic composition ($\delta^{13}C_i$) of the carbon reservoir based on estimations from Bowen (2013). Masses reported in gigatons (Gt) and $\delta^{13}C$ values reported in standard delta notation (δ) in per mil (‰) relative to the international standard Vienna PeeDee Belemnite (VPDB).

$\Delta\delta^{13}C$	$\delta^{13}C_i$	M_i	Carbon Source*	$\delta^{13}C_a$	M_a
			biomass oxidation	−22	2,542
			seaway dessication	−30	1,515
-3	−7.2	10000	thermogenic methane	−35	1,210
			thermogenic methane	−50	754
			methane hydrates	−60	602

*See review in McInerney & Wing (2011) for description of hypothesized sources of carbon.

Table 4. Carbon cycle mass balance calculations for the PETM CIE. The mass of carbon required (M_a) to cause a global CIE ($\Delta\delta^{13}C$) of −2.5‰ or −3‰ (representative of marine records) and −5.7‰ (representative of our terrestrial record) was calculated using multiple carbon sources ($\delta^{13}C_a$) and an initial size (M_i) and isotopic composition ($\delta^{13}C_i$) of the carbon reservoir based on estimations from Bowen (2013). Masses reported in gigatons (Gt) and $\delta^{13}C$ values reported in standard delta notation (δ) in per mil (‰) relative to the international standard Vienna PeeDee Belemnite (VPDB).

$\Delta\delta^{13}C$	$\delta^{13}C_i$	M_i	Carbon Source*	$\delta^{13}C_a$	M_a
			biomass oxidation	−22	6,932
			seaway dessication	−30	5,007
−2.5	1.31	57700	thermogenic methane	−35	4,266
			thermogenic methane	−50	2,955
			methane hydrates	−60	2,453
			biomass oxidation	−22	8,523
			seaway dessication	−30	6,114
−3	1.31	57700	thermogenic methane	−35	5,197
			thermogenic methane	−50	3,583
			methane hydrates	−60	2,969
			biomass oxidation	−22	18,676
			seaway dessication	−30	12,842
−5.7	1.31	57700	thermogenic methane	−35	10,745
			thermogenic methane	−50	7,211
			methane hydrates	−60	5,914

*See review in McInerney & Wing (2011) for description of hypothesized sources of carbon.

CARBON ISOTOPE RECORDS OF PALEOGENE HYPERTHERMAL EVENTS FROM BULK SOIL ORGANIC CARBON AND PEDOGENIC CARBONATE IN THE BIGHORN BASIN, WYOMING

Abstract

The largest and most pronounced of the early Cenozoic hyperthermals include the Paleocene-Eocene thermal maximum (PETM) and Eocene Thermal Maximum 2 (ETM2). These events have been well documented in drilled marine strata and terrestrial outcrops; however, significant uncertainty in the timing and mechanism of carbon release surrounding these global warming events remains. Given the high-quality, high-resolution record of carbon cycle change recorded in Polecat Bench cores, we can look to other regions in the Bighorn Basin to understand the expression of these Cenozoic hyperthermals at other sites. The carbon isotope record from core recovered pedogenic carbonate at Gilmore Hill (GMH; Bighorn Basin, WY) reveals relatively stable background $\delta^{13}C$ and $\delta^{18}O$ values over a host of multicolored floodplain lithologies. The GMH cores show excellent agreement to nearby outcrop studies in background carbon and oxygen isotope values; however, the marked >2‰ negative CIE that characterizes the ETM2 in continental records is missing from our GMH $\delta^{13}C$ curve. We suspect that this interval is located in the thick, poorly cemented, highly weathered sands, which

characterize the upper 25 m of core at this site. Analysis of bulk sedimentary organic matter at Basin Substation (Bighorn Basin, WY) reveals a dramatic decrease in TOC preservation through the interval that we have classified as the PETM; however, the $\delta^{13}C$ record is variable and does not show the expected >2 ‰ shift associated with the PETM CIE, even after several previously proven corrections are applied to the dataset. Comparison of our record to nearby outcrop studies of bulk sedimentary organic matter reveals agreement in the TOC trends to another site in the southeastern Bighorn Basin but notable discrepancies to two other nearby locations. The variability and lack of discernible CIE in our $\delta^{13}C$ record suggests that additional external mechanisms, such as a change in source of organic matter or water stress, likely impacted the preserved organic matter and its associated carbon isotopic signature, and the relationship between these two variables in studies of paleosols requires further investigation.

Background

The last 65 million years of Earth's history records numerous shifts in climate and ecology and provides an ideal foundation with which to study the coupled relationship between global temperatures and the carbon cycle. Early Cenozoic climate, a period of overall warming and increased pCO_2, was interrupted by several transient hyperthermal events associated with large, rapid pulses of carbon into the ocean-atmosphere system (Zachos et al., 2001). These temporary deviations from steady state conditions are similar in timing and magnitude to modern day anthropogenically forced greenhouse conditions and represent the most recent analogues to current human-induced fossil fuel emissions available in the geologic record. The largest and most well-known of these paleo-

warming events, the Paleocene-Eocene thermal maximum (PETM, ca. 55.5 Ma) (Westerhold et al., 2007), occurs at the Paleocene-Eocene boundary. This event was first recognized in marine cores as a ~50% drop in marine carbonate preservation and a >2.5‰ negative carbon isotope excursion (CIE) (Kennett and Stott, 1991; Thomas and Shackleton, 1996; McInerney and Wing, 2011). Further investigation of marine cores indicated another, smaller carbonate dissolution event occurring approximately 1.8 myr after the PETM (Lourens et al., 2005). This hyperthermal event has become known as the Eocene Thermal Maximum 2, or ETM2, and has not been studied in as much detail, especially in continental sections. Comparison of the abundant Paleogene $\delta^{13}C$ records that have been developed over the past decades reveals significant uncertainty in the exact magnitude and timing of carbon release associated with these hyperthermals. In order to determine the triggering mechanisms and better understand the resultant changes to climate and ecology, a coherent account of carbon cycle change through each event must be agreed upon.

As marine records may be affected by carbonate dissolution, low sedimentation rates, and potential time averaging, we can look to the terrestrial record for clues about these past global warming events. If destabilized, carbon stored in deep ocean sediments can propagate into the surface ocean, atmosphere, and biosphere on ~1 kyr timescales. Regardless of the specific triggering mechanism, this isotopically labeled carbon mixes into the atmosphere and will then be incorporated into continental sedimentary archives via the terrestrial biosphere. Stable isotopes of soil organic matter (SOM) and pedogenic carbonate nodules can be used to track such changes in climate, ecology, and the terrestrial carbon cycle (Cerling et al., 1989; Wynn et al., 2006). The isotopic

composition of soil carbonate is derived from that of soil CO_2. Organic matter degradation, plant respiration, and atmospheric CO_2 (CO_{2atm}) all contribute to the $\delta^{13}C$ of soil CO_2 (Wynn, 2007). Twenty to thirty centimeters below the soil surface, atmospheric CO_2 makes up a relatively constant fraction of the soil CO_2 and the isotopic composition of soil carbonate is relatively constant (Cerling et al., 1989). The biologic contribution to soil $\delta^{13}CO_2$ is determined by the carbon isotopic composition of overlying plant material, which is derived from atmospheric $\delta^{13}CO_2$, environmental factors (i.e., water stress), and the photosynthetic pathway used by the plant (C_3, C_4, CAM) (Ehleringer and Monson, 1993). Research suggests that only C_3 plants were in existence during the early Paleogene (Jacobs et al., 1999), and the expected isotopic offset between atmospheric CO_2 and C_3 plants is ~14–19‰ (Arens et al., 2000; Wynn, 2007). Assuming minimal to no influence of water stress, the isotopic composition of soil pedogenic carbonate should track changes in atmospheric $\delta^{13}CO_2$, with some degree of offset from biologic photosynthetic fractionation.

Soil organic carbon (carbon in soil organic matter; SOC) is another useful material that can be used for paleoecologic and paleoclimatic reconstructions. Bulk SOM is derived from biomass living at or near the surface. This biomass incorporates CO_{2atm} during photosynthesis, with the $\delta^{13}C$ signature of the CO_{2atm} preserved with some offset. Thus, by applying the appropriate offset corrections, the $\delta^{13}C$ of the atmosphere can be obtained from bulk SOC sampled at a known period of time. Several other factors may alter the preserved isotopic signature of SOM, however, especially if the SOM sampled is old and has undergone significant changes since initial burial. During the early stages of sedimentation and SOM burial, pedogenic development and microbial degradation may

change the $\delta^{13}C$ of SOC. In studies of fossil soils where more labile organic compounds have been microbially degraded, the remaining $\delta^{13}C$ of bulk SOC will be preferentially shifted towards the signature of the more stable compounds (i.e., lipids, lignins) (Bowen and Beerling, 2004; Wynn, 2007), which can be offset from the original biomass by several ‰ (Balesdent and Mariotti, 1996; Marshall et al., 2007). Additionally, Wynn (2007) and Bowen and Beerling (2004) have suggested that decomposition of SOM during or after burial of soils can result in kinetic fractionation of $^{13}C/^{12}C$, resulting in higher concentrations of ^{13}C-enriched byproducts. Furthermore, deep burial can result in thermal maturation of the SOM, which can also alter the preserved $\delta^{13}C$ signature. Between all of these processes, the $\delta^{13}C$ measured from bulk SOC can be shifted substantially if the SOM has been significantly degraded and/or buried, and these factors must be accounted for in studies of fossil soils, or paleosols.

In the summer of 2011, the Bighorn Basin Coring Project (BBCP) drilled Paleocene and Eocene strata from three locations in the Bighorn Basin, WY, USA (Clyde et al., 2013) (see introductory chapter for additional details). These three sites were targeted for their expected coverage of the PETM or ETM2 and, due to the nature of the coring process, represent unweathered archives that can be correlated to well-studied, adjacent outcropping sections. The Fort Union and Willwood Formations, which span the P-E boundary in the Bighorn Basin, are the thickest and most stratigraphically continuous terrestrial records spanning early Paleogene hyperthermals (Gingerich and Clyde, 2001). The first drilling site, Basin Substation (BSN), is located in the southeastern BHB and is characterized by deposition in a distal, wet, vegetated floodplain of a northwest flowing meandering river system (Neasham and Vondra, 1972; Wing and Harrington, 2001).

Outcrop studies of sediments in this area indicate an abundance of fossil plant material, palynological data and laterally correlative red beds, which characterize the PETM. BSN paleosols contain fossil organic matter at levels of a tenth of a percent to almost ten percent, making them well-suited for studies of organic geochemistry spanning the P-E boundary. Polecat Bench (PCB), discussed in the previous chapter in greater detail, has been well-studied in outcrop, and both outcrop and core data will be included in this chapter for correlations and comparisons. Gilmore Hill (GMH), the last of the three drilling sites, is located in the central portion of the basin in the McCullough Peaks region and is characterized by well-drained floodplain deposits distal from the northwest flowing meandering river system (Neasham and Vondra, 1972; Clyde et al., 1994; Clyde, 1997). It has been studied extensively in a magnetostratagraphic and paleontologic framework, and although the ETM2 interval lies near the Biohorizon B and Wa-4/Wa-5 boundary in the Bighorn Basin, suggesting that the hyperthermal event could have been responsible for mammalian turnover similar to that of the PETM, further studies of the biostratigraphic and chemostratigraphic relationships in the Gilmore Hill outcrop section reveal that the two events are not time equivalent (Abels et al., 2012). Gilmore Hill was targeted for its expected coverage of ETM2 and high density of pedogenic carbonate, as seen in nearby outcropping sediments.

Methods

Gilmore Hill Pedogenic Carbonate

Seventy-nine pedogenic carbonate nodules were collected from Gilmore Hill cores after methods described in the introductory chapter of this text. The exterior surface

of each nodule sample was physically cleaned using deionized water, and samples larger than ~1 cm in diameter were slabbed to expose a clean flat surface. For smaller samples, the exterior surface of the nodule was etched away using a dental drill. Primary micritic carbonate was collected with a dental drill under a binocular microscope. Aliquots of approximately 100 μg were weighed into 10 mL Exitainer vials (for analyses conducted at the University of Utah, 4 mL at Purdue University). The vials were flushed with helium to remove atmospheric carbon dioxide from the headspace and placed on a heating block held at 75 °C, and orthophosphoric acid was manually injected into each vial. The samples were reacted for a minimum of one hour and analyzed using a ThermoFinnigan Gas Bench II coupled to a Delta Plus Isotope Ratio Mass Spectrometer at the University of Utah's SIRFER lab or a ThermoFinnigan Delta V Isotope Ratio Mass Spectrometer at Purdue University's Stable Isotope lab. Analyses of reference carbonates (Carrara Marble, NBS-19 and LSVEC) were used to correct the values for peak area and through-run drift and to calibrate the values to the Vienna PeeDee Belemnite (VPDB) scale. Analytical precision was approximately 0.1‰, for both $\delta^{13}C$ and $\delta^{18}O$, at both labs based on replicate analyses of reference carbonates throughout the course of the analyses. Repeatability of the pedogenic carbonate analyses averaged 0.18‰ for $\delta^{13}C$ and 0.25‰ for $\delta^{18}O$ based on replicate analyses of 23 samples. Pedogenic carbonate nodules that are exposed to meteoric waters may undergo diagenetic alteration and form secondary sparry calcite (Bowen et al., 2001). The isotopic composition of microsampled micritic calcite from GMH core samples is similar to that previously documented from outcropping and core collected Polecat Bench carbonate (Bowen et al., 2001; Chapter 8) and the measured

GMH samples do not show signs of secondary sparry calcite with the characteristic offset $\delta^{18}O$ values (Fig. 9).

Basin Substation Bulk Soil Organic Matter

One hundred two-sediment samples were collected from BSN cores at approximately 1 m intervals during sampling at the Bremen Core Repository (additional details can be found in the introductory chapter of this text). Carbonate nodules found in bulk sediment samples were removed before processing. Any signs of contamination (i.e., exterior sides of sample exposed to organic materials during drilling, sampling, or storage) during the drilling or sampling process were removed from the sample using a cleaned Dremel. Samples were broken into 5–10 cm^3 pieces and dried in a 60 °C drying oven for a minimum of 24 hours to remove moisture. Once dry, ~10 g of sample was powdered and homogenized in a Retsch MM 301 Mill for 20 seconds at 30 Hz. If larger aggregates remained, samples were run for an additional 20 second intervals until all material had been powdered and well mixed. Mill chambers were cleaned by powdering ashed Ottowa sand and cleaning with ethanol before and after every sample and sand run. The powdered sample was placed in an ashed 20 mL glass vial with ashed aluminum foil between the vial and the plastic lid for storage.

Two methods of carbonate removal were evaluated to determine an optimum procedure for our samples. For the first, aliquots of ~30 mg were placed in open silver capsules (5 x 9 mm) on a polypropylene 96-well plate for acid fumigation to remove carbonate from the sample after methods described in Harris et al. (2001). Silver capsules must be used because tin capsules will disintegrate during the fumigation process. Once

capsules were in place in the plate, several drops of deionized water were added to each capsule until samples were saturated in order to ensure complete acid reaction. The plate was placed into a desiccator with 100 mL of a 12N HCl solution in the bottom of it and allowed to react with the acid for 8 hours. After 8 hours, the samples were removed and placed in a 60 °C drying oven for a minimum of 12 hours until samples were fully dried. Capsules were then placed into tin capsules and then folded and sealed with all air removed from the interior of the capsule.

As an alternative method for carbonate removal from our samples, we chose to use a direct acidification method after the methods described in Midwood and Boutton (1998). Approximately 2 g aliquots of the powdered sample were placed in centrifuge tubes and reacted with 30 mL of 2N HCl for 24 hours in a 50 °C water bath with periodic agitations to ensure full exposure to the acid. After the acid reaction, samples were centrifuged at 4500 RPM for 20 minutes, acid was decanted, and samples were rinsed repeatedly with DI water until a pH >5 was reached. Following acid removal, tubes were placed in a 50 °C drying oven for a minimum of 24 hours until samples were dried. Then, powders were reground with a cleaned mortar and pestle and aliquots were weighed into tin capsules. Size varied based on expected organic content of sample and ranged from 0.3–55 mg with an average weight of 20 mg.

Capsules from both carbonate removal techniques were placed in a zero blank autosampler and analyzed on a ThermoFinnigan Elemental Analyzer coupled to a Delta Plus Advantage Continuous Flow Isotope Ratio Mass Spectrometer at the University of Utah's SIRFER Lab. Total organic carbon (TOC) measurements were collected and are reported here in weight percent organic carbon relative to the total sample (wt% C or %

C). Due to extremely low organic carbon content in BSN sediments (average 0.42% C), samples were run only for $\delta^{13}C$ analyses to optimize for CO_2 measurements and maximize the peak areas for carbon. Samples were flash combusted, and carbon isotopic compositions of samples were calculated from measurements of masses 44, 45, and 46. All samples are reported standard δ-notation in per mil (‰) relative to the international standard Vienna PeeDee Belemnite (VPDB). To correct raw instrument data and put measurements into the VPDB scale, National Institute of Standards and Technology (NIST) certified peach leaf references were measured every 5^{th} or 6^{th} sample throughout the sample run. Secondary reference materials of Montana Soil (MT Soil) were used for quality control. Additional MT Soil references were placed at the beginning of the run to correct for any observed weight dependencies. In order to minimize linearity issues, all reference materials were weighed out to fall within range of the expected carbon peak areas (containing between 20 to 40 μg of C).

Repeatability of analyses averaged 0.20‰ for $\delta^{13}C$ and 0.01% for TOC based on replicate analyses of twenty-two samples. Any analyses that yielded carbon peaks below 75 Vs, likely due to low amounts of TOC, were reanalyzed at higher weights. In order to ensure that carbon was not retained from previous runs or that our lab preparation techniques were not introducing organic contaminants, we analyzed eight sand blanks. Sand was ashed in either a plastic centrifuge tube or glass vial, and then half of the samples were treated with acid using the methods described above, while the other half were not acidified. Samples were weighed out to ~30 mg, representative of normal sample weights. Three out of eight samples had peak areas below detection limits and yielded no measurements (Table 5). Of the remaining five samples, the average of all

carbon peak areas (4.5 Vs) represents only ~4% of the normal measured peak areas for samples and reference materials. Additionally, the measured TOC values for those five samples (0.005%) represents only ~1% of the average TOC measured for the entire remaining dataset. There was no discernible relationship between these five samples and their ashing or acid treatments. Due to the values acquired from the five samples which did yield organic carbon measurements, we suspect that lab preparation techniques and/or machine error may account for up to 4% error in our reported values.

Results and Discussion

Gilmore Hill Pedogenic Carbonate

General trends and observations

Consisting of primarily brown mudstones to siltstones throughout the 210 m of total section, the Gilmore Hill cores also host a variety of floodplain-type lithologies, ranging from siltstones to sandstones in colors from gray and green to yellow, red, and purple (Fig. 10). Large, weathered, poorly cemented sand bodies found in the upper 25 m of section were not sampled for pedogenic carbonate due to the likelihood of allocthonous and potentially weathered or altered carbonate (Clyde et al., 2013); thus, the carbon isotope curve spans only 183 m while the total section length (total amount of core collected) spans ~210 m. Several other sands found throughout the cores were not sampled due to the general absence of carbonate, as well as the likelihood for detrital nodules, leaving several ~10 m gaps in the compiled $\delta^{13}C$ record.

The average carbon isotope value at GMH is −10‰, and measured values span a range of approximately 3.5‰ over the ~183 m of section (n = 79, sampled every ~2 m)

(Fig. 10; Table 6). The oxygen isotope record also demonstrates variability throughout the total length of core, with average values of −8.6‰ that span a total range of ~2.6‰. Mean $\delta^{13}C$ and $\delta^{18}O$ values are −10.0‰ and −8.56‰, respectively, and results of an F-test indicate that there is a correlation between the measured variance at 98% confidence ($p < 0.02$).

Carbon isotope ratios decrease by ~2–3‰ from the base of the record up to 175 m and then rebound by ~1‰ in a stratigraphically coherent pattern, with the exception of one value at 192 MCD. Intermediate carbon isotope values are demonstrated throughout the middle part of the record, with a slight increase of 1–1.5‰ up section between 145 and 80 MCD. $\delta^{13}C$ values through this interval show a higher range of variability in the lower ~20 m, with the remainder of the section exhibiting a relatively tight trend towards higher values. Above the sampling gap at ~70 MCD, values are low and stable to the top of the carbon isotope record. The oxygen isotope record shows relatively stable values through the entire length of section, with some small <1‰ shifts exhibited over 10 to 20 m intervals. The middle portion of the record between 145 and 80 MCD, however, demonstrates a slight ~0.5–1‰ increase up section, similar to the $\delta^{13}C$ record. Intervals of coupled increases in both $\delta^{13}C$ and $\delta^{18}O$ suggest that perhaps an increase in temperature and a decrease in soil respiration rates locally or an increase in temperatures and a shift in the atmospheric $\delta^{13}C$ values globally may have led to these measured patterns. Additionally, intervals which reveal a distinctive shift in the carbon isotope record without the matching $\delta^{18}O$ changes (i.e., the lower ~50 m of section) suggest that local or global changes in plant respiration or $\delta^{13}C_{atm}$ did not occur coeval to a marked temperature or hydrological cycle change. A detailed assessment of the host lithologies

for each carbonate nodule and a comparison of these patterns to other records across the globe would help clarify the forcing mechanisms that may have caused these measured shifts.

Regional comparisons between core and outcrop

Due to land management restrictions, the GMH site chosen for drilling was ~600 m away from the previously studied GMH outcrop site that captured the ETM2 $\delta^{13}C$ excursion (Abels et al., 2012). Two large sandstones between ~890–863 m at the GMH outcrop site were originally thought to be the time-equivalent of ETM2 with the measured $\delta^{13}C$ excursion of H2 lying stratigraphically above; however, the correlation of this interval to the magnetic reversal of C24r reveals that this measured excursion corresponds to ETM2 (W. Clyde, personal communication, August 2013). A closer comparison of the GMH core to outcrop reveals excellent agreement between average background $\delta^{13}C$ values (both −10.0‰), with the largest difference being the ~2.5‰ negative CIE associated with ETM2 captured in outcrop (Fig. 11).

Another outcrop section that has been studied for its coverage of ETM2 is Upper Deer Creek (UDC) (~12 km from the GMH drill site) (Abels et al., 2012). Pedogenic carbonate from this site exhibit average background values that are slightly lower than at GMH (−10.2‰), and this outcrop section shows two distinct negative $\delta^{13}C$ CIE's, a −4‰ excursion associated with ETM2 and a −2.5‰ excursion associated with H2, a smaller (in both magnitude and duration) hyperthermal event occurring ~100 kyr after ETM2 (Fig. 11). Although $\delta^{18}O$ data from the nearby GMH and UDC outcrop collected carbonate were not available, comparison between a compilation of pedogenic carbonate

analyses from the McCullough Peaks region (Koch et al., 2003) and this study reveal agreement of $\delta^{18}O$ values, averaging around −8.5‰ for the early Eocene. All sites demonstrate an abundance of brown mudstones and siltstones, with periodic sandstones and multicolored mudstones, but the GMH cores have more gray, bluish-gray, and gray-green units, possibly due to these drilled strata lacking exposure to meteoric waters and being less weathered.

Based on correspondence with collaborators, it is predicted that the upper 25 m of weathered sands in the GMH cores that were not sampled represent the expected interval of ETM2 (Fig. 11) (W. Clyde, personal communication, August 2013). The coupled $\delta^{13}C$ and $\delta^{18}O$ shifts in the top 10 m of core support this hypothesis, suggesting that perhaps early carbon cycle perturbation and warming may have led up to ETM2. The presence of these thick sequential packages of sands where the expected ETM2 excursion should be may indicate a climatic response to the hyperthermal, where increased warming and an enhanced hydrological cycle led to more rapid accumulation of coarser grained sediments. Additionally, the proximity of these units to the top of the cored section reveals that they lie within the zone of weathering and were not conducive to sampling.

When compared to the continental expression of the PETM from drilled Polecat Bench (PCB) strata (previous chapter), several notable observations can be made from closer examination of the litho- and isotope stratigraphy (Fig. 12). While GMH strata are largely brown mudstones with some gray, blueish-gray and gray-green mudstones and siltstones, PCB cores consist primarily of gray to green mudstones and siltstones, with some characteristic red and purple beds. This could point towards a higher amount of oxidation in GMH strata due to better drained soils or drier conditions (Kraus and

Riggins, 2007), although both sites are interpreted as having been deposited in a well-drained floodplain environment distal from the main meandering trunk channel (Neasham and Vondra, 1972; Clyde, 1997; Gingerich, 2001). Background $\delta^{13}C$ values at PCB average around −8‰ while GMH average background values are −10‰, and GMH $\delta^{18}O$ values are ~0.5‰ lower than those recorded at PCB. These differences may be caused by local or global changes in temperature, the hydrological cycle, or biotic respiration or productivity.

Global comparisons/implications

The marine record of ETM2 has been well documented in sediments on Walvis Ridge, off the southwestern coast of Africa (Lourens et al., 2005; Stap et al., 2009). In a series of five cores collected at varying depths by Ocean Drilling Program (ODP) Leg 208, ETM2 is characterized by a decrease in carbonate abundance, the presence of a deep-red clay layer and a ~1.0‰ and ~0.7‰ negative excursion in the carbon and oxygen isotope values, respectively, all which occur just before the C24r/C24n magnetostratigraphic boundary. Additionally, Lourens et al. (2005) established that the observed $\delta^{18}O$ change through the ETM2 interval indicated overall warming of up to 3 °C. In cores collected from the shallowest drilling location, where the highest sedimentation rates and the lowest amount of reworked or secondary calcite exist, $\delta^{13}C$ and $\delta^{18}O$ excursions from bulk carbonate are ~1.6‰ each. Differences in the magnitude of carbon and oxygen isotopic change between benthic and planktonic foraminifera suggest that perhaps the absolute amount of change was greater in shallower sections or

given the overall larger mass of the deep ocean, the relative amount of change was less for this reservoir.

Compared to the terrestrial record of carbon cycle change at Gilmore Hill and Upper Deer Creek, the marine record reveals a smaller magnitude CIE. While the continental expression of ETM2 is a −2.5‰ (at Gilmore Hill) and −4‰ (at Upper Deer Creek) CIE, the marine excursion of −1 to −1.6‰ suggests that perhaps dissolution or bioturbation led to a muted marine signal, or enhanced biotic respiration on land may have led to a more enhanced terrestrial signal. Using basic steady-state mass balance calculations (described in previous chapter) (Table 2), modeled scenarios suggest that two to four times as much carbon (assuming a −60‰ $\delta^{13}C$ source) would be required to explain the larger −2.5 to −4‰ CIE recorded on land (Table 7). Assuming that the marine carbon isotope record represents a more accurate global representation of carbon cycle change, the magnitude of carbon release with a −60‰ $\delta^{13}C$ signature required to observe the ETM2 CIE is ~2 to 2.5 times less than that required for the PETM CIE, suggesting that ETM2 was about half of the size of the PETM in terms of the magnitude of carbon cycle change.

Basin Substation Bulk Soil Organic Matter

General trends and observations

Samples that were processed for carbonate removal using the acid fumigation method yielded very low carbon voltages and inconsistent stable isotope values when run on the IRMS. In addition, reproducibility of values for reference materials was poorer than usual for these runs. Although the exact mechanism that caused this is unknown, we

suspect that very low TOC values combined with either a reaction of residual HCl in the capsule during the combustion process, a build-up of sulfur in the combustion column, or potentially residual siderite left in samples that was not removed during the fumigation process may have caused the unreliable results. Thus, all data reported for this study are based on lab preparation techniques of direct acidification to remove carbonate.

Analysis of SOM from BSN cores reveals a substantial amount of variability in both $\delta^{13}C$ and TOC across the total length of section (Fig. 13, Table 8). The average TOC values range from 0.05% to 8.88% C; however, a clear trend is noticeable. Average TOC drops to 0.12% for the interval between 43.46 and 93.09 MCD, where these low values do not rise above 0.23% for the entire ~50 m section (denoted by the gray field in Fig. 13). Below 93.09 MCD, where the lowest average $\delta^{13}C$ values are expressed, the average TOC is higher than in any over interval (average = 1.03% C), whereas above 43.46 MCD, the average TOC is 0.45% C. Sections with high TOC and generally low $\delta^{13}C$ values (lower ~35 m of carbon isotope curve) correspond in most cases to brown, gray, and black mudstones and carbonaceous shales, some of which contain flecks of coal. The ~50 m section characterized by very low TOC is characterized primarily by dark gray, drab mudstones, siltstones, and sandstones. Above 43.46 MCD, where median TOC values are demonstrated, there is an increase in the amount of brown mudstones, similar to the lithological expression in the lower portion of the core. Additionally, the top ~23 m of the core contain periodic yellow sandstones, which likely represent a zone of weathering and exposure to modern meteoric waters. Based on lithological patterns, preliminary correlation to nearby outcrop strata (S. Wing, personal communication,

November 2012), and the patterns of TOC preservation, we estimate that the PETM CIE is expressed between ~43 to 93 MCD.

Carbon isotope values also exhibit a wide range of variability across the total length of section (Fig. 13, Table 8). The average $\delta^{13}C$ value of BSN SOM is −24.6‰, similar to soil organic matter derived from a C_3 plant source (Cerling et al., 1989). Carbon isotope values vary as much as 10.6‰ over the ~125 m of core and although a clear 2–3‰ negative shift characteristic of the PETM CIE in terrestrial SOC (Magioncalda et al., 2004) is not apparent in our record, several discernible trends are noticeable. The lowest 35 m of section feature the lowest mean $\delta^{13}C$ values, averaging around −25.5‰ and spanning a range of 3.8‰. The middle ~35 m of core, between ~54 and ~89 MCD, displays a positive shift in average $\delta^{13}C$ values, with the highest average $\delta^{13}C$ values through the entire section (−24‰) and the highest range of values spanning 9.8‰. Above ~54 MCD, values decrease slightly to an average of −24.5‰ and display much more stratigraphic coherence than the middle interval below it. Although some large scale trends in average carbon isotope values exist, the individual points reveal a substantial amount of variability across the total length of measured section.

The Basin Substation bulk organic record shows substantial variability in both $\delta^{13}C$ and TOC concentrations across the ~125 m of core analyzed in this study. Additionally, the distinctive negative carbon isotopic shift of >2‰ in bulk organic carbon, which is expected to characterize the PETM CIE in the BHB (Magioncalda et al., 2004), is missing from our raw dataset. In order to ensure that measured samples had all inorganic carbon removed, we reconsidered any samples which yielded $\delta^{13}C$ values above −23‰. We selected this cutoff point because values above this level were higher

than most other $\delta^{13}C$ values throughout the dataset, and they may reflect the combined analysis of both organic and inorganic carbon. Fifteen samples (representing 14% of the total dataset) were collected and reprocessed, using the direct acidification procedures described above. Following reacidification, $\delta^{13}C$ values decreased by between 0.9 to 9.6‰, suggesting that all fifteen samples chosen for this procedure had retained some amount of inorganic carbonate after only one acidification (Fig. 14; Table 8). These fifteen samples demonstrated a strong correlation ($R^2 = 0.79$) between the original $\delta^{13}C$ values and the total change in $\delta^{13}C$ values after reacidification, suggesting that the higher the original $\delta^{13}C$ value, the more inorganic carbon there was left in the sample.

We grouped all $\delta^{13}C$ and TOC analyses in terms of their host lithologies to determine any patterns between organic matter preservation and lithology. Samples with low TOC through the middle section of the core, from ~43 to ~93 MCD, mainly come from drab sandstones, siltstones, and massive mudstones. In particular, samples collected in sandstone lithologies have very low organic content (0.08% on average, relative to 1.26% for other host lithothologies). Due to the high potential for exogenously derived plant material as the source for the SOM in sandstone lithologies, we removed all sandstone analyses from the dataset used for subsequent analysis (Fig. 15). Sandstone-derived $\delta^{13}C$ analyses also exhibit higher standard deviations (0.7‰ for 1 σ) than the mudstone, siltstone, and carbonaceous shale derived analyses (0.1‰ for 1 σ), providing further support to exclude these data. Even after removal of sandstone analyses, the expected negative CIE is not clear in the $\delta^{13}C$ record from bulk organics in BSN cores (Fig 15B). Patterns of carbon preservation exhibited in the TOC values through these strata, however, although variable, do exhibit coherent stratigraphic changes through

specific intervals. This pattern of change may indicate a decrease in ecosystem productivity, resulting in less overall biomass available, or the possibility of enhanced decomposition of SOM in the middle 50 m of section, resulting in the preservation of only a fraction of the original biomass preserved, which would likely exhibit different $\delta^{13}C$ offsets relative to the original organic material (Bowen and Beerling, 2004; Wynn, 2007).

In order to determine if the measured $\delta^{13}C$ values varied systematically with the amount of carbon preserved in a sample, we examined the relationship of these two variables across three intervals of distinctive carbon preservation (Fig. 16). The first interval, from 20.48 to 42.23 MCD, represents a stratigraphically continuous section of median TOC values (average 0.34%) that are below the zone of potential alteration from weathering (Clyde et al., 2013). The second interval, from 43.46 to 93.09 MCD, characterizes a section of stratigraphically continuous low TOC values (average 0.14%), and the third section, from 94.17 to 114.04 MCD, is from stratigraphically continuous overall high (but still variable) TOC values (average 1.35%, with highest measured value 8.88%). The relationship between the isotopic composition and concentration of bulk SOM is nonlinear and best explained by the natural log of TOC as a linear function of the $\delta^{13}C$ value (Wynn, 2007). The strongest relationship is seen in the interval of high SOC concentrations in the lower section of core ($R^2 = 0.56$), and a trend correction using this regression equation was applied to the entire data set. Wing et al. (2005) conducted a comparable test for samples collected approximately 62 km (39 miles) southeast at Cabin Fork (BHB, WY) and found similar but stronger correlations between SOC concentrations and $\delta^{13}C$ values for PETM and non-PETM intervals. Although the cause

of this observed relationship is not discussed in detail here, several hypothesized mechanisms include preferential preservation of less labile organic compounds with a lower (depleted in ^{13}C) $\delta^{13}C$ signal; enhanced microbial degradation of samples within a given interval, resulting in a preferentially higher (enriched in ^{13}C) $\delta^{13}C$ signal; or natural kinetic fractionation during maturation of SOC (Wynn, 2007). Future studies should include a detailed assessment of (1) lithological properties for each sample, (2) specific organic compounds preserved in these different intervals, and (3) the amount of degradation the organic matter has undergone.

Following application of the TOC preservation trend correction, the bulk organic carbon isotope data from BSN cores presented were calculated as an anomaly relative to the bottom 25 m of section (Fig. 16, 17; Table 9). This interval was chosen to represent expected pre-PETM "baseline values" (S. Wing, personal communication, November 2012) without the potential for recent alteration due to weathering, as would be expected for post-PETM "baseline values" at the top of the core. Application of this trend correction reduces the total amount of variability slightly and results in an overall smoothing of average $\delta^{13}C$ values (Fig. 17). Average $\delta^{13}C$ values are ~0.5‰ lower than the baseline average in the lower 45 m of the carbon isotope record. In the middle section, from ~40–80 MCD, average $\delta^{13}C$ values display no anomaly relative to defined baseline conditions, and the upper section of the core exhibit an overall ~1‰ positive shift. Although the low values demonstrated in the lowest part of the core are not sustained up section, a ~2‰ negative shift occurring at 93.09 MCD likely correlates to the onset of the PETM CIE, where measured TOC values plummet to <0.1%. The shift towards higher values around 40–45 MCD also matches the stratigraphic interval of

increasing TOC, which may suggest further support for this interval representing the end of the PETM. Interpretation of this interval as the PETM is supported by preliminary studies of pollen types and abundances measured by colleagues on the BBCP (P. Jardine, personal communication, unpublished data, August 2013). Numerous swings in the individual $\delta^{13}C$ values in stratigraphically adjacent intervals, however, make finer scale interpretations of the carbon isotope record more difficult.

Higher concentrations of organic matter found in sediments prior to the onset of the PETM, below 93 MCD, are likely a result of sedimentation and organic matter deposition in a swampy environment, where carbonaceous shales and lithologies containing coal are present. During the PETM, however, the low SOC preservation in our record may be suggestive of a change to a more limited biomass supply during initial sedimentation or enhanced microbial degradation of the organic material through this interval, supporting previous interpretations of increased aridity and drying during the PETM (Kraus and Riggins, 2007; Wing et al., 2005).

Due to the high frequency and large magnitude of carbon isotope shifts recorded in BSN bulk organic $\delta^{13}C$, it is difficult to discern whether the pre-onset excursion (POE; discussed in previous chapter) is present in this additional drilled PETM section. A ~1‰ excursion and very slight (~0.2‰) recovery exists in $\delta^{13}C$ values ~1.3 meters prior to the presumed onset; however, variability (in terms of the magnitude and frequency of $\delta^{13}C$ shifts) is prevalent in strata leading up to the PETM, and this feature may be an artifact of the wt.% C trend correction that was applied to the whole dataset. Accumulation rates predicted for the nearby Highway 16 site (0.25–0.33 m/kyr) (Kraus et al., 2013) applied to BSN cores suggest that the potential POE and recovery would have occurred in ~4.1–

5.4 kyr. Applying these accumulation rates to the onset of the PETM CIE onset at BSN, which spans ~3 m from 90.07–93.09 MCD, reveals that ^{13}C-depleted carbon release would have occurred in ~9–12 kyr. These calculations agree with previous estimations for the duration of the PETM CIE onset (Bowen et al., 2001; McInerney and Wing, 2011), but do not align with timing predictions made for Polecat Bench cores in the previous chapter. The discrepancy could be due to differing accumulation rates at BSN, indicating that perhaps sedimentation was more rapid, and the 3 m accumulated in <9 kyr; however, the δ^{13}C record is quite unclear, and there may be significant time averaging of the preserved SOC δ^{13}C. Development of site specific sedimentation rates, carbon isotope analysis of specific organic compounds or specific types of preserved organic matter (mineral bound versus free light fraction [Bataille et al., 2013]), or collection of total nitrogen data may provide additional information regarding organic matter source or the degree of degradation throughout the PETM interval at BSN, and future studies should include this work.

Regional comparisons between core and outcrop

When placed in a regional context, the BSN organic record reveals several notable similarities and differences to other organic studies conducted in the BHB (Magioncalda et al., 2004; Wing et al., 2005; Baczynski et al., 2013; Kraus et al., 2013). In the four studies highlighted in this text, the PETM CIE is characterized by 40–60 m of fluvial strata ranging from alluvial backswamp and pedogenically modified mudrocks to coarser grained heterolithic deposits characteristic of higher energy floodplain deposition and periodic river avulsions (Fig. 18) (Kraus et al., 2013). In general, cored strata at

Basin Substation are more drab and dark in color and appear less weathered than surrounding outcrops. The purple and red beds that mark the onset and recovery intervals of the PETM in most BHB outcrop sections are largely missing from BSN cores. The only prominent red bed is located ~25–30 m above the onset in BSN cores, and this unit may correspond to the well-documented upper double red beds first characterized at Polecat Bench (Gingerich, 2001; W. Clyde, personal communication, August 2013). Brown mudstones located near the onset and termination of the CIE in BSN cores may represent the less oxidized red and purple beds found in outcrop. Additionally, all sites except Highway 16 seem to have coarser grained units near the onset of the PETM, perhaps indicating a basin wide climatic response to initiation of the hyperthermal.

Organic carbon concentrations through all four sections are similar and typically below 1% (Fig. 19). In general, similar patterns of TOC preservation are displayed between BSN and Cabin Fork and between Polecat Bench and Highway 16. The BSN and Cabin Fork sections have very high TOC concentrations in pre-PETM intervals, with low TOC during the PETM and a slight increase in TOC concentrations after the PETM. These two sections are the only sites to exhibit TOC concentrations >1%, and dark mudstones and carbonaceous shales appear to be the host lithologies for these organic rich intervals. These organic rich lithologies indicate that they were most likely deposited in a swampy environment, where water saturated sediments and abundant overlying biomass resulted in these high measured TOC values. Polecat Bench and Highway 16 demonstrate similar patterns of TOC change to one another through the measured sections, with an increase in organic carbon concentrations near the onset of the PETM and a logarithmic decrease in TOC towards the end of the event. These two sections also

demonstrate the lowest average TOC concentrations of the four sites. Both of these outcrop sections appear to have cyclic patterns of TOC preservation throughout the entire measured section. This pattern of carbon preservation coupled with the host lithologic units throughout the sections suggests some larger forcing mechanism that may have driven sedimentology and paleosol development (measured by color, among other things) and ultimately organic carbon preservation. Previous research on bulk organic matter at Polecat Bench has suggested that this rhythmic pattern corresponds to the Milankovitch precession cycle, with this astronomical mechanism driving climatic variation and ultimately sedimentation and paleosol development (Aziz et al., 2008). It is unusual, however, that this cyclic pattern is demonstrated in Polecat Bench and Highway 16 strata, but not Cabin Fork and Basin Substation strata, given their close proximity to the Highway 16 site. This lack of correlation may be a result of local differences in topography or sedimentation.

When compared to the outcrop studies, the $\delta^{13}C$ record in BSN cores does not exhibit the expected >2‰ negative PETM CIE shift that is measured in the other three sections (Fig. 20). The lack of CIE signal could be a result of several different mechanisms that may alter the amount or $\delta^{13}C$ of the preserved organic matter. Mixing of the original autochthonous carbon with ^{13}C-enriched allochthonous carbon may lead to a muted CIE. This phenomenon would be expected in coarser grained avulsion deposits which are more prevalent through the PETM interval. Oxidation and microbial respiration during degradation of the SOM may result in a preferentially enriched signal (Bowen and Beerling, 2004; Bataille et al., 2013); however, our darker strata that are missing the more oxidized red beds characteristic of the PETM in outcrop section

indicate that our sediments were likely less oxidized than the surrounding outcrop examples and therefore should show a stronger CIE signal. After early deposition of SOM, further microbial decomposition resulting in ^{13}C-enriched residues or selective preservation of less labile compounds could also mute the carbon isotope signal of preserved SOC (Clechenko et al., 2007; Bataille et al., 2013). If these mechanisms are responsible for the overall highly variable and muted CIE signal in our record, then we would expect to see these factors play a more important role in the nearby outcrop $\delta^{13}C$ records. This does not seem to be the case, however. Finally, Bowen and Beerling (2004) suggest that sampling of specific paleosoil horizons may help resolve the total contribution of microbial decomposition on bulk $\delta^{13}C$; however, paleo-soil horizons were not sampled specifically in this study. We cannot conclusively evaluate each of these hypotheses; however, ongoing analysis of specific organic compounds would provide pertinent information towards determining the origin of the SOM and the amount of degradation that it has undergone, helping to resolve some of these important uncertainties.

Conclusions

Gilmore Hill Pedogenic Carbonate

The BBCP cores provides an opportunity not only to study environmental changes from unweathered, drilled terrestrial sediments, but also allows for the detailed and close comparison of core to nearby outcrop records of these environmental changes. In the case of the GMH site, this idea proved especially important, as the carbon isotope stratigraphy was lacking features that we expected to see from these cores. General

agreement in the $\delta^{13}C$ background values exists between pedogenic carbonate from the GMH core and the Gilmore Hill and Upper Deer Creek outcrop sites (Abels et al., 2012) as well as in $\delta^{18}O$ background values between the GMH core and outcrops in the McCullough Peaks region (Koch et al., 2003). The presence of several tens of meters of yellow, unconsolidated sands at the top of the GMH cores suggests a very deep weathering horizon and highlights the possibility of secondary alteration from more modern meteoric waters. These thick weathered sands represent the expected stratigraphic placement of ETM2, and this interval in GMH cores may represent either sedimentation during the ETM2 or subsequent erosion and redeposition at a later time. If the former is the case, the presence of thick sands through this section may point towards a climatic response to the onset of the hyperthermal.

When compared to the pedogenic carbonate record from PCB cores, the background $\delta^{13}C$ values are ~2‰ lower at GMH, indicating an isotopically shifted atmospheric carbon pool during the early Eocene compared to the Paleocene/Eocene transition. Additionally, background $\delta^{18}O$ values are ~0.5 ‰ higher at GMH compared to PCB, equating to a 1–2 °C warming (assuming no changes to hydrological conditions). These observations are supported by the extensive research conducted on marine sediments spanning the early Cenozoic (Zachos et al., 2001). Although $\delta^{18}O$ values were not available for the outcrop studies at GMH and UDC, a coupled analysis of these measurements would add to these comparisons and provide more quantitative detail on temperatures through this period of time.

Mass balance accounting for ETM2 using the measured CIEs from Abels et al. (2012) and Lourens et al. (2005) suggests that ETM2 was about half the size of the

PETM in terms of the mass of isotopically light carbon required to cause the observed CIEs. This interpretation is corroborated by existing research, and since the ETM2 excursion is not accompanied by major biotic change like the PETM (Abels et al., 2012), these calculations may provide constraints on the carbon cycle thresholds required for ecological turnover during hyperthermal events.

Basin Substation Bulk Soil Organic Matter

Initial observations of the $\delta^{13}C$ and TOC measurements through the BSN bulk organic record reveals that the acid fumigation technique to remove inorganic carbonate was not effective for our samples. Due to very low measured carbon voltages for both samples and reference materials, results were highly unreliable and likely incorrect. Although the exact cause is unknown, we hypothesize that this phenomenon may be a result of residual HCl in the capsules, remaining inorganic carbon in the form of siderite in the capsules, or a build-up of sulfur in the combustion column of the mass spectrometer during sample runs. We found the direct acidification technique to be much more affective, yielding much higher carbon voltages and reproducible results, although some samples did require additional rounds of acid treatment due to residual inorganic carbon left over in the sample.

The raw bulk organic $\delta^{13}C$ and TOC records from BSN cored strata are highly variable through the entire length of measured section. Several different screening techniques were employed to filter the raw $\delta^{13}C$ data, including removal of sandstone derived samples and a wt.% C trend correction; however, the resultant $\delta^{13}C$ record still does not demonstrate the stratigraphically coherent >2‰ negative CIE over 40+ m of

strata associated with the PETM in other studies of bulk organic carbon. An abrupt decrease of ~2‰ in $\delta^{13}C$ values, however, is observed near the measured decrease in TOC values, which likely indicates initiation of the PETM CIE. The lack of sustained low values which mark the CIE could be a result of several different mechanisms which may alter the amount or $\delta^{13}C$ of the preserved organic matter. Further investigation of specific organic biomarkers, total nitrogen, and sedimentological change from BSN cores may help to filter some of the noise in the $\delta^{13}C$ record, address potential sources of alteration on organic carbon preservation, and aid in environmental change interpretations.

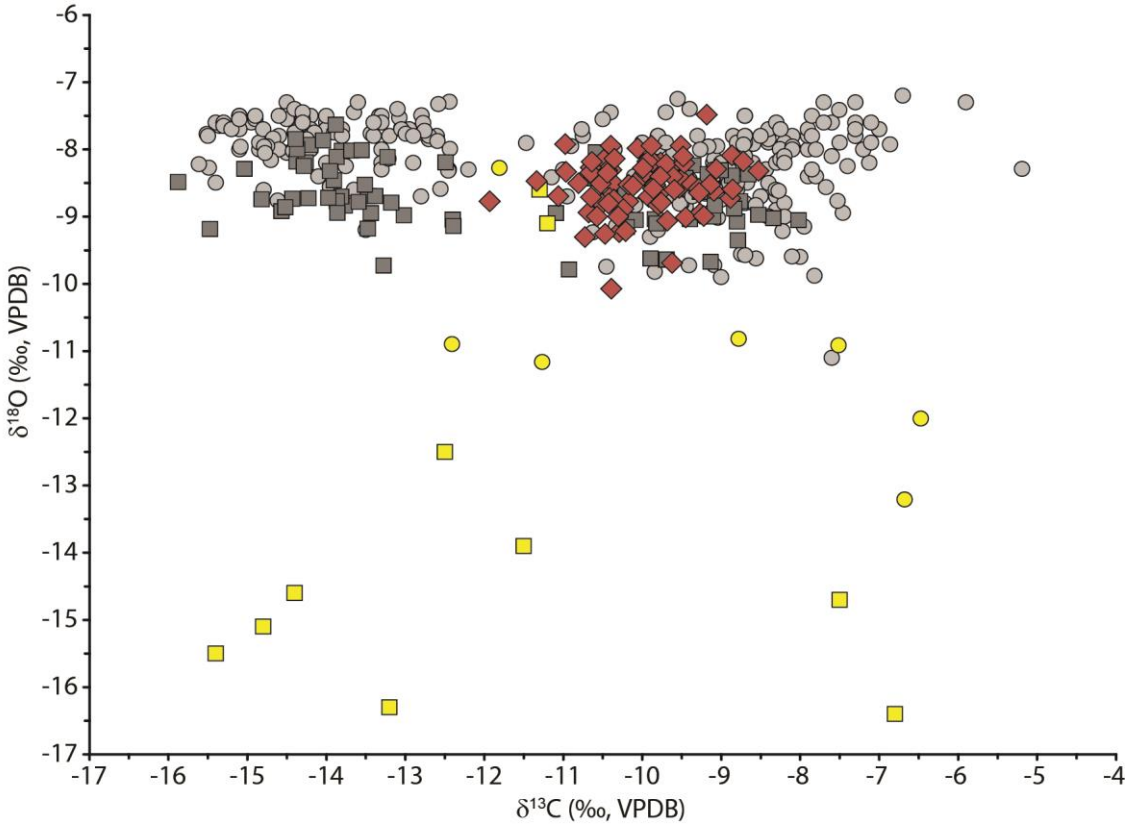

Fig. 9. Variation in primary micritic calcite versus secondary sparry calcite in pedogenic carbonate collected from Gilmore Hill (GMH) cores and Polecat Bench (PCB) cores and outcrop. Carbon-oxygen isotope cross plot showing typical $\delta^{13}C$ and $\delta^{18}O$ values for primary micritic calcite (red diamonds = GMH core; gray circles = PCB core; gray squares = PCB outcrop) and secondary diagenetic sparry calcite (yellow circles = PCB core; yellow squares = PCB outcrop).

Fig. 10. Pedogenic carbonate carbon isotope stratigraphy and lithostratigraphy at Gilmore Hill. Compiled lithostratigraphy (left panel), carbon isotope data (middle panel, gray circles), and oxygen isotope data (right panel, gray circles) across ~210 m of drilled strata. The five point running average is denoted by the black lines, and breaks in the line indicate a sampling gap of >10 m.

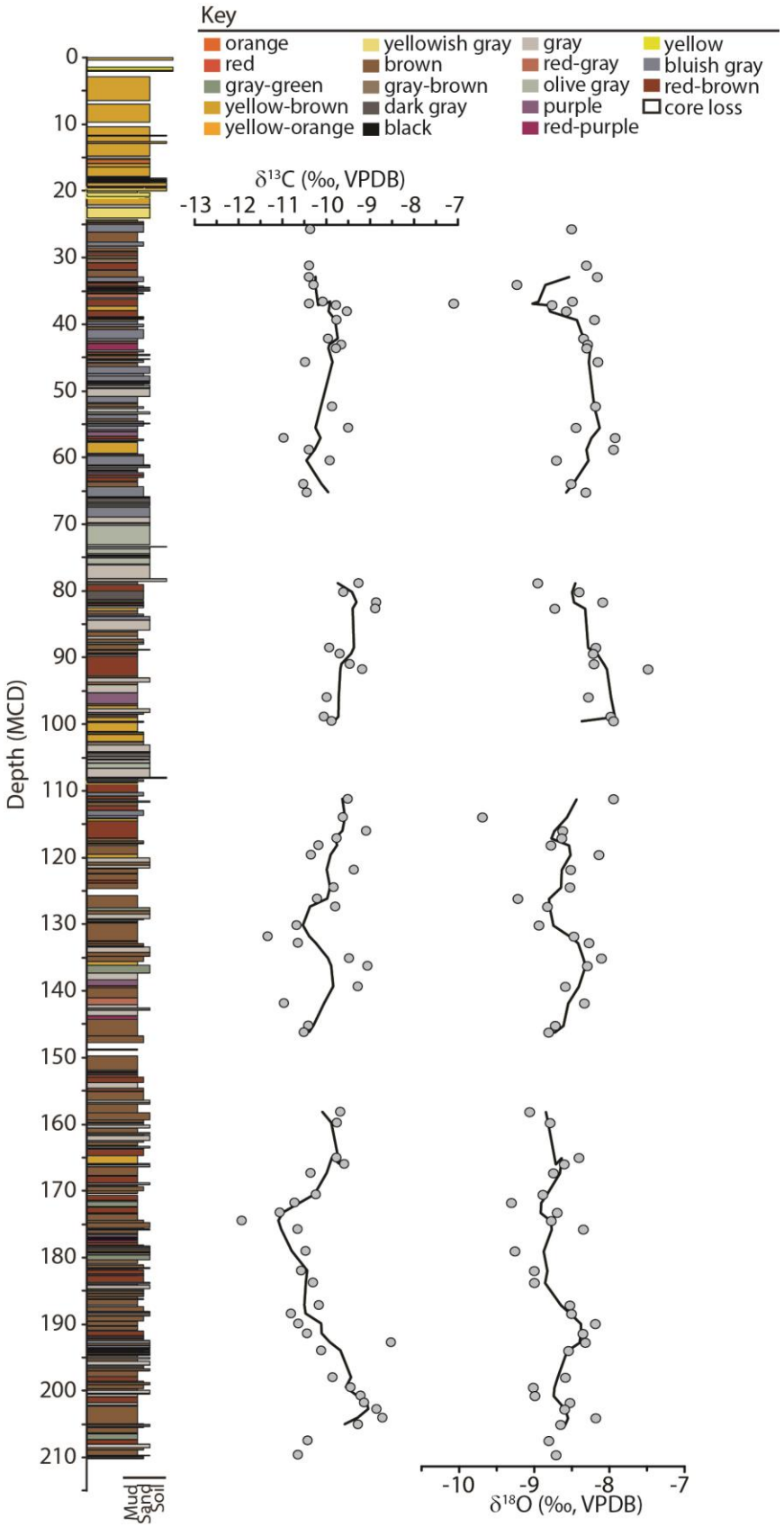
Key
orange
red
gray-green
yellow-brown
yellow-orange
yellowish gray
brown
gray-brown
dark gray
black
gray
red-gray
olive gray
purple
red-purple
yellow
bluish gray
red-brown
core loss
δ13C (‰, VPDB)
-13 -12 -11 -10 -9 -8 -7
Depth (MCD)
0 10 20 30 40 50 60 70 80 90 100 110 120 130 140 150 160 170 180 190 200 210
Mud
Sand
Soil
-10 -9 -8 -7
δ18O (‰, VPDB)

Fig. 11. Comparison of outcrop and core lithostratigraphy and carbon isotope records from terrestrial Eocene strata in the Bighorn Basin, WY. Lithostratigraphy and carbon isotope stratigraphy of (A) the Upper Deer Creek outcrop section, (B) the Gilmore Hill outcrop section, and (C) the Gilmore Hill core section showing the correlative carbon isotope excursion and magnetochrons (outcrop only), which characterize the ETM2 (gray field). Black lines represent five point running averages, and stratigraphic positions/depths are equally scaled for all sections.

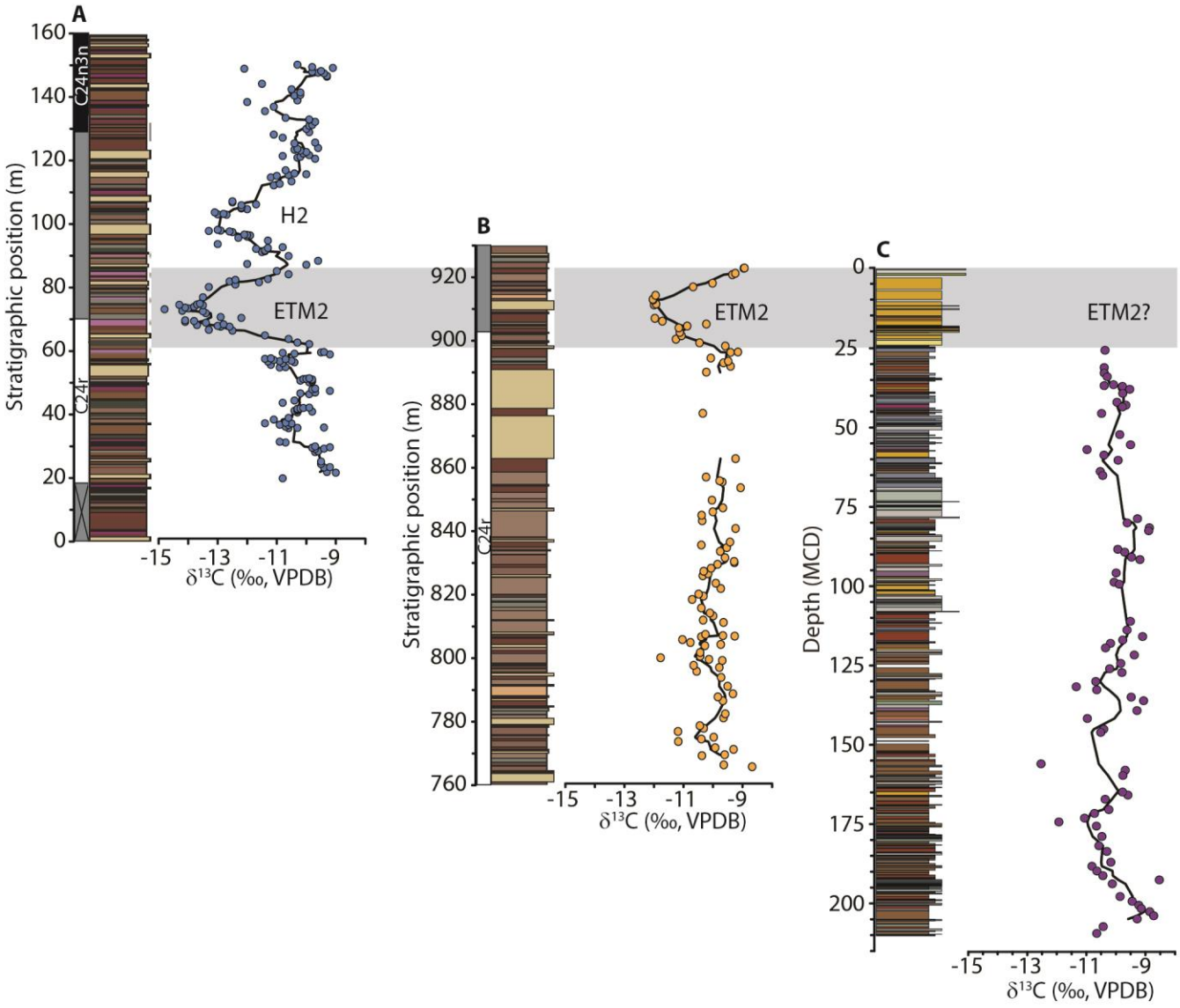
A
B
C
Stratigraphic position (m)
Depth (MCD)
C24n3n
C24r
H2
ETM2
ETM2?
δ13C (‰, VPDB)
-15
-13
-11
-9

Fig. 12. Comparison of cored lithostratigraphy and carbon isotope stratigraphy from two Bighorn Basin sites. Lithostratigraphy and carbon isotope stratigraphy from (A) drilled Gilmore Hill strata and (B) drilled Polecat Bench strata. Carbon isotope values are derived from pedogenic carbonate analyses, black lines denote a running five point average, and stratigraphic depths are equally scaled for both sections.

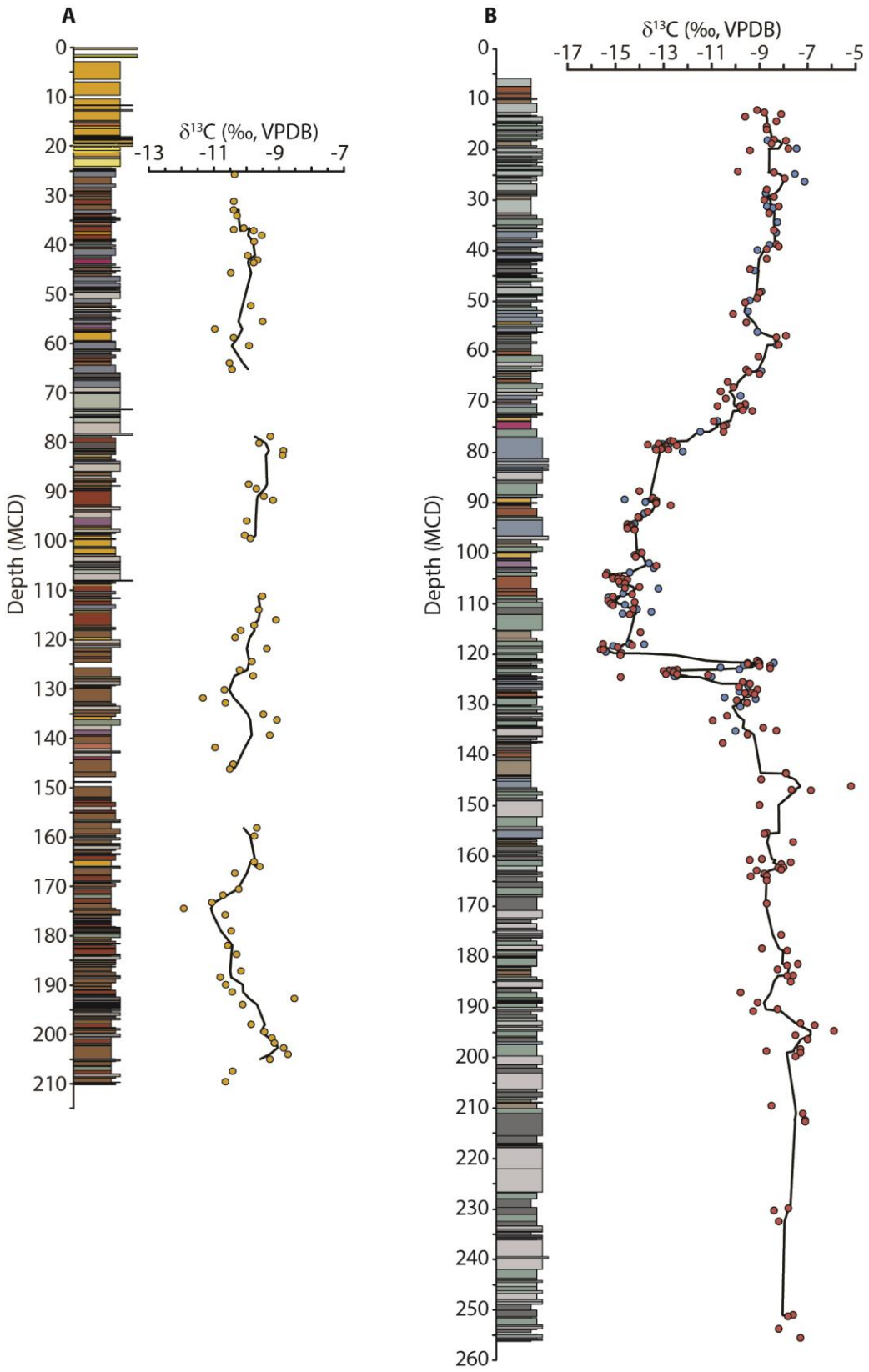
A
B
δ13C (‰, VPDB)
-13
-11
-9
-7
-17
-15
-13
-11
-9
-7
-5
Depth (MCD)
0
10
20
30
40
50
60
70
80
90
100
110
120
130
140
150
160
170
180
190
200
210
220
230
240
250
260

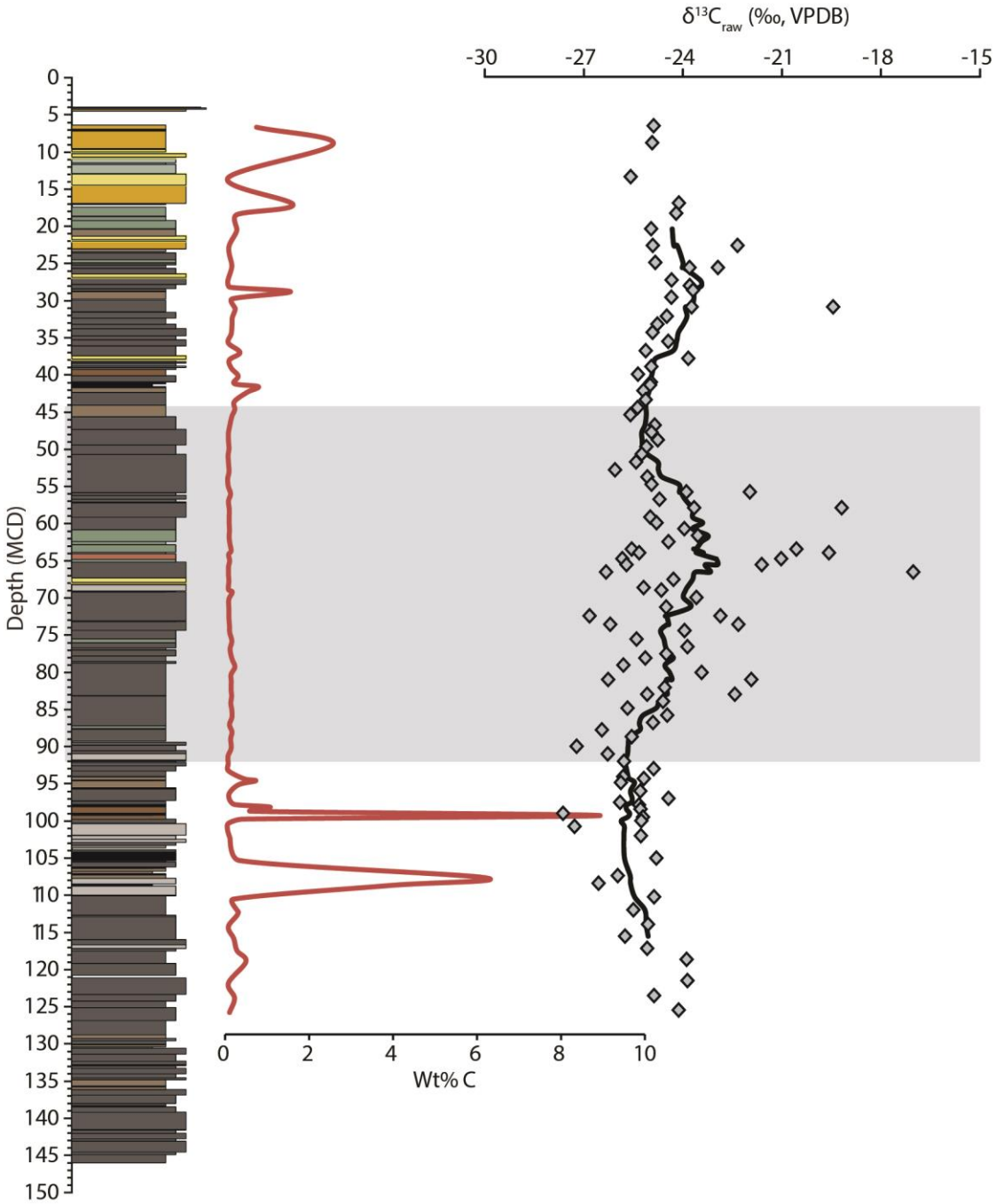

Fig. 13. Lithostratigraphy, total organic carbon (TOC) concentrations, and bulk organic matter carbon isotope stratigraphy at Basin Substation. Compiled lithostratigraphy (left panel), bulk soil organic matter carbon concentrations (middle panel, red line), and bulk soil organic matter carbon isotope data (right panel, gray diamonds) across ~130 m of drilled strata. The eleven point running average of $\delta^{13}C$ values is denoted by the black line, and the middle interval of very low TOC concentrations between ~43 and ~93 MCD is denoted by the gray field.

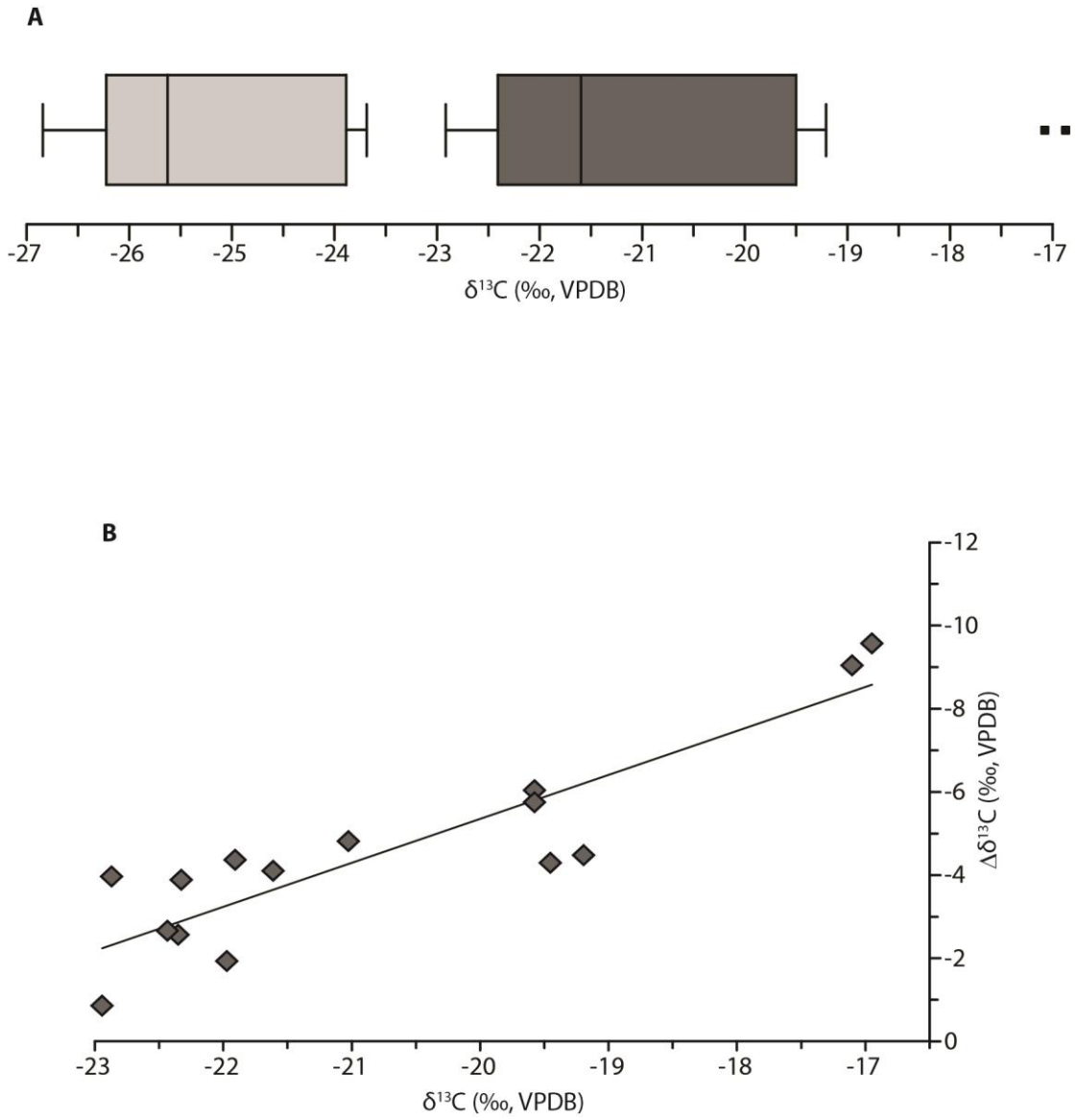

Fig. 14. Test for the presence of inorganic carbonate in Basin Substation bulk organic matter samples. Fifteen samples with $\delta^{13}C$ values above −23‰ after the first acidification (dark gray field with two outliers) were reacidified to remove any remaining inorganic carbonate (lighter gray field). Average values shifted 4.55‰ lower following reacidification.

Fig. 15. Basin Substation bulk organic carbon isotope record highlighting values derived from sandstone lithologies. (A) raw $\delta^{13}C$ values (gray diamonds) showing the location of sandstone derived analyses (yellow diamonds) and the eleven point running average (black line). (B) $\delta^{13}C$ values (gray diamonds) after sandstone values were removed with the new eleven point running average (black line).

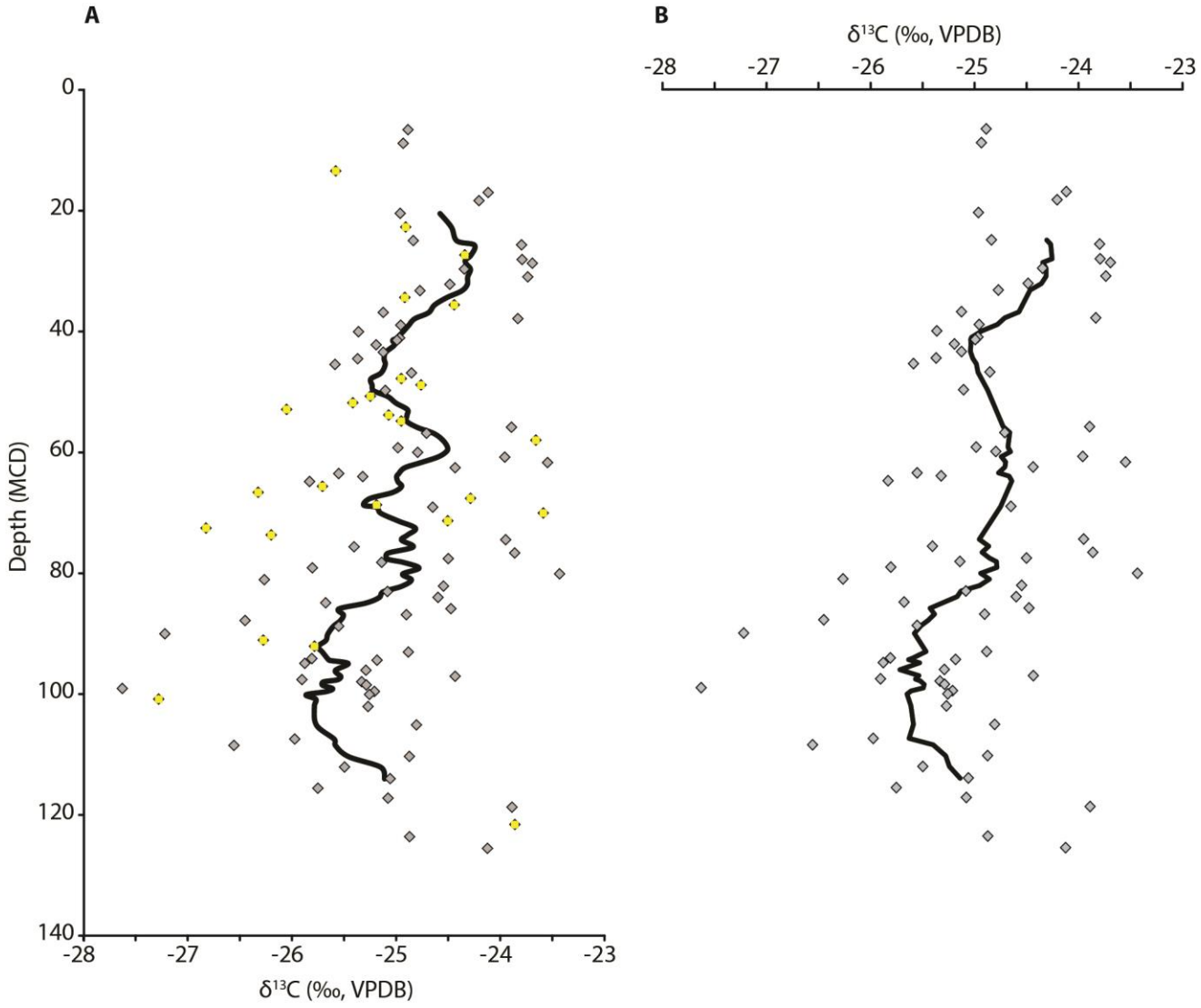
A
B
Depth (MCD)
0
20
40
60
80
100
120
140
-28
-27
-26
-25
-24
-23
δ13C (‰, VPDB)

Fig. 16. TOC trend corrections calculated and applied to $\delta^{13}C_{org}$ data at Basin Substation. (A) relationship between the natural logarithm of wt. % C and $\delta^{13}C$ values to test for carbon preservation dependency in carbon isotope values. Values are separated into three distinct groups of TOC preservation, which are stratigraphically defined: low TOC (43.46–93.09 MCD) (red diamonds), median TOC (20.48–42.23 MCD) (green diamonds), and high TOC values (94.17–114.04) (blue diamonds). Best fit lines are shown for each group in black. (B) $\delta^{13}C$ values (gray diamonds) after the wt. % C trend was corrected for. These values are reported as an anomaly relative to the lowest 25 m of section (baseline values), and the eleven point running average is denoted by the black line.

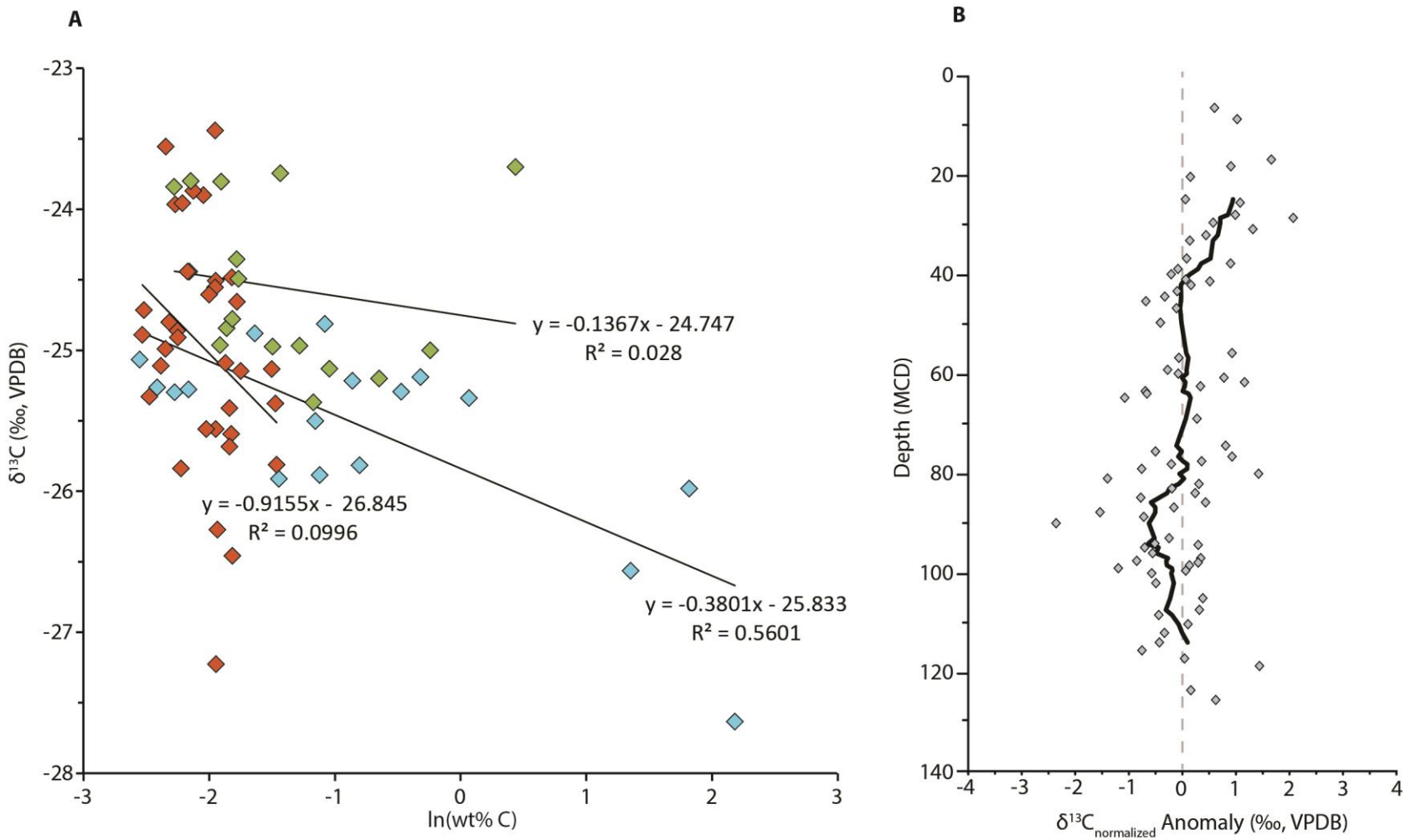
A
B
δ13C (‰, VPDB)
ln(wt% C)
y = -0.1367x - 24.747
R² = 0.028
y = -0.9155x - 26.845
R² = 0.0996
y = -0.3801x - 25.833
R² = 0.5601
Depth (MCD)
δ13Cnormalized Anomaly (‰, VPDB)

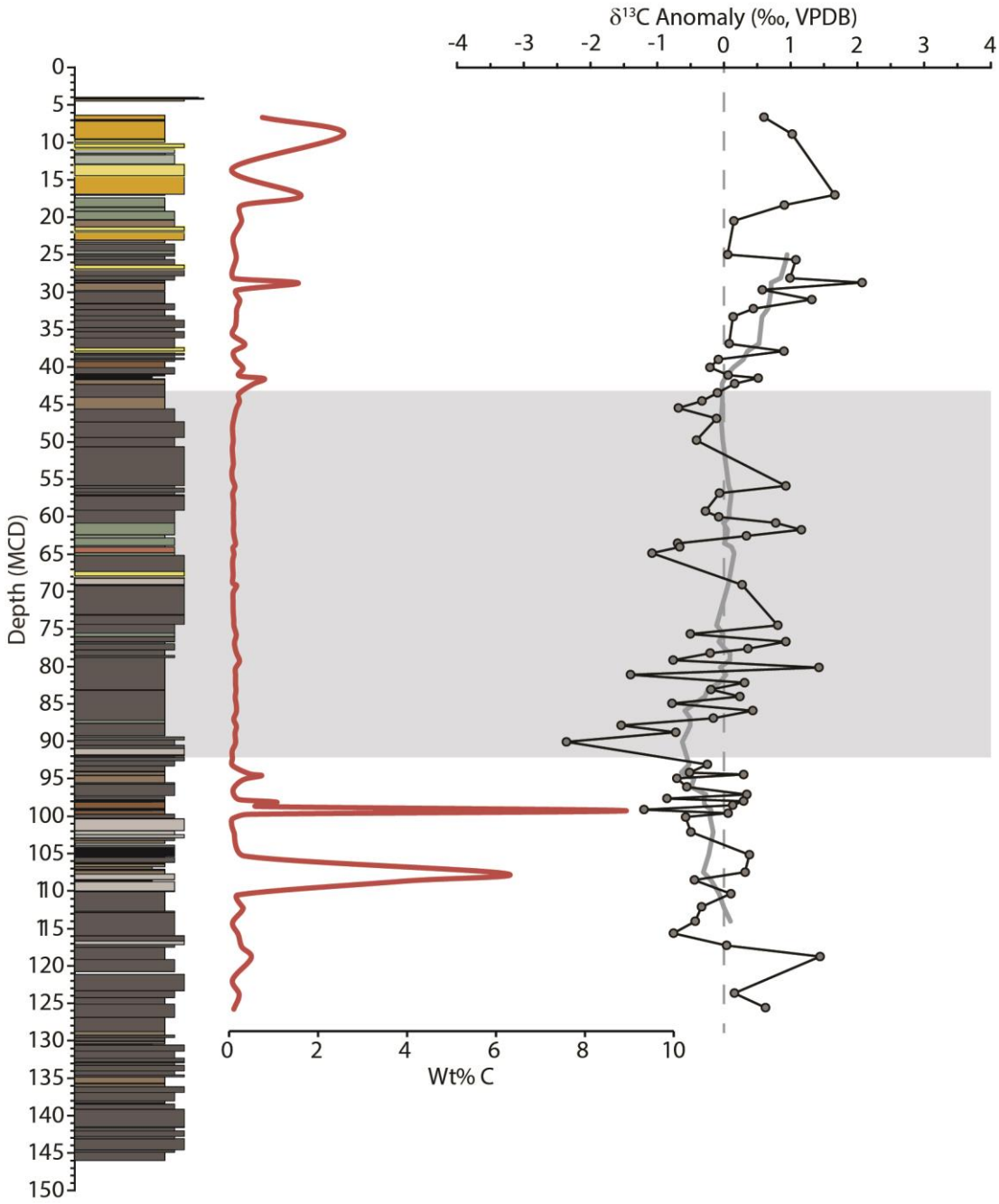

Fig. 17. Lithostratigraphy, total organic carbon (TOC) concentrations, and corrected bulk organic matter carbon isotope stratigraphy at Basin Substation. Compiled lithostratigraphy, TOC preservation (weight % carbon, Wt% C), and corrected $\delta^{13}C$ values measured from Basin Substation bulk sedimentary organic matter. $\delta^{13}C$ values (gray circles) are reported after both sandstone values were removed and the Wt% C trend was corrected for. These values are reported as an anomaly relative to the lowest 25 m of section (baseline values). The eleven point running average is denoted by the gray line and the interval interpreted as the PETM (based on low TOC values between ~43 and 93 MCD) is denoted by the gray field.

Fig. 18. Location and stratigraphy of four Bighorn Basin bulk organic matter studies. Lithostratigraphy of (A) Basin Substation core (this study), (B) Cabin Fork outcrop (Wing et al., 2005), (C) Polecat Bench outcrop (Magioncalda et al., 2004), and (D) Highway 16 (Baczynski et al., 2013; Kraus et al., 2013) and map of Bighorn Basin showing the location of the four sites used in this comparison (red circles). Stratigraphic levels/depths are equally scaled for all sections and gray fields represent the predicted interval of the PETM CIE, with a gradational boundary representative of a range of possible end members and a solid boundary representative of a definitive end member. All sections are aligned to the start of the PETM CIE.

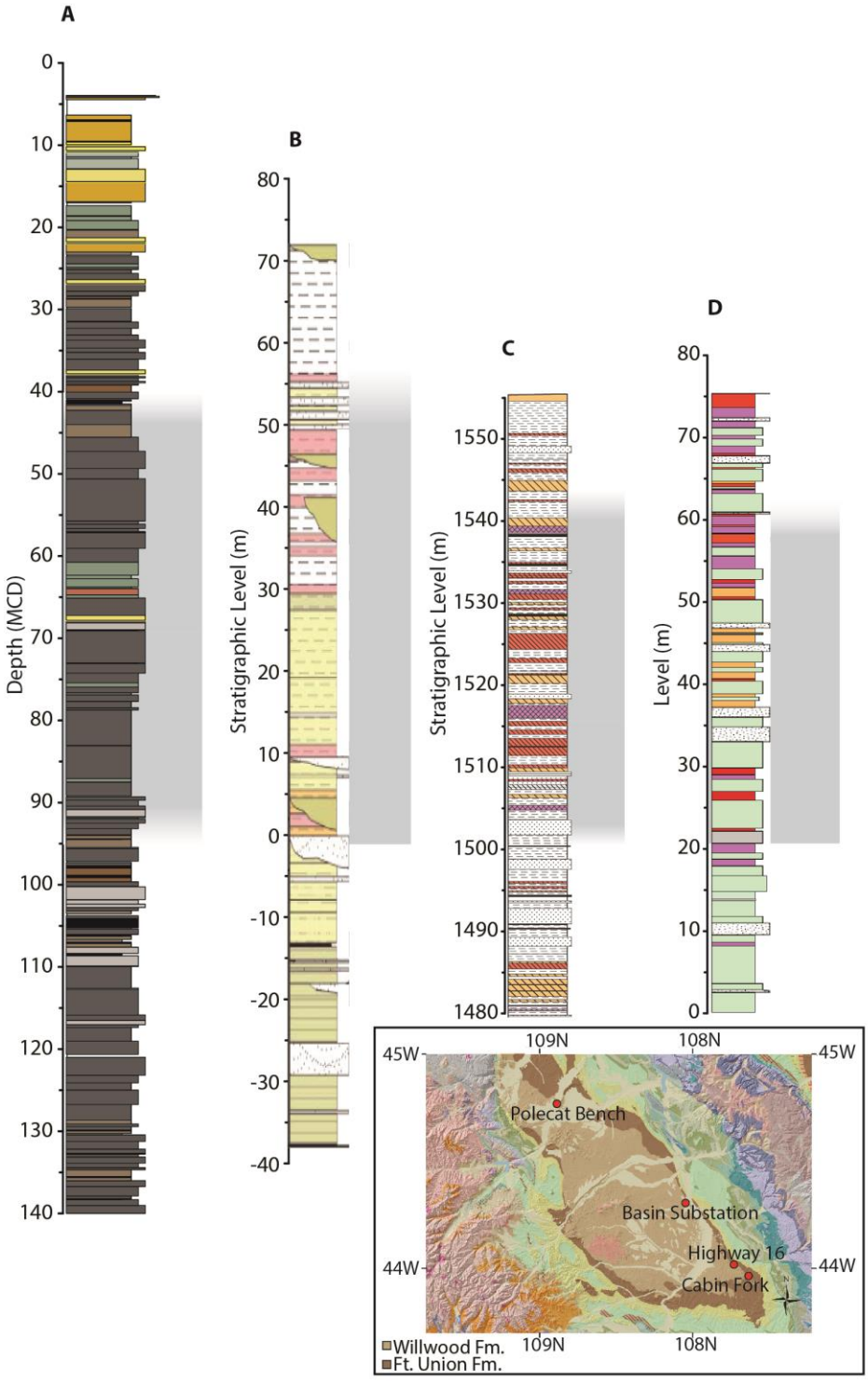
A
B
C
D
Depth (MCD)
Stratigraphic Level (m)
Stratigraphic Level (m)
Level (m)
0
10
20
30
40
50
60
70
80
90
100
110
120
130
140
80
70
60
50
40
30
20
10
0
-10
-20
-30
-40
1550
1540
1530
1520
1510
1500
1490
1480
80
70
60
50
40
30
20
10
0
109N
108N
45W
44W
Polecat Bench
Basin Substation
Highway 16
Cabin Fork
Willwood Fm.
Ft. Union Fm.

Fig. 19. Comparison of total organic carbon records from four sites located in the Bighorn Basin, WY. Total organic carbon (TOC) concentrations (red lines) from (A) Basin Substation, (B) Cabin Fork (Wing et al. 2005), (C) Polecat Bench (Magioncalda et al., 2004), and (D) Highway 16 (Baczynski et al., 2013; Kraus et al., 2013). Note that TOC concentrations are plotted on a logarithmic scale. Stratigraphic levels/depths are equally scaled for all sections and the gray fields in each plot represent the predicted interval of the PETM CIE, with a gradational boundary representative of a range of possible end members and a solid boundary representative of a definitive end member.

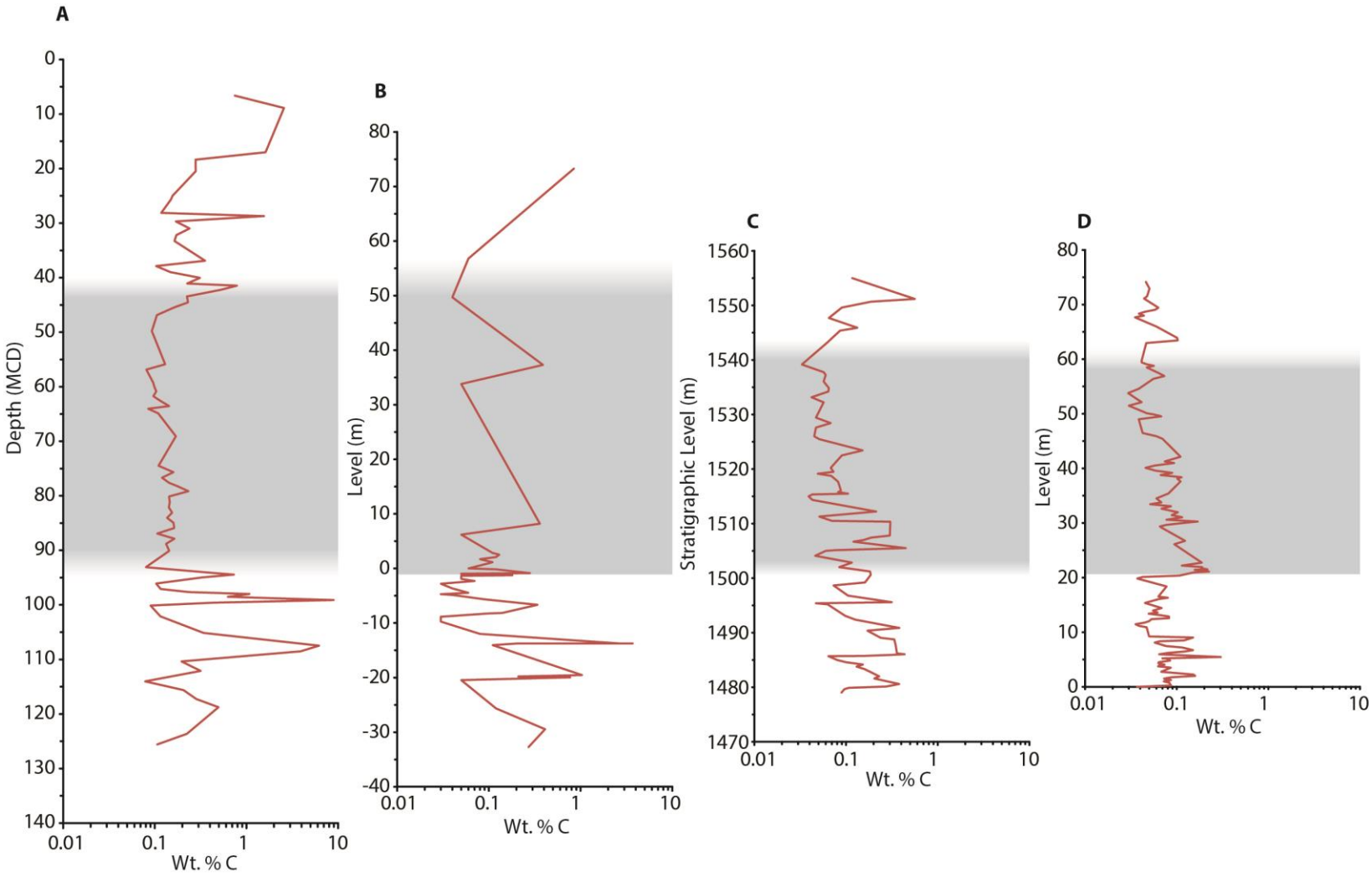
A
Depth (MCD)
0
10
20
30
40
50
60
70
80
90
100
110
120
130
140
0.01
0.1
1
10
Wt. % C
B
Level (m)
80
70
60
50
40
30
20
10
0
-10
-20
-30
-40
0.01
0.1
1
10
Wt. % C
C
Stratigraphic Level (m)
1560
1550
1540
1530
1520
1510
1500
1490
1480
1470
0.01
0.1
1
10
Wt. % C
D
Level (m)
80
70
60
50
40
30
20
10
0
0.01
0.1
1
10
Wt. % C

Fig. 20. Comparison of bulk organic carbon isotope records from four sites located in the Bighorn Basin, WY. (A) Basin Substation (gray circles), (B) Cabin Fork (gray diamonds; Wing et al. 2005), (C) Polecat Bench (gray squares; Magioncalda et al., 2004), and (D) Highway 16 (gray triangles; Baczynski et al., 2013; Kraus et al., 2013) carbon isotope stratigraphy. For (A), (C), and (D), the red line denotes an eleven point running average and carbon isotope values are reported as an anomaly relative to the lower 20-25 m of section. For (B), the red line denotes the five point running average and values are normalized by calculating the observed minus the predicted δ13C values outlined in (Wing et al., 2005). Stratigraphic levels/depths are equally scaled for all sections, and the gray fields in each plot represent the predicted interval of the PETM CIE, with a gradational boundary representative of a range of possible end members and a solid boundary representative of a definitive end member.

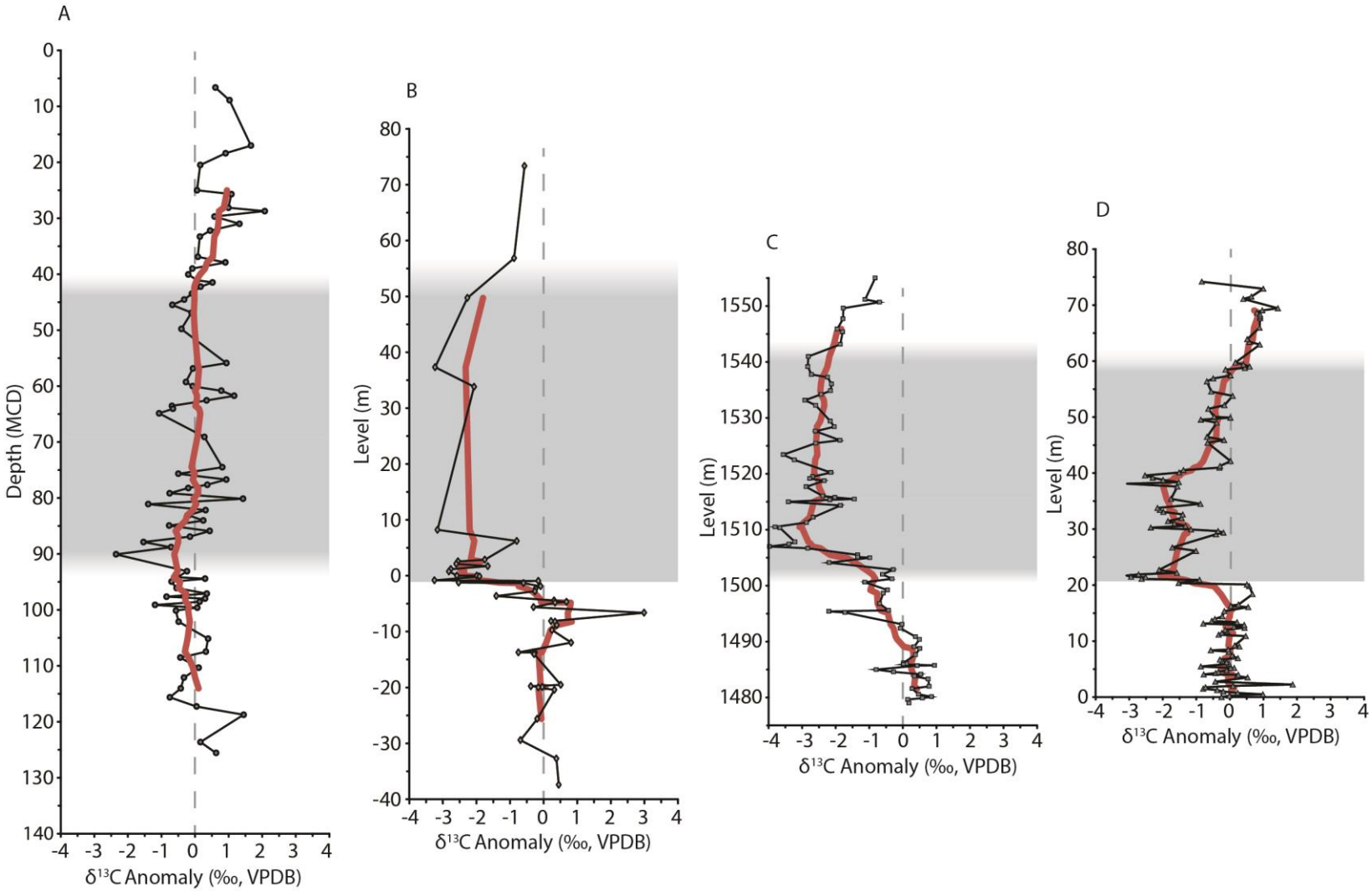
A
Depth (MCD)
0
10
20
30
40
50
60
70
80
90
100
110
120
130
140
-4 -3 -2 -1 0 1 2 3 4
δ13C Anomaly (‰, VPDB)
B
Level (m)
80
70
60
50
40
30
20
10
0
-10
-20
-30
-40
-4 -3 -2 -1 0 1 2 3 4
δ13C Anomaly (‰, VPDB)
C
Level (m)
1550
1540
1530
1520
1510
1500
1490
1480
-4 -3 -2 -1 0 1 2 3 4
δ13C Anomaly (‰, VPDB)
D
Level (m)
80
70
60
50
40
30
20
10
0
-4 -3 -2 -1 0 1 2 3 4
δ13C Anomaly (‰, VPDB)

Table 5. Sand blank test for residual organic carbon during sample analysis.

Analysis ID	Notes	Sample weight (mg)	Peak Area (Vs)	TOC (wt% C)
310	small	32.70	4.40	0.00
311	no peak	28.01	0.00	0.00
312	no peak	31.67	0.00	0.00
313	small	29.75	4.33	0.00
314	no peak	23.33	0.00	0.00
315	small	28.05	4.13	0.00
316	small	36.21	4.48	0.00
317	small	30.89	5.05	0.01

Table 6. Carbon and oxygen isotope stratigraphy from Gilmore Hill core collected carbonate nodules. Isotope data is reported in standard delta notation (δ) in per mil (‰) relative to the international standard Vienna PeeDee Belemnite (VPDB).

MCD	Sample ID	Avg. $\delta^{13}C$	Avg. $\delta^{18}O$	Count
25.65	3106128	−10.4	−8.5	1
31.10	3107592	−10.4	−8.3	1
32.81	3107612	−10.4	−8.2	1
33.99	3107638	−10.3	−9.2	1
36.50	3107682	−10.1	−8.5	1
36.80	3107680	−10.4	−10.1	1
37.03	3107678	−9.8	−8.8	1
37.97	3107704	−9.5	−8.6	1
39.25	3107728	−9.8	−8.2	1
42.05	3107784	−10.0	−8.3	1
42.96	3107804	−9.7	−8.3	1
43.51	3107806	−9.8	−8.3	1
45.57	3107826	−10.5	−8.2	1
52.23	3107920	−9.9	−8.2	1
55.43	3107970	−9.5	−8.4	1
56.95	3107992	−11.0	−7.9	1
58.70	3108014	−10.4	−7.9	1
60.33	3108048	−9.9	−8.7	1
63.85	3108128	−10.5	−8.5	1
65.13	3108154	−10.4	−8.3	1
78.73	3108264	−9.3	−9.0	1
80.07	3108294	−9.6	−8.4	1
81.59	3108336	−8.9	−8.1	1
82.54	3108350	−8.9	−8.7	1
88.39	3108416	−9.9	−8.2	1
89.31	3108432	−9.7	−8.2	1
90.85	3108440	−9.5	−8.2	1
91.64	3108462	−9.2	−7.5	1
95.84	3108540	−10.0	−8.3	1
98.75	3108588	−10.1	−8.0	1
99.40	3108592	−9.9	−7.9	1
111.10	3108808	−9.5	−7.9	1
113.83	3108876	−9.6	−9.7	3
115.88	3108890	−9.1	−8.6	1
116.98	3108904	−9.8	−8.6	2
118.03	3108908	−10.2	−8.8	1

Table 6 Continued

MCD	Sample ID	Avg. $\delta^{13}C$	Avg. $\delta^{18}O$	Count
121.71	3108974	−9.4	−8.5	1
124.34	3109018	−9.8	−8.5	2
126.05	3109048	−10.2	−9.2	2
127.25	3109064	−9.8	−8.8	2
130.04	3109106	−10.7	−8.9	2
131.71	3109126	−11.3	−8.5	2
132.69	3109150	−10.6	−8.3	2
134.98	3109172	−9.5	−8.1	2
136.13	3109190	−9.1	−8.3	1
139.22	3109214	−9.3	−8.6	2
141.72	3109238	−11.0	−8.3	2
145.08	3109292	−10.4	−8.7	2
146.09	3109306	−10.5	−8.8	2
156.01	3109402	−12.5	−9.9	2
158.02	3109422	−9.7	−9.1	1
159.65	3109432	−9.8	−8.8	1
165.84	3109490	−9.6	−8.6	1
164.89	3109496	−9.8	−8.4	2
167.18	3109510	−10.4	−8.7	1
170.42	3109540	−10.2	−8.9	2
171.64	3109558	−10.7	−9.3	1
173.12	3109574	−11.1	−8.7	1
174.34	3109590	−11.9	−8.8	1
175.62	3109616	−10.7	−8.3	1
178.90	3109650	−10.5	−9.3	1
181.84	3109670	−10.6	−9.0	1
183.63	3109692	−10.3	−9.0	2
187.01	3109744	−10.2	−8.5	2
188.28	3109762	−10.8	−8.5	2
189.78	3109766	−10.6	−8.2	1
191.26	3109790	−10.4	−8.4	1
192.59	3109816	−8.5	−8.3	1
193.82	3109828	−10.1	−8.5	2
197.84	3109876	−9.9	−8.6	1
199.34	3109890	−9.4	−9.0	2
200.58	3109916	−9.2	−9.0	2
201.62	3109926	−9.1	−8.5	2
203.91	3109958	−8.7	−8.2	1

Table 6 Continued

MCD	Sample ID	Avg. $\delta^{13}C$	Avg. $\delta^{18}O$	Count
207.31	3109996	−10.43	−8.81	1
209.46	3110024	−10.65	−8.71	1

Table 7. Carbon cycle mass balance calculations for the ETM2. The mass of carbon required (M_a) to cause four different CIE's ($\Delta\delta^{13}C$) was calculated using terrestrial and marine end member CIE estimations using a methane hydrate carbon source ($\delta^{13}C_a$). Masses reported in gigatons (Gt), and $\delta^{13}C$ values reported in standard delta notation (δ) in per mil (‰) relative to the international standard Vienna PeeDee Belemnite (VPDB).

	$\Delta\delta^{13}C$	$\delta^{13}C_i$	M_i	Carbon Source‡	$\delta^{13}C_a$	M_a
Terrestrial end member*	−2.5	1.31‰	57,700	methane hydrates	−60‰	2,453
	−4					4,027
Marine end member†	−1					957
	−1.6					1,546

‡ See review in McInerney & Wing (2011) for description of hypothesized sources of carbon.
*Terrestrial record end members are based on work by Abels et al. (2012).
†Marine record end members are based on work by Lourens et al. (2005).

Table 8. Carbon isotope stratigraphy and total organic carbon (TOC, wt% C) from Basin Substation bulk sedimentary organic matter. Isotope data are reported in standard delta notation (δ) in per mil (‰) relative to the international standard Vienna PeeDee Belemnite (VPDB). Samples in italics represent high initial $\delta^{13}C$ values indicative of the presence of inorganic carbonate. The duplicate value listed (not in italics) represents the $\delta^{13}C$ value after reacidification that was used in the final dataset.

MCD	Sample ID	Avg. $\delta^{13}C$	Avg. TOC	Count
6.62	3101140	−24.9	0.75	1
8.89	3101166	−24.9	2.57	1
13.46	3101188	−25.6	0.07	1
17.00	3101198	−24.1	1.62	2
18.37	3101210	−24.2	0.28	1
20.48	3101222	−25.0	0.28	1
22.72	3101240	−24.9	0.09	1
22.72	3101240	*−22.4*	*0.08*	*1*
24.99	3101256	−24.8	0.16	1
25.69	3101268	−23.8	0.15	1
25.69	3101268	*−22.9*	*0.12*	1
27.37	3101274	−24.3	0.06	1
28.12	3101280	−23.8	0.12	3
28.72	3101286	−23.7	1.56	1
29.68	3101298	−24.4	0.17	1
30.98	3101310	−23.7	0.24	1
30.98	3101310	*−19.5*	*0.29*	*1*
32.20	3101318	−24.5	0.17	2
33.28	3101334	−24.8	0.16	1
34.39	3101346	−24.9	0.15	1
35.61	3101358	−24.4	0.08	2
36.88	3101370	−25.1	0.35	1
37.89	3101382	−23.8	0.10	1
38.99	3101394	−25.0	0.15	1
40.05	3101406	−25.4	0.31	1
41.08	3101418	−25.0	0.23	1
41.47	3101424	−25.0	0.79	1
42.23	3101436	−25.2	0.53	1
43.46	3101454	−25.1	0.22	2
44.54	3101472	−25.4	0.23	1
45.48	3101484	−25.6	0.16	1
46.87	3101502	−24.9	0.11	1
47.83	3101514	−25.0	0.08	1
48.86	3101526	−24.8	0.08	1
49.79	3101538	−25.1	0.09	1
50.75	3101550	−25.3	0.07	1
51.84	3101562	−25.4	0.08	1

Table 8 Continued

MCD	Sample ID	Avg. $\delta^{13}C$	Avg. TOC	Count
52.90	3101576	−26.1	0.09	1
53.86	3101588	−25.1	0.06	1
54.85	3101600	−25.0	0.07	1
55.88	3101612	−23.9	0.13	1
55.88	3101612	*−22.0*	*0.12*	1
56.85	3101624	−24.7	0.08	1
58.00	3101636	−23.7	0.10	1
58.00	3101636	*−19.2*	*0.09*	1
59.26	3101648	−25.0	0.10	2
60.02	3101660	−24.8	0.10	1
60.82	3101672	−24.0	0.10	1
61.74	3101684	−23.6	0.10	1
62.56	3101696	−24.4	0.11	2
63.54	3101708	−25.6	0.14	2
63.54	3101708	*−20.6*	*0.12*	*2*
64.04	3101714	−25.3	0.08	1
64.04	3101714	*−19.6*	*0.10*	*1*
64.86	3101726	−25.8	0.11	1
64.86	3101726	*−21.0*	*0.09*	*1*
65.65	3101738	−25.7	0.08	1
65.65	3101738	*−21.6*	*0.07*	*1*
66.64	3101750	−26.3	0.08	2
66.64	3101750	*−17.0*	*0.09*	*2*
67.64	3101758	−24.3	0.09	1
68.72	3101768	−25.2	0.08	1
69.09	3101772	−24.7	0.17	1
70.06	3101782	−23.6	0.09	2
71.34	3101794	−24.5	0.09	1
72.55	3101802	−26.8	0.09	1
72.55	3101802	*−22.9*	*0.08*	*1*
73.69	3101812	−26.2	0.11	1
73.69	3101812	*−22.3*	*0.09*	*1*
74.50	3101832	−24.0	0.11	2
75.66	3101850	−25.4	0.16	1
76.70	3101862	−23.9	0.12	1
77.63	3101874	−24.5	0.14	1
78.22	3101886	−25.1	0.18	2
79.15	3101898	−25.8	0.23	1
80.14	3101910	−23.4	0.14	1
81.10	3101922	−26.3	0.15	1
81.10	3101922	*−21.9*	*0.12*	*2*
82.16	3101934	−24.6	0.14	1

Table 8 Continued

MCD	Sample ID	Avg. $\delta^{13}C$	Avg. TOC	Count
83.07	3101946	−25.1	0.16	2
83.07	3101946	*−22.4*	*0.13*	*1*
84.02	3101958	−24.6	0.14	1
84.94	3101974	−25.7	0.16	2
85.90	3101994	−24.5	0.16	1
86.91	3102014	−24.9	0.11	1
87.87	3102024	−26.5	0.16	1
88.79	3102044	−25.6	0.13	1
90.07	3102066	−27.2	0.14	2
91.11	3102092	−26.3	0.07	1
92.12	3102112	−25.8	0.07	1
93.09	3102128	−24.9	0.08	1
94.17	3102146	−25.8	0.45	2
94.43	3102152	−25.2	0.73	1
94.95	3102162	−25.9	0.33	1
96.09	3102178	−25.3	0.10	1
97.09	3102190	−24.4	0.12	2
97.64	3102196	−25.9	0.24	1
97.98	3102208	−25.3	1.08	1
98.53	3102214	−25.3	0.63	1
99.11	3102226	−27.6	8.93	1
99.59	3102232	−25.2	0.43	1
100.12	3102238	−25.3	0.09	1
100.88	3102248	−27.3	0.05	2
102.10	3102256	−25.3	0.12	2
105.15	3102290	−24.8	0.34	1
107.48	3102318	−26.0	6.21	1
108.52	3102330	−26.6	3.89	2
110.35	3102342	−24.9	0.20	1
112.11	3102354	−25.5	0.32	1
114.04	3102370	−25.1	0.08	2
115.63	3102382	−25.8	0.21	1
117.27	3102392	−25.1	0.28	1
118.75	3102404	−23.9	0.50	2
121.63	3102418	−23.9	0.08	1
123.63	3102428	−24.9	0.22	1
125.57	3102440	−24.1	0.11	1

Table 9. Raw and corrected $\delta^{13}C$ values for Basin Substation bulk organic matter. TOC trend corrected $\delta^{13}C$ values are based on the relationship between TOC and δ13C in samples between 94.17–114.04 MCD. The TOC trend corrected $\delta^{13}C$ values are reported as an anomaly relative to the lowest 25 m of strata (baseline values). Data are reported in standard delta notation (δ) in per mil (‰) relative to the international standard Vienna PeeDee Belemnite (VPDB).

MCD	Avg. $\delta^{13}C$	Avg. TOC	TOC-corrected $\delta^{13}C$	TOC-corrected anomaly
6.62	−24.89	0.75	0.83	0.60
8.89	−24.94	2.57	1.26	1.02
17.00	−24.12	1.62	1.89	1.66
18.37	−24.21	0.28	1.14	0.90
20.48	−24.97	0.28	0.38	0.15
24.99	−24.84	0.16	0.29	0.05
25.69	−23.80	0.15	1.31	1.08
28.12	−23.80	0.12	1.22	0.99
28.72	−23.70	1.56	2.30	2.07
29.68	−24.35	0.17	0.81	0.57
30.98	−23.74	0.24	1.55	1.31
32.20	−24.49	0.17	0.67	0.44
33.28	−24.78	0.16	0.37	0.14
36.88	−25.13	0.35	0.31	0.08
37.89	−23.84	0.10	1.13	0.90
38.99	−24.96	0.15	0.15	−0.09
40.05	−25.37	0.31	0.02	−0.21
41.08	−24.97	0.23	0.29	0.06
41.47	−25.00	0.79	0.75	0.51
42.23	−25.20	0.53	0.39	0.16
43.46	−25.13	0.22	0.14	−0.10
44.54	−25.37	0.23	−0.10	−0.33
45.48	−25.59	0.16	−0.45	−0.68
46.87	−24.86	0.11	0.12	−0.11
49.79	−25.11	0.09	−0.18	−0.41
55.88	−23.90	0.13	1.16	0.93
56.85	−24.71	0.08	0.16	−0.07
59.26	−24.99	0.10	−0.05	−0.28
60.02	−24.80	0.10	0.16	−0.08
60.82	−23.96	0.10	1.01	0.77
61.74	−23.55	0.10	1.39	1.16
62.56	−24.44	0.11	0.57	0.34
63.54	−25.56	0.14	−0.46	−0.70
64.04	−25.33	0.08	−0.43	−0.66
64.86	−25.84	0.11	−0.84	−1.08
69.09	−24.65	0.17	0.51	0.27

Table 9 Continued

MCD	Avg. $\delta^{13}C$	Avg. TOC	TOC-corrected $\delta^{13}C$	TOC-corrected anomaly
74.50	−23.95	0.11	1.04	0.80
75.66	−25.41	0.16	−0.27	−0.51
76.70	−23.87	0.12	1.16	0.93
78.22	−25.14	0.18	0.03	−0.21
79.15	−25.81	0.23	−0.53	−0.76
81.10	−26.27	0.15	−1.17	−1.40
82.16	−24.55	0.14	0.54	0.31
83.07	−25.09	0.16	0.04	−0.20
84.02	−24.60	0.14	0.47	0.24
84.94	−25.68	0.16	−0.54	−0.78
85.90	−24.48	0.16	0.66	0.43
86.91	−24.91	0.11	0.07	−0.16
87.87	−26.45	0.16	−1.31	−1.54
88.79	−25.56	0.13	−0.49	−0.72
90.07	−27.22	0.14	−2.13	−2.36
93.09	−24.89	0.08	−0.02	−0.25
94.17	−25.81	0.45	−0.28	−0.52
94.43	−25.19	0.73	0.53	0.29
94.95	−25.88	0.33	−0.47	−0.71
96.09	−25.29	0.10	−0.32	−0.56
97.09	−24.44	0.12	0.58	0.34
97.64	−25.91	0.24	−0.62	−0.86
97.98	−25.34	1.08	0.53	0.29
98.53	−25.29	0.63	0.36	0.13
99.11	−27.63	8.93	−0.97	−1.20
99.59	−25.21	0.43	0.29	0.06
100.12	−25.26	0.09	−0.34	−0.58
102.10	−25.27	0.12	−0.26	−0.50
105.15	−24.81	0.34	0.61	0.38
107.48	−25.98	6.21	0.55	0.31
108.52	−26.56	3.89	−0.21	−0.45
110.35	−24.88	0.20	0.34	0.10
112.11	−25.50	0.32	−0.10	−0.34
114.04	−25.06	0.08	−0.20	−0.43
115.63	−25.76	0.21	−0.52	−0.76
117.27	−25.08	0.28	0.27	0.04
118.75	−23.89	0.50	1.67	1.44
123.63	−24.88	0.22	0.39	0.15
125.57	−24.13	0.11	0.85	0.62

SUMMARY AND FUTURE WORK

Assessment of pedogenic carbonate or bulk sedimentary organic matter from three cored terrestrial locales in the Bighorn Basin, WY reveals new structure or confirms existing records of carbon cycle change through early Paleogene hyperthermals. High-resolution, stratigraphically continuous carbon isotope data from Polecat Bench (PCB) show that the PETM is characterized by a sustained >5‰ negative shift in $\delta^{13}C$, which characterizes the Paleocene-Eocene thermal maximum (PETM) carbon isotope excursion CIE. The onset of this event is characterized by two distinct, rapid negative shifts, separated by a short recovery back to near background values, suggesting that initiation of the PETM CIE was from two, not one, massive releases of carbon. Following the onset of the CIE, low values are sustained for approximately 40 m, where they gradually recover back towards background values over about 20 m. The sustained low $\delta^{13}C$ values which characterize the body of the CIE and the gradual recovery of values back to baseline agree in terms of the timing and magnitude of change with existing studies; however, the volatility demonstrated in the early phases of initiation of the CIE represent previously unrecognized structure in the carbon isotope stratigraphy. Basic steady-state mass balance calculations combined with an existing internal age model suggest that during each release, carbon entered the surface ocean and/or atmosphere at rates similar to modern fossil fuel emission rates. Therefore, this new highly-resolved terrestrial

carbon isotope record suggests that the PETM is an excellent analogue to modern day anthropogenic carbon release.

Two additional sites that contain strata spanning either the PETM or the Eocene Thermal Maximum 2 (ETM2) were also drilled in the Bighorn Basin, WY. Analysis of bulk sedimentary organic matter from Basin Substation (BSN) cores reveals a dramatic decrease in TOC preservation through the interval that we have classified as the PETM; however, the $\delta^{13}C$ record is variable and does not show the expected >2‰ shift associated with the PETM CIE, even after several previously proven corrections are applied to the dataset. Comparison of our record to nearby outcrop studies of bulk sedimentary organic matter reveals agreement in the TOC trends to another site in the southeastern Bighorn Basin but notable discrepancies to two other nearby locations. The variability and lack of discernible CIE in our $\delta^{13}C$ record suggests that additional external mechanisms likely impacted the preserved organic matter and its associated carbon isotopic signature, and the relationship between these two variables in studies of paleosols requires further investigation. The carbon isotope record from core recovered pedogenic carbonate at Gilmore Hill (GMH) reveals relatively stable background $\delta^{13}C$ and $\delta^{18}O$ values over a host of multicolored floodplain lithologies. The GMH cores show excellent agreement to nearby outcrop studies in background carbon and oxygen isotope values; however, the marked >2‰ negative CIE that characterizes the ETM2 in continental records is missing from our GMH $\delta^{13}C$ curve. We suspect that this interval is located in the thick, poorly cemented, highly weathered sands, which characterize the upper 25 m of core at this site and may represent a climatic response to the warming event. Although the BSN and GMH sites did not contain the expected CIE associated

with the PETM or ETM2, the PCB record shows volatile behavior in Earth's carbon cycle and indicates that the PETM is a strong analogue to current and future carbon cycle perturbation in both magnitude and rate of change.

The results presented in this text represent a first order assessment of carbon cycle change through this interval of significant environmental change. Due to the nature of the Bighorn Basin Coring Project, many opportunities are available for ongoing and future work. For Polecat Bench cores, analysis of bulk sedimentary organic matter at high resolution across the section would create another record of carbon isotopic change at this site and allow for comparison to the paleosol carbonate $\delta^{13}C$ record. This coupled assessment of $\delta^{13}C$ change may provide valuable information regarding soil carbon dynamics, global carbon dynamics, and the exchange of CO_2 between organic and inorganic carbon phases. Analysis of specific organic compounds and their $\delta^{13}C$ values at Basin Substation would provide pertinent information towards determining the origin of the SOM, the amount of degradation that it has undergone, and/or ecologic responses to the hyperthermal event helping to resolve some of the important uncertainties highlighted in this text. Additionally, a detailed study of the host lithologies and paleosoil horizons that were sampled may help constrain some of the environmental conditions both during the time of sediment and organic matter deposition and during burial. Although the expected ETM2 CIE is missing from the GMH cores, comparison of the $\delta^{18}O$ record from our site to nearby outcrop sites may help to constrain background temperatures in the early Eocene. Additionally, a detailed assessment of the lithologic change coupled to isotope values may help provide additional information on some of the smaller scale, regional coupled environmental and carbon cycle changes.

REFERENCES

Abels, H.A., Clyde, W.C., Gingerich, P.D., Hilgen, F.J., Fricke, H.C., Bowen, G.J., and Lourens, L.J., 2012, Terrestrial carbon isotope excursions and biotic change during Paleogene hyperthermals: Nature Geoscience, v. 5, p. 326–329.

Andres, R.J., Boden, T.A., Bréon, F.M., Ciais, P., Davis, S., Erickson, D., Gregg, J.S., Jacobson, A., Marland, G., and Miller, J., 2012, A synthesis of carbon dioxide emissions from fossil-fuel combustion: Biogeosciences Discussions, v. 9, no. 1, p. 1299–1376.

Archer, D., 2007, Methane hydrate stability and anthropogenic climate change: Biogeosciences, v. 4, p. 521–544.

Arens, N.C., Jahren, A.H., and Amundson, R., 2000, Can C3 plants faithfully record the carbon isotopic composition of atmospheric carbon dioxide?: Paleobiology, v. 26, no. 1, p. 137–164.

Aziz, H.A., Hilgen, F.J., van Luijk, G.M., Sluijs, A., Kraus, M.J., Pares, J.M., and Gingerich, P.D., 2008, Astronomical climate control on paleosol stacking patterns in the upper Paleocene-lower Eocene Willwood Formation, Bighorn Basin, Wyoming: Geology, v. 36, no. 7, p. 531–534.

Baczynski, A.A., McInerney, F.A., Wing, S.L., Kraus, M.J., Bloch, J.I., Boyer, D.M., Secord, R., Morse, P.E., and Fricke, H.C., 2013, Chemostratigraphic implications of spatial variation in the Paleocene-Eocene Thermal Mazimum carbon isotope excursion, SE Bighorn Basin, Wyoming: Geochemistry Geophysics Geosystems.

Bains, S., Corfield, R.M., and Norris, R.D., 1999, Mechanisms of climate warming at the end of the Paleocene: Science, v. 285, no. 5428, p. 724–727.

Bains, S., Norris, R.D., Corfield, R.M., Bowen, G.J., Gingerich, P.D., and Koch, P.L., 2003, Marine-terrestrial linkages at the Paleocene-Eocene boundary, *in* Wing, S.L., Gingerich, P.D., Schmitz, B., and Thomas, E., eds., Causes and Consequences of Globally Warm Climates in the Early Paleogene: Boulder, Colorado, Geological Society of America Special Paper 369, p. 1–9.

Balesdent, J., and Mariotti, A., 1996, Measurement of Soil Organic Matter Turnover Using 13C Natural Abundance, *in* Boutton, T. W., and Yamasaki, S. I., eds., Mass spectrometry of soils: New York, NY, Marcel Dekker, Inc.

Bataille, C.P., Mastalerz, M., Tipple, B.J., and Bowen, G.J., 2013, Influence of organic provenance and preservation on the carbon isotope variations of dispersed organics in ancient floodplain sediments: Geochemistry Geophysics Geosystems (in press).

Bottinga, Y., and Craig, H., 1968, Oxygen Isotope Fractionation between CO_2 and Water and Isotopic Composition of Marine Atmospheric CO_2: Earth and Planetary Science Letters, v. 5, no. 5, p. 285–295.

Bowen, G.J., 2013, Up in smoke: A role for organic carbon feedbacks in Paleogene hyperthermals: Global and Planetary Change, v. 109, p. 18–29.

Bowen, G.J., and Beerling, D.J., 2004, An integrated model for soil organic carbon and CO_2: Implications for paleosol carbonate pCO_2 paleobarometry: Global Biogeochemical Cycles, v. 18, GB1026, doi:10.1029/2003GB002117.

Bowen, G.J., Beerling, D.J., Koch, P.L., Zachos, J.C., and Quattlebaum, T., 2004, A humid climate state during the Palaeocene-Eocene thermal maximum: Nature, v. 432, p. 495–499.

Bowen, G.J., Bralower, T.J., Delaney, M.L., Dickens, G.R., Kelly, D.C., Koch, P.L., Kump, L.R., Meng, J., Sloan, L.C., Thomas, E., Wing, S.L., and Zachos, J.C., 2006, Eocene hyperthermal event offers insight into greenhouse warming: Eos, v. 87, no. 17, p. 165–169.

Bowen, G.J., Koch, P.L., Gingerich, P.D., Norris, R.D., Bains, S., and Corfield, R.M., 2001, Refined isotope stratigraphy across the continental Paleocene-Eocene boundary on Polecat Bench in the Northern Bighorn Basin, *in* Gingerich, P.D., ed., Paleocene-Eocene Stratigraphy and Biotic Change in the Bighorn and Clarks Fork Basins, Wyoming: Ann Arbor, MI, University of Michigan Museum of Paleontology, p. 73–88.

Bowen, G.J., and Zachos, J.C., 2010, Rapid carbon sequestration at the termination of the Paleocene-Eocene thermal maximum: Nature Geoscience, v. 3, p. 866–869.

Bown, T.M., and Kraus, M.J., 1987, Integration of channel and floodplain suites, I: Developmental sequence and lateral relations of alluvial Paleosols: Journal of Sedimentary Petrology, v. 57, no. 4, p. 587–601.

Cerling, T.E., 1984, The stable isotopic composition of modern soil carbonate and its relationship to climate: Earth and Planetary Science Letters, v. 71, p. 229–240.

Cerling, T.E., 1999, Stable carbon isotopes in palaeosol carbonates: Palaeoweathering, palaeosurfaces and related continental deposits, p. 43–60.

Cerling, T.E., Quade, J., Wang, Y., and Bowman, J.R., 1989, Carbon isotopes in soils and palaeosols as ecology and palaeoecology indicators: Nature, v. 341, p. 138–139.

Clechenko, E.R., Kelly, D.C., Harrington, G.J., and Stiles, C.A., 2007, Terrestrial records of a regional weathering profile at the Paleocene-Eocene boundary in the Williston Basin of North Dakota: Geological Society of America Bulletin, v. 119, no. 3, p. 428–442.

Clyde, W.C., 1997, Stratigraphy and mammalian paleontology of the McCullough Peaks, Northern Bighorn Basin, Wyoming: Implications for biochronology, basin development, and community reorganization across the Paleocene-Eocene boundary [Dissertation]: University of Michigan, Ann Arbor, Michigan.

Clyde, W.C., and Gingerich, P.D., 1998, Mammalian community response to the latest Paleocene thermal maximum: An isotaphonomic study in the northern Bighorn Basin, Wyoming: Geology, v. 26, no. 11, p. 1011–1014.

Clyde, W.C., Gingerich, P.D., and Wing, S.L., 2012, Coring project in Bighorn Basin: Drilling phase complete: Eos, Transactions American Geophysical Union, v. 93, no. 4, p. 41–42.

Clyde, W.C., Gingerich, P.D., Wing, S.L., Röhl, U., Westerhold, T., Bowen, G.J., Johnson, K., Baczynski, A.A., Diefendorf, A.F., McInerney, F., Schnurrenberger, D., Noren, A., Brady, K., and the Bighorn Basin Science Team, 2013, Bighorn Basin Coring Project (BBCP): A Continental Perspective on Early Paleogene Hyperthermals: Scientific Drilling (in press).

Clyde, W.C., Hamzi, W., Finarelli, J.A., Wing, S.L., Schankler, D., and Chew, A., 2007, Basin-wide magnetostratigraphic framework for the Bighorn Basin, Wyoming: GSA Bulletin, v. 119, p. 848–859.

Clyde, W.C., Stamatakos, J., and Gingerich, P.D., 1994, Chronology of the Wasatchian land-mammal age (early Eocene): Magnetostratigraphic results from the McCullough Peaks section, northern Bighorn Basin, Wyoming: Journal of Geology, v. 102, no. 4, p. 367–377.

Cramer, B.S., and Kent, D.V., 2005, Bolide summer: The Paleocene/Eocene thermal maximum as a response to an extraterrestrial trigger: Palaeogeography Palaeoclimatology Palaeoecology, v. 224, p. 144–166.

Cui, Y., Kump, L.R., Ridgwell, A.J., Charles, A.J., Junium, C.K., Diefendorf, A.F., Freeman, K.H., Urban, N.M., and Harding, I.C., 2011, Slow release of fossil carbon during the Palaeocene-Eocene thermal maximum, Nature Geoscience, , v. 4, no. 7, p. 481–485.

DeConto, R., Galeotti, S., Pagani, M., Tracy, D., Schaefer, K., Zhang, T., Pollard, D., and Beerling, D.J., 2012, Past extreme warming events linked to massive carbon release from thawing permafrost: Nature, v. 484, p. 87–92.

Dickens, G.R., Castillo, M.M., and Walker, J.C.G., 1997, A blast of gas in the latest Paleocene: Simulating first-order effects of massive dissociation of oceanic methane hydrate: Geology, v. 25, no. 3, p. 259–262.

Dickens, G.R., O'Neil, J.R., Rea, D.K., and Owen, R.M., 1995, Dissociation of oceanic methane hydrate as a cause of the carbon isotope excursion at the end of the Paleocene: Paleoceanography, v. 10, no. 6, p. 965–971.

Ehleringer, J.R., and Monson, R.K., 1993, Evolutionary and ecological aspects of photosynthetic pathway variation: Annual reviews, v. 24, p. 411–439.

Gingerich, P.D., 2001, Biostratigraphy of the continental Paleocene-Eocene boundary interval on Polecat Bench in the Northern Bighorn Basin: University of Michigan Papers on Paleontology, v. 33, p. 37–71.

Gingerich, P.D., 2006, Environment and evolution through the Paleocene–Eocene thermal maximum: Trends in Ecology & Evolution, v. 21, no. 5, p. 246–253.

Gingerich, P.D., and Clyde, W.C., 2001, Overview of mammalian biostratigraphy of the Paleocene-Eocene Fort Union and Willwood formations of the Bighorn and Clarks Fork basins: University of Michigan Papers on Paleontology, v. 33, p. 1–14.

Harris, D., Horwath, W.R., and Van Kessel, C., 2001, Acid fumigation of soils to remove carbonates prior to total organic carbon or carbon-13 isotopic analysis: Soil Science Society of America Journal, v. 65, p. 1853–1856.

Higgins, J.A., and Schrag, D.P., 2006, Beyond methane: Towards a theory for the Paleocene-Eocene Thermal Maximum: Earth and Planetary Science Letters, v. 245, no. 3-4, p. 523–537.

IPCC, 2007, Climate Change 2007: Impacts, adaption and vulnerability: Contribution of Working Group I to the Fourth Assessment Report of the Intergovernmental Panel on Climate Change: Cambirdge, UK, Cambridge University Press, 996 pp.

IPCC, 2013, Climate Change 2013: The physical science basis: Working Group I Cpmtribution to the Fifth Assessment Report of the Intergovernmental Panel on Climate Change (in press).

Jacobs, B.F., Kingston, J.D., and Jacobs, L.L., 1999, The origin of grass-dominated ecosystems: Annals of the Missouri Botanical Garden, v. 86, no. 2, p. 590–643.

Katz, M.E., Pak, D.K., Dickens, G.R., and Miller, K.G., 1999, The source and fate of massive carbon input during the latest Paleocene thermal maximum: Science, v. 286, p. 1531–1533.

Kennett, J.P., and Stott, L.D., 1991, Abrupt deep-sea warming, palaeoceanographic changes and benthic extinctions at the end of the Palaeocene: Nature, v. 353, no. 6341, p. 225–229.

Koch, P.L., Clyde, W.C., Hepple, R.P., Fogel, M.L., Wing, S.L., and Zachos, J.C., 2003, Carbon and oxygen isotope records from paleosols spanning the Paleocene-Eocene boundary, Bighorn Basin, Wyoming, *in* Wing, S. L., Gingerich, P.D., Schmitz, B., and Thomas, E., eds., Causes and Consequences of Globally Warm Climates in the Early Paleogene: Boulder, Colorado, Geological Society of America, p. 49–64.

Kraus, M.J., and Gwinn, B., 1997, Facies and facies architecture of Paleogene floodplain deposits, Willwood Formation, Bighorn Basin, Wyoming, USA: Sedimentary Geology, v. 114, p. 33–54.

Kraus, M.J., McInerney, F.A., Wing, S.L., Secord, R., Baczynski, A.A., and Bloch, J.I., 2013, Paleohydrologic response to continental warming during the Paleocene-Eocene Thermal Maximum, Bighorn Basin, Wyoming: Palaeogeography Palaeoclimatology Palaeoecology, v. 370.

Kraus, M.J., and Riggins, S., 2007, Transient drying during the Paleocene–Eocene Thermal Maximum (PETM): Analysis of paleosols in the Bighorn Basin, Wyoming: Palaeogeography Palaeoclimatology Palaeoecology, v. 245, p. 444–461.

Kraus, M.J., and Wells, T.M., 1999, Recognizing avulsion deposits in the ancient stratigraphic record, *in* Smith, N. D., and Rogers, J., eds., Fluvial Sedimentology VI: Special Publication 28 of the International Association of Sedimentologists: Hoboken, New Jersey, International Association of Sedimentologists Series, p. 251–268.

Lourens, L.J., Sluijs, A., Kroon, D., Zachos, J.C., Thomas, E., Röhl, U., Bowles, J., and Raffi, I., 2005, Astronomical pacing of late Palaeocene to early Eocene global warming events: Nature, v. 435, p. 1083–1087.

Magioncalda, R., Dupuis, C., Smith, T., Steurbaut, E., and Gingerich, P.D., 2004, Paleocene-Eocene carbon isotope excursion in organic carbon and pedogenic carbonate: Direct comparison in a continental stratigraphic section: Geology, v. 32, no. 7, p. 553–556.

Marshall, J.D., Brooks, J.R., and Lajtha, K., 2007, Sources of variation in the stable isotopic composition of plants, *in* Michener, R., and Lajtha, K., eds., Stable

Isotopes in Ecology and Environmental Science: Malden, Massachusettes, Blackwell Publishing.

McInerney, F.A., and Wing, S.L., 2011, The Paleocene-Eocene thermal maximum: A perturbation of carbon cycle, climate, and biosphere with implications for the future: Annual Review of Earth & Planetary Sciences, v. 39, p. 489–516.

Midwood, A.J., and Boutton, T.W., 1998, Soil carbonate decomposition by acid has little effect on the d13C or organic matter: Soil Biology & Biochemistry, v. 30, p. 1301–1307.

Moore, E.A., and Kurtz, A.C., 2008, Black carbon in Paleocene-Eocene boundary sediments: A test of biomass combustion as the PETM trigger: Palaeogeography Palaeoclimatology Palaeoecology, v. 267, p. 147–152.

Murphy, B.H., Farley, K.A., and Zachos, J. C., 2010, An extraterrestrial ^{3}He-based timescale for the Paleocene-Eocene thermal maximum (PETM) from Walvis Ridge, IODP Site 1266: Geochimica et Cosmochimica Acta, v. 74, p. 5098–5108.

Neasham, J.W., and Vondra, C.F., 1972, Stratigraphy and petrology of the Lower Eocene Willwood Formation, Bighorn Basin, Wyoming: Geological Society of America Bulletin, v. 83.

National Oceanic & Atmospheric Administration, 2013, Earth System Research Laboratory, Global Monitoring Division, Trends in Atmospheric Carbon Dioxide: http://www.esrl.noaa.gov/gmd/ccgg/trends/

Petit, J.R., Jouzel, J., Raynaud, D., Barkov, N.I., Barnola, J.M., Basile, I., Bender, M., Chappellaz, J., Davis, M., Delaygue, G., Delmotte, M., Kotlyakov, V.M., Legrand, M., Lipenkov, V.Y., Lorius, C., Pepin, L., Ritz, C., Saltzmann, E., and Stievenard, M., 1999, Climate and atmospheric history of the past 420,000 years from the Vostok ice core, Antarctica: Nature, v. 399, no. 6735, p. 429–436.

Rampino, M.R., 2013, Peraluminous igneous rocks as an indicator of thermogenic methane release from the North Atlantic Volcanic Province at the time of the Paleocene-Eocene Thermal Maximum (PETM): Bulletin of Volcanology, v. 75, p. 1–5.

Röhl, U., Westerhold, T., Bralower, T.J., and Zachos, J.C., 2007, On the duration of the Paleocene-Eocene thermal maximum (PETM): Geochemistry Geophysics Geosystems, v. 8, Q12002.

Royer, D.L., 1999, Depth to pedogenic carbonate horizon as a paleoprecipitation indicator?: Geology, v. 27, p. 1123–1126.

Rozanski, K., Araguas-Araguas, L., and Gonfiantini, R., 1993, Isotopic patterns in modern global precipitation, *in* Swart, P. K., Lohmann, K. C., McKenzie, J., and Savin, S., eds., Climate change in continental isotopic records: Washington, D.C., American Geophysical Union, p. 1–36.

Secord, R., Gingerich, P.D., Lohmann, K.C., and MacLeod, K.G., 2010, Continental warming preceding the Palaeocene-Eocene thermal maximum: Nature, v. 467, p. 955–958.

Sluijs, A., Brinkhuis, H., Schouten, S., Bohaty, S., John, C.M., Zachos, J.C., Reichart, G.J., Sinninghe Damste, J.S., Crouch, E.M., and Dickens, G.R., 2007, Environmental precursors to rapid light carbon injection at the Palaeocene/Eocene boundary: Nature, v. 2007, p. 1218–1222.

Sluijs, A., Schouten, S., Pagani, M., Woltering, M., Brinkhuis, H., Sinninghe Damsté, J.S., Dickens, G.R., Huber, M., Reichart, G.J., Stein, R., Matthiessen, J., Lourens, L.J., Pedentchouk, N., Backman, J., and Moran, K., 2006, Subtropical Arctic Ocean temperatures during the Palaeocene/Eocene thermal maximum: Nature, v. 441, p. 610–613.

Sluijs, A., Zachos, J.C., and Zeebe, R.E., 2012, Constraints on hyperthermals: Nature Geoscience, v. 5.

Stap, L., Sluijs, A., Thomas, E., and Lourens, L., 2009, Patterns and magnitude of deep sea carbonate dissolution during Eocene Thermal Maximum 2 and H2, Walvis Ridge, southeastern Atlantic Ocean: Paleoceanography, v. 24, PA1211.

Svensen, H., Planke, S., Malthe-Sorenssen, A., Jamtveit, B., Myklebust, R., Eidem, T.R., and Rey, S.S., 2004, Release of methane from a volcanic basin as a mechanism for initial Eocene global warming: Nature, v. 429, no. 6991, p. 542–545.

Thomas, D.J., Zachos, J.C., Bralower, T.J., Thomas, E., and Bohaty, S., 2002, Warming the fuel for the fire: Evidence for the thermal dissociation of methane hydrate during the Paleocene-Eocene thermal maximum: Geology, v. 30, no. 12, p. 1067–1070.

Thomas, E., and Shackleton, N.J., 1996, The Paleocene-Eocene benthic foraminiferal extinction and stable isotope anomalies: Geological Society Special Publications, v. 101, p. 401–441.

Westerhold, T., Röhl, U., and Laskar, J., 2012, Time scale controversy: Accurate orbital calibration of the early Paleogene: Geochemistry Geophysics Geosystems, v. 13.

Westerhold, T., Röhl, U., Laskar, J., Raffi, I., Bowles, J., Lourens, L.J., and Zachos, J.C., 2007, On the duration of magnetochrons C24r and C25n and the timing of early

Eocene global warming events: Implications from the Ocean Drilling Program Leg 208 Walvis Ridge depth transect: Paleoceanography, v. 22, PA2201.

Wing, S.L., and Harrington, G.J., 2001, Floral response to rapid warming in the earliest Eocene and implications for concurrent faunal change: Paleobiology, v. 27, no. 3, p. 539–563.

Wing, S.L., Harrington, G.J., Smith, F.A., Bloch, J.I., Boyer, D.M., and Freeman, K.H., 2005, Transient floral change and rapid global warming at the Paleocene-Eocene boundary: Science, v. 310, p. 993–996.

Wyoming State Geological Survey, 2013, Bighorn Basin: http://www.wsgs.uwyo.edu/research/stratigraphy/BigHornBasin/Default.aspx

Wynn, J.G., 2007, Carbon isotope fractionation during decomposition of organic matter in soils and paleosols: implications for paleoecological interpretations of paleosols: Palaeogeography Palaeoclimatology Palaeoecology, v. 251, p. 437–448.

Wynn, J.G., Harden, J.W., and Fries, T.L., 2006, Stable carbon isotope depth profiles and soil organic carbon dynamics in the lower Mississippi Basin: Geoderma v. 131, no. 1-2, p. 89–109

Zachos, J.C., Dickens, G.R., and Zeebe, R.E., 2008, An early Cenozoic perspective on greenhouse warming and carbon-cycle dynamics: Nature, v. 451.

Zachos, J.C., Pagani, M., Sloan, L., Thomas, E., and Billups, K., 2001, Trends, rhythms, and aberrations in global climate 65 Ma to present: Science, v. 292, no. 5517, p. 686–693.

Zachos, J.C., Röhl, U., Schellenberg, S.A., Sluijs, A., Hodell, D.A., Kelley, D.C., Thomas, E., Nicolo, M., Raffi, I., Lourens, L.J., McCarren, H., and Kroon, D., 2005, Rapid acidification of the ocean during the Paleocene-Eocene thermal maximum: Science, v. 308, p. 1611–1615.

Zachos, J.C., Schouten, S., Bohaty, S., Quattlebaum, T., Sluijs, A., Brinkhuis, H., Gibbs, S.J., and Bralower, T.J., 2006, Extreme warming of mid-latitude coastal ocean during the Paleocene-Eocene Thermal Maximum: Inferences from TEX_{86} and isotope data: Geology, v. 34, no. 9, p. 737–740.

Zeebe, R.E., 2013, What caused the long duration of the Paleocene-Eocene Thermal Maximum?: Paleoceanography.

Zeebe, R.E., Zachos, J.C., and Dickens, G.R., 2009, Carbon dioxide forcing alone insufficient to explain Palaeocene-Eocene Thermal Maximum warming: Nature Geoscience, v. 2, p. 576–580.